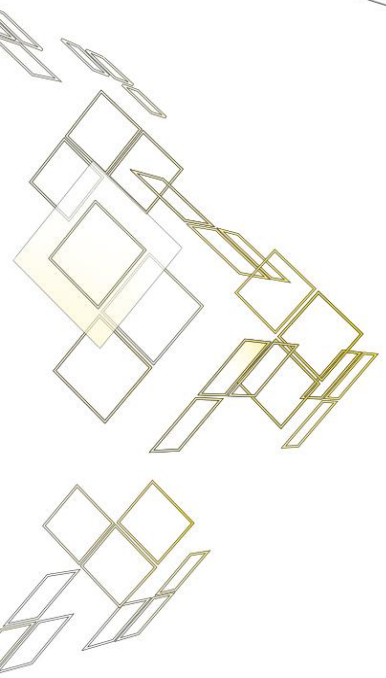

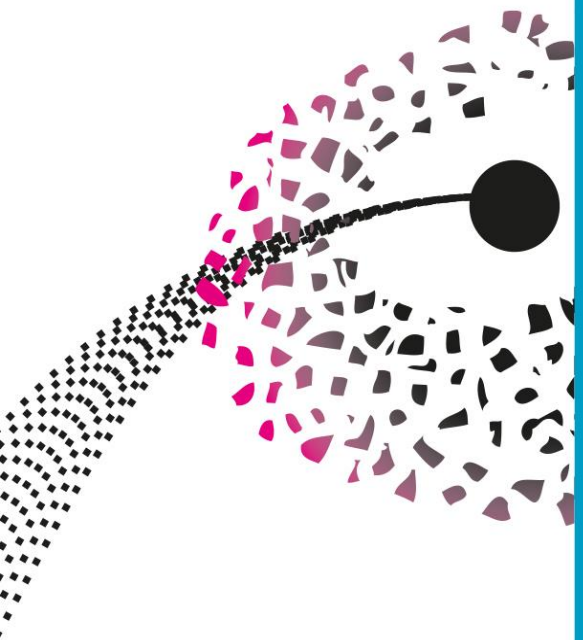

FACULTY OF ENGINEERING TECHNOLOGY

LIDAR MEASUREMENTS OF SWASH-EVENT BED DYNAMICS

MASTER'S THESIS

ARTIS MURNIEKS (S2203383)

02.10.2022

UNIVERSITY OF TWENTE.

COLOPHON

MANAGEMENT
Department of Engineering Technology

DATE
02.10.2022

VERSION
1.

STATUS
Final

PROJECT
Master's Thesis

PROJECT NUMBER
201800116

AUTHOR(S)
Artis Mūrnieks

TELEPHONE
0613440546

EMAIL
a.murnieks@student.utwente.nl

POSTAL ADDRESS
P.O. Box 217
7500 AE Enschede

WEBSITE
www.utwente.nl

REGISTRATION DETAILS
Registration details

UNIVERSITY OF TWENTE

LIDAR MEASUREMENTS OF SWASH-EVENT BED DYNAMICS

Investigation of LiDAR Application to Monitor Beach Evolution at the Inter-Swash Scale

Master's Thesis

Author:

Name: A. (Artis) Mūrnieks
Programme: MSc. Civil Engineering and Management
River and Coastal Engineering
Institute: University of Twente
Enschede, The Netherlands
E-mail: a.murnieks@student.utwente.nl

Graduation Committee:

Dr. ir. J.J. (Jebbe) van der Werf	University of Twente/Deltares
Dr. ir. E.M. (Erik) Horstman	University of Twente
M.Sc. S. (Sara) Dionisio Antonio	University of Twente

ACKNOWLEDGEMENTS

The Master's thesis was the final step of my educational journey before I step into the professional world as a qualified engineer. Therefore, I would like to take the time to thank the involved parties who were part of this journey in the last two years.

Firstly, I would thank the members of the graduation committee. Special thanks to Sara Dionisio Antonio, MSc for providing daily supervision, discussions, and enthusiasm throughout the master's thesis period. I wish you the best of luck with attaining your PhD. Similarly, I would thank Dr Ir. Jebbe van der Werf and Dr Ir. Erik Horstman for guidance and support in times when progress was difficult to attain. Second, I would like to express my deepest appreciation to the University of Twente. During my study period, I was always surprised by the quality of education, the possibilities that are offered to students and the level of organization. It was an honour to study River and Coastal Engineering which was taught by highly knowledgeable lecturers. The lessons learned during the study period have made me a more well-rounded professional. I am also grateful for the opportunity to be part of the Design Lab's family. The time spent there and the work together with fellow Dream Teamers has allowed me to grow as a person. In addition, I would like to thank the University of Twente for always being there for the students.

Finally, I would like to thank my family and friends. The mental support and your trust have helped me to overcome times when I lost confidence. There are no words to describe how lucky I am to have you all by my side no matter what the situation is. I wish you a pleasant time reading the thesis which could give you new insight into LiDAR capabilities and swash zone bed dynamics.

Thank you all again!

Artis Murnieks
Enschede, September 2022

SUMMARY

The swash zone is the dynamic interface between the land and ocean that is alternately covered and exposed by onshore- and offshore-directed water movement. The challenge associated with the swash zone is the ability to obtain reliable measurements of its bed dynamics. As the result, the knowledge about the processes occurring in the swash zone is limited. To overcome the challenge, it is proposed to make use of LiDAR (light detection and ranging), which is an optical remote sensing technology that makes use of laser beams to detect the distance between LiDAR and an object or surface. The benefit of LiDAR use is its ability to replace point measurement systems and make spatially and temporally dense measurements without interfering with the observed environment.

The objective of this research is to make use of available raw LiDAR data gathered in large-scale wave flume experiments and to examine if it is possible to quantify the inter-swash morphodynamical contribution of individual swash events to the longer-term, event-averaged morphological evolution of the sandy beach.

In the validation part of this research, the LiDAR measurements along the horizontal and vertical axis were compared to other measurement devices. It was found that LiDAR error along the horizontal axis for the dry bed is below ~5mm margin, while if there are objects present on the slopes, the error can increase by one order of magnitude. Along the y-axis, not all the vertical positions of the obtained beach profile measurements were within the allowed error margin. The main cause for differences along the y-axis could be caused by measuring two separate locations or the inherent error of the mechanical measurement devices. The LiDAR error along the vertical axis of the static beach slope did not exceed ~5mm.

Subsequently, the LiDAR data on the water level was separated from the bed level of the beach. In this case, three different methods were compared: varying variance, decreased variance and relative signal strength index. Both, the variance and decreased variance methods provided similar results. The extracted water lines were capable of following the water column that is higher than ~20mm. The method with relative strength index was capable of better capturing the swash lens's temporal variability than the variance methods. However, it was concluded that for the calculation of bed level changes the water line determined with the varying variance method, derived from data in the validation section, provided the best match to the researchers' observations of maximum run-up, average run-up, maximum run-down and relative elevation change image in time.

Finally, the observed bed level changes between consecutive profiles were quantified. In this case in total, 165 swash events with the majority of events being short than 11s were identified. Out of 165 events, 77 accretive and 88 erosive events were observed. While the majority of all these events caused bed level changes below $0.05m^2$, the smaller scale events did not contribute to the net morphological change of the beach slope. The events that did contribute the most to the net morphological change of the slope were larger than $0.05m^2$. In addition, the largest event was determined to induce bed level change which was 50% of the net morphological change over a ~30min period. Additionally, to the bed level changes along the full length of the swash zone, the point measurements were also examined. At the point of maximum accretion and erosion during 30min period, the bed level changes at these points in inter swash scale most of the time were below 2mm. Furthermore, the correlation between the length of the swash event and the change in the swash zone was examined. It was concluded, that there is no correlation between the two latter variables.

This research implies that although LiDAR is capable of monitoring the morphological evolution of the swash zone in the period of 30min, the device's error is too large to deterministically analyse the bed level changes at the inter-swash scale. This occurs, because at the inter-swash scale, most of the changes that occur are below the LiDAR error margin (<~5mm).

Table of Contents

LIST OF FIGURES

LIST OF TABLES

1. INTRODUCTION

The swash zone can be defined as an interface between the land and ocean (or sea) that is alternately covered by uprush (onshore-directed water movement) and exposed by backwash (offshore-directed water movement). This is illustrated in Figure 1-1. The swash event at a certain point on the beach slope as a function of water depth is shown in Figure 1-2. To be precise, the swash events are defined by a period of water depths greater than zero and are separated by periods of zero water depths. If the water level stays above the defined threshold (the bed is immersed on the beach slope), the same swash event is continuing. However, when the beach emerges, the swash event ends. Inter-swash scale or swash event scale is the time scale that refers to the time interval between consecutive swash events (Hughes & Moseley, 2007).

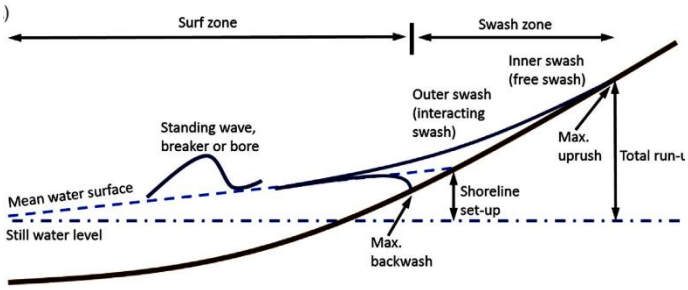

Figure 1-1: The swash zone (Hughes & Baldock, 2020)

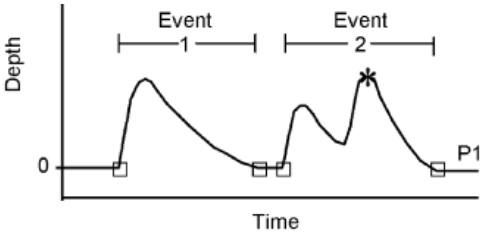

Figure 1-2: The swash event (Hughes & Moseley, 2007)

Brocchini & Baldock (2008) presented a description of recent and ongoing research in the field of swash zone dynamics. Authors suggested that there is a need to improve the sediment transport and morphological models predicting the beach face evolution over longer durations of time (minutes and hours). However, before the latter can be achieved, field and experimental studies with spatially dense data are needed to make a robust description of bed level changes at the single and multiple swash scales. Blenkinsopp et al., (2011) managed to quantify cross-shore sediment fluxes for thousands of swash events during a variety of wave/tide conditions while at the same time describing the spatial and temporal distribution of cross-shore sediment fluxes. However, to achieve this, the authors had to make use of a relatively large network of sensors (89 in total). Following the methodology by Blenkinsopp et al. (2011) Puleo et al. (2014) studied inner surf and swash-zone bed level change during periods of inundation throughout a tidal cycle. Nevertheless, the authors mentioned that networks of sensors are limited to measurements only at a predetermined location. So, if, for example, large-scale bed level changes occurred next to the location of the sensor, the bed level change would not be accurately captured. Another issue with the sensors was that sometimes the sensors get buried by the moving sediment. As a result, incomplete data sets are obtained and this limits the analysis of the results.

To replace the networks of sensors to quantify the bed dynamics a LiDAR (light detection and ranging) could be used. LiDAR is an optical remote sensing technology that makes use of laser beams to provide detect the distance between LiDAR and an object or surface. The application of LiDAR technology in coastal engineering has become progressively more popular during the last two decades. LiDAR has gained popularity for several reasons. Firstly, its ability to replace the system of point measurement devices for bed and water levels with just one apparatus to obtain full profiles of bed and water levels (Blenkinsopp et al., 2012). Secondly, the instrument makes measurements while not interfering with hydrodynamic or morphodynamic processes and therefore minimizing measurement errors (Harry et al. 2018). Thirdly, LiDAR can make measurements at the temporal and spatial scales that are beyond the capability of other common in situ instruments (Martins, Blenkinsopp, & Zang, 2016). Besides, there have been several scientific articles on LiDAR application in coastal environments

across various temporal and spatial scales. Furthermore, several studies show the successful application of LiDAR in making profile measurements. In spatial scales up to several hundreds of meters, Kotilainen & Kaskela (2016) proved that LiDAR is capable of imaging bathymetry at a higher resolution than the acoustic survey method. On a scale of up to a few meters, Blenkinsopp et al. (2012) found that LiDAR devices can measure free water surface measurements at a much higher resolution than conventual laboratory instrumentation such as wave probes. On a scale up to tens of centimetres, Stringari & Power (2021) successfully measured the daily changes in the beach profile elevation with LiDAR.

The knowledge gap associated with the swash zone is uncertainty if the LiDAR's could be applied to monitor bed level changes at inter-swash scale where a spatial resolution is millimetres and a temporal resolution is seconds. In particular, there is no information available what is the quality of the data or the actual error made the device measuring the swash zone.

1.1 RESEARCH OBJECTIVE & QUESTIONS

The objective of this research is to make use of available raw LiDAR data gathered in controlled flume experiments and examine if it is possible to quantify the inter-swash morphodynamical contribution of individual swash events to the longer-term, event-averaged morphological evolution on the sandy beach. To achieve this research objective, the following main research questions and research sub-questions are defined:

1) **How accurate is the LiDAR data?**
   a) How well does LiDAR capture objects (reference boxes) on the beach slope?
   b) How large is the difference between the bed levels measured by the mechanical bed profiler and LiDAR?

2) **How to identify swash events in the LiDAR data?**
   a) How can bed level and water surface be distinguished in the LiDAR data?
   b) How can consecutive swash events be identified in the water level profile?

3) **What is the contribution of individual swash events or groups of swash events to the total net morphological change of the beach?**
   a) How do bed levels change over individual swash events or groups of swash events?
   b) What is the smallest time scale at which bed level changes (greater than the instrument uncertainty) can be measured?
   c) What is the distribution of the magnitude of measured erosive and/or accretive events or groups of events in a 30-minute observation period?

1.2 SCOPE

There are several limiting aspects to the research. The limiting aspects originate from the experimental setup and time dedicated to research.

The research focus will be the swash zone. The swash zone will be characterized by a slope of 1:15 consisting of sand. The dynamics in the surf zone and interactions between the surf and swash zone will remain out of the scope of the research. The research will be limited to the examination of only one wave condition's influence on the beach slope's morphology. The duration of this one wave condition will be roughly 30 minutes. Bed level changes in the swash zone will focus only on changes in the cross-shore direction. This means that cross-shore sediment transport, long-shore bed level changes and long-shore sediment transport will remain out of the scope of this research. Study of variables that influence the bed level changes, e.g., bed shear stress, will also remain out of scope.

1.3 OUTLINE OF THE REPORT

In Figure 1-3 the conceptual model of the research outline is presented. First, theoretical research is provided. Here, additional information about the swash zone dynamics and the LiDAR device is described. Next, is the research methodology where details regarding applied methods used to study bed level changes at the inter-swash scale with LiDAR are detailed. After that comes the validation of the LiDAR observations. For each of the 2D axes, the x (cross-shore)- and y(height)- axis respectively, the accuracy of the LiDAR was determined. Following the validation, the data smoothing of the elevation matrix and variance is described. Next, the bed level was separated from the water level within the LiDAR data. The water level was separated from the bed level using three different methods, namely, varying variance, decreased variance and RSSI. Once the observations of water level and bed level are separated, the bed level changes were calculated. The bed level changes between consecutive LiDAR observations were then quantified at the inter-swash scale and full observation period.

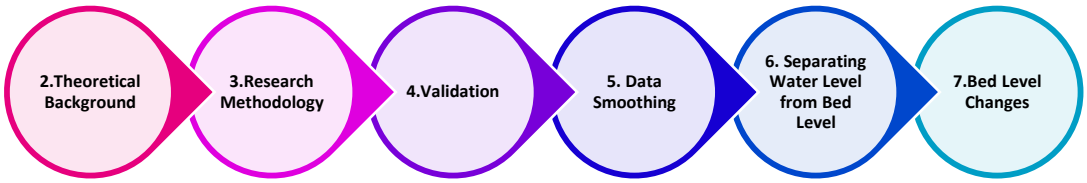

Figure 1-3: Conceptual Model of the Research

2. THEORETICAL BACKGROUND

2.1 SWASH ZONE

Usually, when the swash zone is addressed in detail, it is subdivided into two sections, the inner and outer swash zone (Figure 1-1), or sometimes three sections: upper, mid, and lower swash zone (Hughes & Moseley, 2007; Blenkinsopp et al., 2011; Zanden, et al., 2019). The outer (lower) swash zone is where the waves and swashes are interacting with each other. The inner (upper) swash zone is free from wave-swash interactions. The mid-swash zone is where wave-swash interactions occur part of the time.

The swash zone is referred to as the most energetic region of beach sediment transport. The swash zone in general is characterized by high turbulence levels, unsteady flows, and rapid bed level changes. Ultimately, processes occurring in the swash zone determine beach slope evolution. In other words, swash processes determine whether the beach will be accreting or eroding.

As mentioned in the introduction, swash motions consist of two parts, uprush, and backwash. The uprush is characterized by the dominance of onshore-directed turbulent flows. During the uprush, the flow is decelerating leading to the thinning of the water column. During the backwash, the offshore-directed flow starts to accelerate due to gravity force and beach profile inclination. The initial stages of backwash and late stages of backwash are characterized by supercritical flows, whilst subcritical flows prevail during the mid-stages. Besides, it is essential to recognize that backwash in the different swash zones may start at various times. At the lower swash zone, the backwash may start even before the uprush has reached its maximum height. Therefore, it is found that the duration of the uprush is generally shorter than the backwash. The peak uprush velocities are either higher or comparable to the peak backwash velocities. However, the backwash water depths are shallower compared to the uprush water depths (Masselink & Puleo, 2006; Chardón-Maldonado et al., 2015; Bergsma, et al., 2019). The turbulence in the swash zone is generated by waves arriving and collapsing at the shoreline. In particular, turbulence can be subdivided into two smaller categories, namely bed-related and bore-related turbulence. The bed-related turbulence is present during both the upwash and backwash stages, however, bore-related turbulence occurs only during the uprush phase (Puleo et al., 2000; Aagaard & Hughes, 2006; Zhang & Liu, 2008; Sou et al., 2010).

The pressure gradient describes the direction and rate of pressure change along with the chosen location on the slope. It is one of three components that characterize fluid momentum. Kranenburg et al. (2012) estimated that pressure gradient may be responsible for 1/3 of the total bed shear stress and therefore it has a significant influence on sediment transport. Baldock & Hughes (2006) and Pedrozo-Acuña et al. (2011) found that the pressure gradient in the swash zone has a maximum negative horizontal value just before the bore collapse. During the rest of the swash cycle, the leading edge maintains the positive pressure gradient which is nearly horizontal. Besides, the pressure gradient hinders the onshore flow, while it aids the offshore flow.

Wave-swash interactions occur when the wave arrives at the shoreline, and it interacts with either the preceding wave travelling to the shoreline or either backwash induced by the preceding wave breaking on the shoreline. In Figure 2-1 three types of interactions are defined in the swash zone: swash overtakes (wave-uprush interaction) and weak or strong wave-backwash interaction (Caceres & Alsina, 2012). Swash overtake – during the uprush phase, the following wave breaks on the beach and amplifies the existing uprush. Wave-backwash interaction – the backwash phase is ended by the incoming wave which breaks and starts the uprush (Hughes & Moseley, 2007). This interaction can be weak and strong wave-backwash interaction (Figure 2-1). Weak wave-backwash is described as the event in which the backwash from the previous wave is relativity weaker than the uprush from the incoming wave. As a result, the net onshore flow occurs (Caceres & Alsina, 2012). However, in the case

of a strong wave-backwash, the backwash flow of the previous wave is relatively stronger than the uprush from the incoming wave. As a result, there is net offshore flow occurs (Caceres & Alsina, 2012).

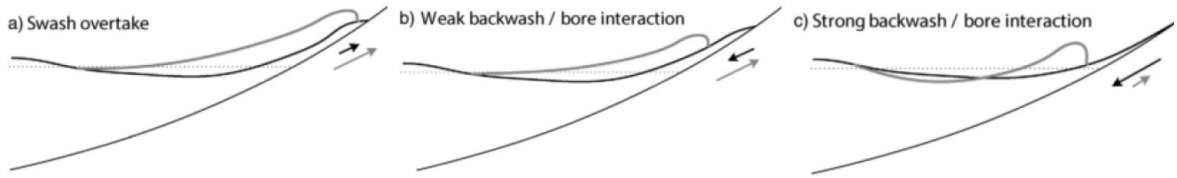

Figure 2-1: Wave-swash interaction (Caceres & Alsina, 2012). The dotted line is the still water line, the foreshore is represented by the thin black line, the initial swash event is the thick black line, and the grey line is the following bore motion

Austin et al., (2009) by studying the onshore sediment transport on sandy beaches found that wave asymmetry and skewness is a relevant factor for sediment transport in a swash zone. Although, the wave asymmetry and wave skewness have no direct influence on the sediment transport in the swash zone, the wave asymmetry and wave skewness influence the run-up limit and velocities of the swash events, as a result, influencing the sediment transport. The sinusoidal, skewed and asymmetric waves are shown in Figure 2-2. The sinusoidal wave is symmetric at both the crest and trough. The skewed wave has a sharp triangle-like crest and parabolic-like trough while the asymmetric wave's onshore part is steeper than the offshore part. Grasso et al., (2011) found that relatively small wave asymmetry in a combination with a relatively strong wave skewness induces offshore sediment transport. However, relatively large wave skewness with a relatively strong skewness results in onshore-directed sediment transport.

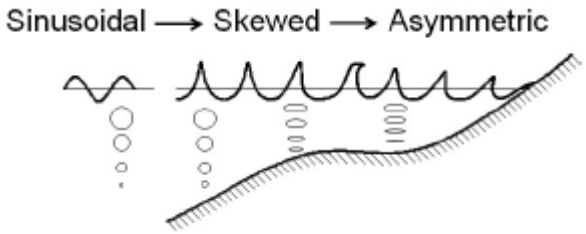

Figure 2-2: Nonlinearities of wave propagating (Rocha, 2014)

In general, in the swash zone, the sediments are transported as sheet flow and suspended load. If during the swash cycle the sediment transport onshore exceeds the sediment transport offshore, the net sediment flux is onshore directed and therefore the beach is accreting. If it is vice versa, the net sediment flux is negative and therefore the beach is eroding (Pritchard & Hogg, 2005; Masselink & Puleo, 2006; Bergsma, et al., 2019; Hughes & Baldock, 2020). Masselink & Hughes (1998) found that the largest sediment loads and largest transport rates occur in either the lower or mid-swash zone. This occurs because most of the wave energy is dissipated in the previously mentioned region.

When the onshore and offshore sediment transport rates are almost equal, it is referred to as an equilibrium state (Hardisty, 1986). When the beach face is flatter than the equilibrium stage, the uprush will transport more sediment onshore than the backwash offshore. As a result, there will be net onshore sediment transport. So, the beach face will become steeper and steeper. However, if the beach face is too steep, then onshore sediment transport will be relatively smaller than offshore sediment transport and therefore flatting the beach gradient. This phenomenon occurs due to the relationship between the sediment transport capacity and the beach slope gradient. For example, the steeper the beach, the larger energy is required to transport the sediment onshore (Masselink & Puleo, 2006). Also, the beach gradient influences the period of the swash motion. The steeper the gradient

the shorter the swash motion will be (Komar, 1998). This is also shown in equation 2-1 which is derived by Baldock & Holmes (1999), where T_s is the natural period of swash, U_0 is initial water velocity, g is the gravitational acceleration and β is the beach slope.

$$T_s = \frac{2U_0}{g*sin\beta} \qquad 2\text{-}1$$

Also, it is essential to recognize that beach gradient especially at the bottom of the swash zone influences the wave breaking pattern and therefore the amount of turbulence and sediment transport fluxes. While plunging and collapsing waves are regarded as onshore sediment transport promoters, the spilling and surging waves will have more limited onshore transport capacity (Masselink & Puleo, 2006) & (Chardón-Maldonado, Pintado-Patiño, & Puleo, 2015).

As mentioned above, in the swash, zone sediments are transported via two modes, namely, as suspended sediment and as a sheet flow. The thickness of sheet flow may extend over several centimetres above the beach bed; however, the suspended sediment is spread across the water column. During the swash motion, the maximum total sediment transport fluxes occur at the uprush initiation phase. This occurs due to relatively high turbulence and bed shear levels during the early uprush stages. Here, bedload flux exceeds the suspended sediment flux (Puleo et al., 2015). At the point where uprush is reversed into backwash, the suspended and sheet flow concentrations are neglectable since, the particles have settled, and the decreasing flow velocity cannot entrain sediment particles. During the backwash, the concentration of suspended and sheet flow sediment transport rates increases. However, the sheet flow is more dominant than the suspended sediment transport mode. At the end of the backwash, the suspended sediment transport is not present anymore. It can be explained by flow deacceleration and thinning. Therefore, it is assumed that also at this point, bedload transport is the dominant transport mode (Chardón-Maldonado, Pintado-Patiño, & Puleo, 2015).

Blenkinsopp et al., (2011) quantified net cross-shore sediment fluxes for thousands of swash events during a variety of wave/tide conditions on a stretch of sandy beach located on the South-West Atlantic coast of France while at the same time describing the spatial and temporal distribution of cross-shore sediment fluxes. To achieve this, the authors had to make use of a network of sensors. In total 89 sensors were installed on a beach face. Besides the instruments themselves, also an additional relatively large (4m x 28m) scaffolding was necessary to attach the sensors. They addressed the influence of swash–swash interactions on the magnitude and direction of sediment transport, and spatial and temporal distribution of cross-shore sediment fluxes. It was found that, in general, the swash-by-swash bed-level changes in the mid to lower swash zone are normally distributed, meaning that there are approximately equal amounts of erosive and accretive events. Most of the time (approximately 90%), the bed level changes were smaller than ±10mm and 60% of the time the bed level changes were smaller than ±2mm (Figure 2-3). Interestingly, irregular single-event bed level changes were observed' magnitudes were similar (in order of tens of millimetres) to the net morphological change at a point on the beach face over a complete tidal cycle. Additionally, it was found that the largest sediment fluxes were observed at the seaward location of the beach slope, while relatively smaller sediment fluxes occurred at the upper part of the beach slope. However, direct quantification of this fact may be complicated to resolve, since for each specific tide and wave condition the position of the swash zone varies. Nevertheless, the phenomenon of relatively larger sediment fluxes occurring in the mid to lower part of the swash zone could be explained by the greater dominance of wave-swash interactions compared to the upper part of the swash zone. Another explanation for the relatively larger sediment occurring in the mid to lower swash zone could be explained by findings by Zanden, et al., (2019) who studied sand transport processes and bed level changes induced by two alternating laboratory swash events. It was found that relatively larger mean flow depths were observed in the mid to lower part of the swash zone, resulting in a larger sediment

transport capacity. However, the definitive underlying forcing mechanisms that cause these large-scale accretive or erosive events were not described and remain unknown.

Masselink et al., (2009) studied the net sediment transport and morphological change in the swash zone. Masselink et al., (2009) concluded that the beach face over time does not erode or accrete rapidly (over a 10 min period) due to frequent reversals of relatively larger sediment fluxes that balance the beach's sand volume.

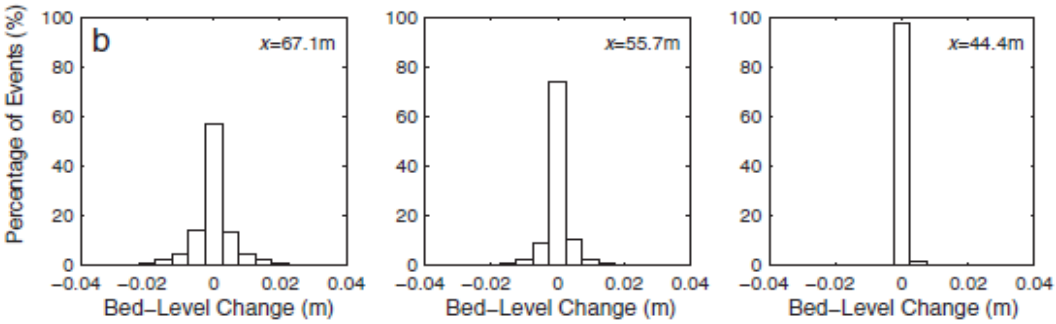

Figure 2-3: Percentage occurrence of bed-level changes at three different locations on the beach slope (Blenkinsopp et al., 2011). X=67.1 - lower swash zone, x=55.7 - mid swash zone & x=44.4 upper swash zone

Currently, there are available a variety of models that could be used to predict sediment transport in the swash zone, for example, the bed shear stress model formulation and run-up formulation by Larson et al., (2004). While the bed shear stress model includes the parameters such as bed shear stress, wave skewness and asymmetry and bed slope, the run-up model is only limited to the wave skewness and asymmetry and bed slope. None of the models above describes the influence of groundwater, bore turbulence, wave-swash interaction, pore pressure and response time. To account for the missing pore pressure, it is possible to modify the Shield parameters of the bed shear stress model according to Nielsen et al., (2001) or Francalanci et al., (2008). The shield parameter is a method to determine the initiation of the motion and transported volume of sediment caused by water flow (Shields, 1936). Nielsen et al., (2001) suggest incorporating the effective sediment weight and ventilated boundary layer according to the description provided by Conely and Inman (1994). However, Francalanci et al., (2008) proposed to include the effective sediment weight forced by the seepage in the Shields parameter. One of the more complete sediment transport models known is the Van Thiel – Van Rijn model (Van Thield De Vries, 2009). The model separates the suspended and bed load while taking into account factors such as depth-averaged flow velocity, sediment and water densities, incident wave motion, near-bed turbulence, diffusion coefficient, etc. Although there are varying methods with different complexities in how to calculate sediment transport, there are still more processes occurring in the swash zone than researches have been capable of incorporating into models. The selection of the required model for the study is still largely limited to the subject of interest, time constrain and computational power. Potential advancements may result from fully (or weakly) connected techniques, but these haven't been put to the test in greater time- and/or realistic-scaled environments. Besides, not many depth-resolving models have emphasized predicting sediment transport and their influence might only be on short time horizons which are equal to the swash events (Chardón-Maldonado et al., 2015).

2.2 LIDAR

LiDAR (light detection and ranging) is an optical remote sensing technology that makes use of laser beams to provide a representation of the surveyed environment. The LiDAR device emits infrared beams that are deflected on an internal mirror that is rotating over a predetermined degree field of view, for example, 190° for 2D LiDAR. After the beam is deflected on an internal mirror, it is then transmitted into the environment. Once the beam reaches the target, it is partially reflected back to the device. Then the time of travel between the incident and reflected beams is used to calculate the distance between the device and the object in the environment (Blenkinsopp et al., 2012; Almeida et al., 2020; Stringari & Power, 2021). The LiDAR operation principles are illustrated in Figure 2-4.

As for the challenges associated with LiDAR, Harry et al. (2018) mention a variety of factors that can have a significant effect on data quality. First, the capability of the measured surface to reflect the infrared beams plays an essential role. If the surface reflectivity is not maintained according to the specified manufacturer regulations, the scatter of measurement will increase. For example, SICK AG specifies that for LiDAR devices LMS511 surface reflectivity must be at least 2% for the device to detect an object in the environment. However, the maximum range of the device could only be attained if the surface reflectivity is at least 10% (SICK, 2022). Second, a minor effect could be assigned to the angle of incidence. It must be noted that the signal is always stronger just beneath the device, where the surface is positioned more perpendicular to the device than at the high angles of incidence. As a result, the elongation of the beam pulse in a combination with reduced beam reflection by the surface may cause erroneous measurements. Third, especially when LiDAR is applied in the field setting, one must be aware that environmental conditions may cause inconsistencies in the measurements. For example, raindrops and sea spray may alter the emitted and reflected beam. However, the latter is of minor concern in this study since the data used were collected in a controlled laboratory environment.

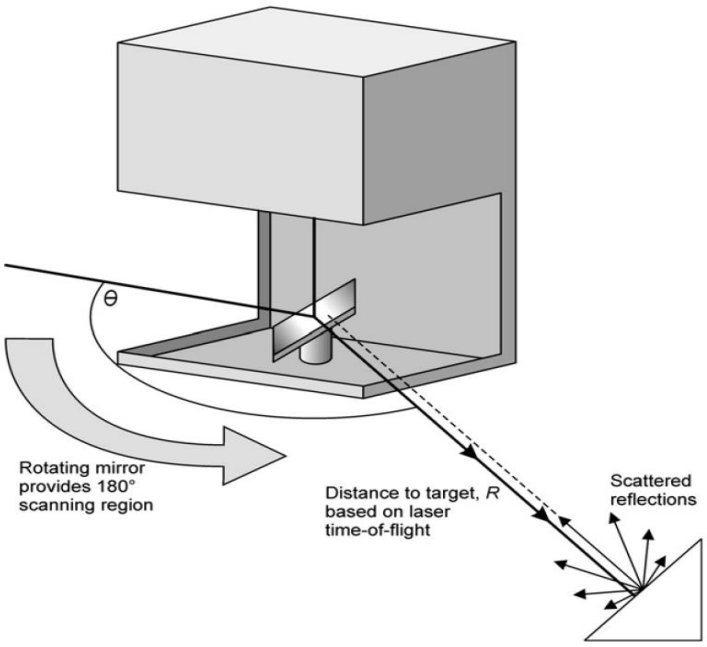

Figure 2-4: The LiDAR's working principle (Blenkinsopp, et al., 2012)

Blenkinsopp et al. (2012) studied time-varying free water surface profiles with LiDAR. An essential characteristic of LiDAR measurements noted in this study was the LiDAR's tendency to systematically underestimate the free water surface elevation at points upstream of the instrument location. However, downstream of the instrument location, the measurements were systematically

overestimated. This could be explained by three main reasons. First, as the wave propagates in the flume the angle of incidence between the LiDAR beam and the water surface is constantly changing. Second, the emitted beam diameter of the point measurement is increasing linearly as the measurement distance increases. Third, the instrument measurements are based on a linear interpolation between the two closest adjacent measurement points, which move with varying free-surface elevation. Almeida et al. (2020) mentioned that LiDAR data in raw format does not provide a direct distinction between topography and the water surface. However, topography can be separated from the water surface by applying a moving-average time window variance filter to the measurements. To extract bed level changes from topography measurements, the difference between two consecutive cross-shore beach profiles must be determined.

3. RESEARCH METHODOLOGY

3.1 DATA COLLECTION

The data was collected in wave flume experiments at the Universitat Politècnica de Catalunya (UPC, Barcelona, Spain). Figure 3-1 shows the general setup in the flume. The flume was 100m long, 4.50m deep and 3m wide. The still water level was at 2.47m high, measured from the bottom of the flume, and it extended up to the longitudinal distance mark of 77.44 m. The slope of the beach was 1:15. The beach profile consisted of sand with d50=0.25mm. Besides, on the beach profile, two dividers were added to reduce the cross-flume flows and bed asymmetries in the swash zone. The dividers were positioned in a manner that splits the flume into 3 parts with a dimension of 0.9m, 1.2m and 0.9m in width. The narrower sections were positioned on the sides, while the wider section was in the middle. The dividers with a thickness of 3mm, a height of 0.70m and a length of 3m were buried approximately 0.40m deep into the initial bed. The LiDAR was mounted on the side of the flume. It was positioned at 4.76m above the beach slope at a longitudinal distance mark of 77.891 m (Figure 3-6) which is 0.451m onshore in relation to the still water line. While the LiDAR measured the bed roughly 70cm from the side of the flume, the bed profiler made the measurements of the beach slope in the middle of the flume. The cross-section and longitudinal section of the flume are shown in Figure 3-2.

The 2D LMS511 LiDAR manufactured by the company SICK AG is used in this flume experiment. The LiDAR measured at a frequency of 25 Hz with an angular resolution of 0.1667 degrees. The LiDAR's systematic and statistical error is shown in Table 3-1. Systematic error refers to the inaccuracy that is inherent in the system while statistical error refers to the difference between the obtained value and the true value. As the measurement distance from the LiDAR to the object in the environment increases, both systematic and statistical errors increase. Figure 3-3 shows how the LiDAR's beam diameter changes over distance. As the distance to the object increases, the beam diameter also increases. Furthermore, as the beam diameter increases, the measured surface of the device increases. Therefore, it is important to note, that if the object at the measured distance is smaller than the beam itself, the object cannot be measured properly due to inaccurate energy reflection from the object. It is also essential to note that LiDAR also has the capability of generating a received signal strength indicator (RSSI) for measurements. RSSI is a measurement of power received by the sensor, relative to the power of the signal emitted, and it is an arbitrary unit with a logarithmic characteristic. The RSSI values range from 0 to 255 where the 0 value represents the situation when the power of the received signal was too low to generate a valid RSSI value, 1 is the weakest valid signal strength possible, 254 is the strongest valid signal possible, and 255 represents the situation when the LiDAR device was "dazzled" or the power of received signal was too high. The RSSI values are dependent on two factors, namely, distance to the object and the object's ability to reflect the light of in this case the incoming laser beam. The manufacturer (SICK AG, 2017) has provided different approximate curves for the RSSI ranges depending on objects' remission or ability to reflect light (Figure 3-4)

Figure 3-1: Flume Set-up

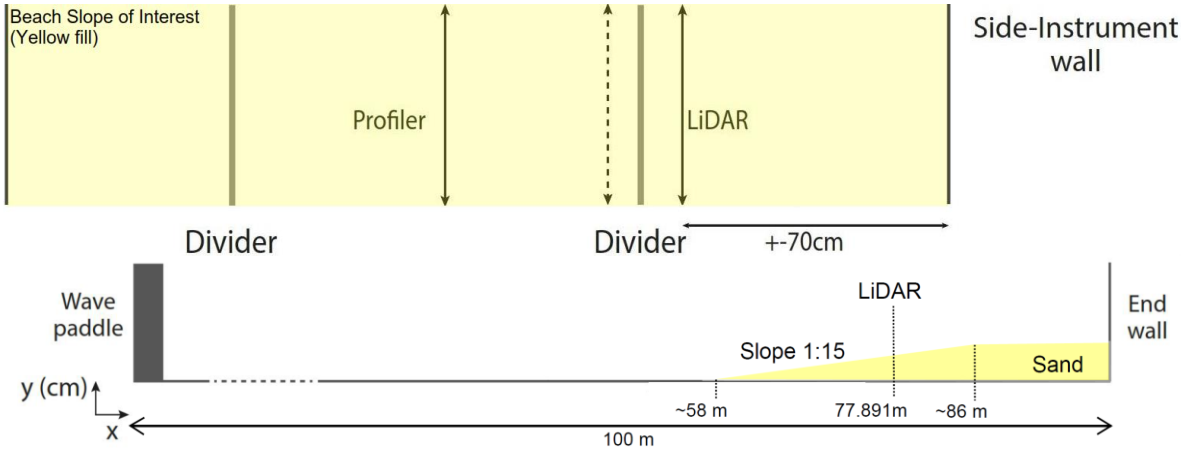

Figure 3-2: Cross-Section (upper image) and Longitudinal Section (lower image) of the Flume

Table 3-1: LiDAR's LMS511 total error along both axis (x and y) simultaneously (SICK AG, 2017)

	Distance Range [m]	Error [mm]
Systematic Error	1-10	± 25
	10-20	± 35
	20-30	± 50
Statistical Error	1-10	± 6
	10-20	± 8
	20-30	± 14

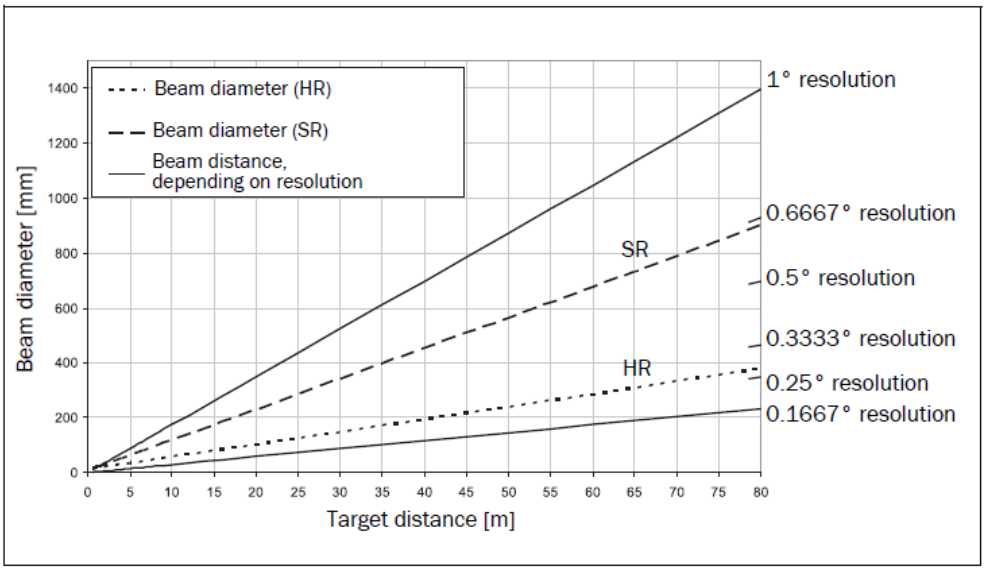

Figure 3-3: LiDAR's beam diameter (SICK AG, 2017)

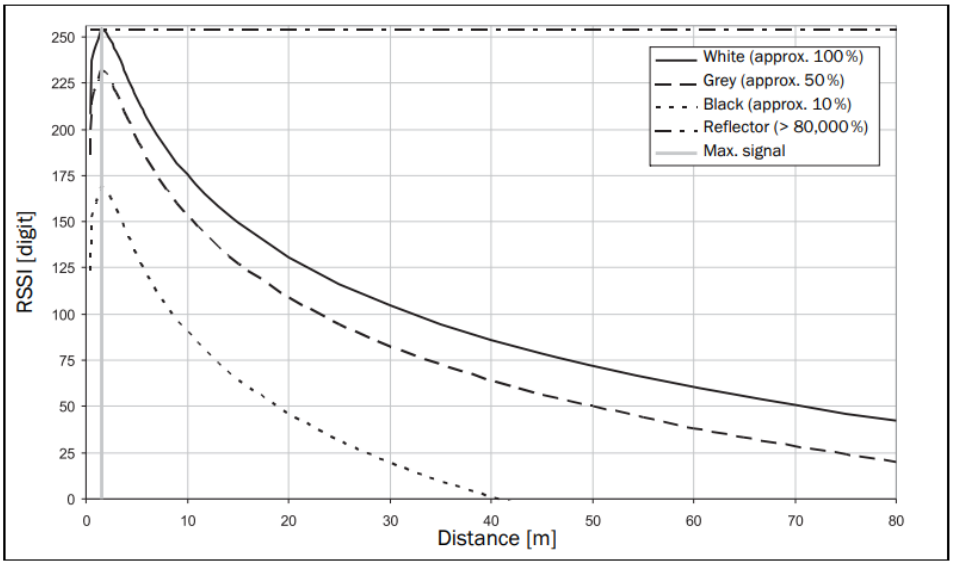

Figure 3-4: Typical RSSI values based on range and object's remission (SICK AG, 2017)

3.1.1 Experimental Setup for Static Validation

During the validation runs, no water was present in the flume. In total three measurement runs were made with the LiDAR. For each run, a reference box (RefP1, RefP2 & RefP3) with a size of ~50x50mm was placed on the slope at different longitudinal locations. Once the box was placed on the slope, the x-coordinates of the reference box bottom edge closest to the LiDAR (the representative edge for each of the box is illustrated in Figure 3-5) was measured manually with a sinker (counter-weight), string, and ruler on the side of the flume. The estimated error for such a measurement is ±10-30mm. The RefP1's representative edge was measured to be at the 71.96m mark, RefP2's at 75.17 and RefP3's at 80.5m (Figure 3-5). The LiDAR measurement runs for each reference box lasted for a couple of minutes. The y-coordinates of the reference boxes representative edge in the wave flume were not measured directly, therefore, are neglected in further research. In addition, the beach slope was also measured with the mechanical bed profiler. The device's measurement error is ±20mm along the x-axis and ±10mm along the y-axis (Dionísio Antónioa, et al., 2021). The mechanical bed profile only measured the beach profile up until the 82.609m longitudinal mark while LiDAR up until the 86.01m mark. The above-described setup is illustrated in Figure 3-5.

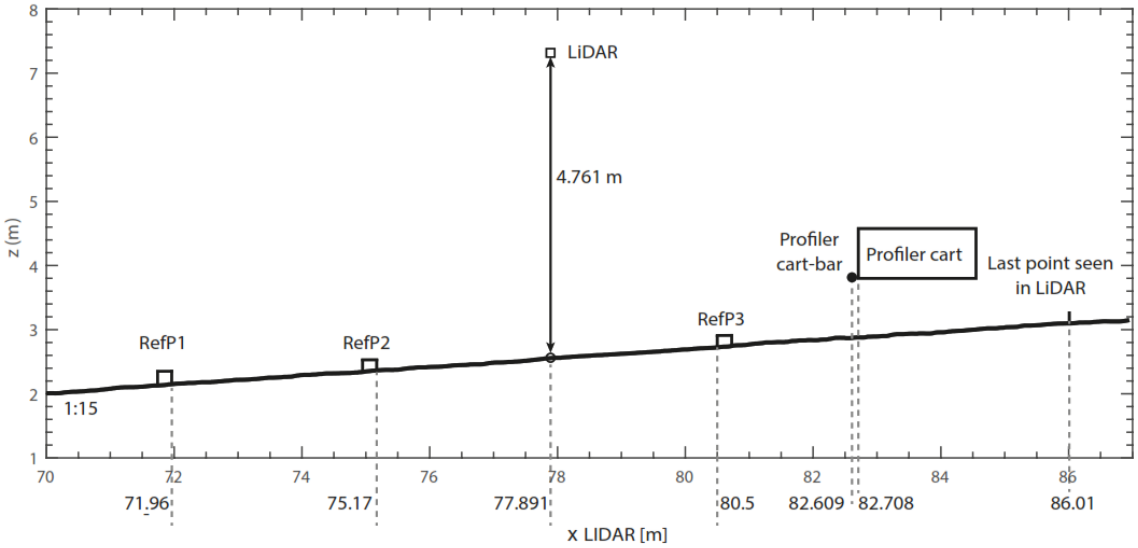

Figure 3-5: Static Validation Set-Up

3.1.2 Experimental Setup for Bed Dynamics

As for the experimental set-up for bed dynamics in the swash zone, the flume was filled up with water to reach the previously described water height mark and the beach was then exposed to a wave sequence with different wave heights and wave periods. All the irregular JONSWAP wave conditions with their relevant parameters are summarized in table 1.

Table 3-2: Wave conditions that were simulated in the flume experiments at the Universitat Politècnica de Catalunya.

Wave Condition		Significant Wave Height [m]	Wave Peak Period [s]	Time [min]	JONSWAP spectrum [-]
B	Benchmark	0.42	4.00	15	3.33
E1	High Energy 1	0.45	3.50	180	3.33
A1	Low Energy 1	0.25	5.20	600	1.33
E2	High Energy 2	0.55	3.50	180	3.33
E3	High Energy 3	0.65	3.50	180	3.33

Due to time constraints, not all wave conditions were feasible to explore. Therefore, it was decided to focus on the first 30 minutes of wave condition E2. This was done because already Dionísio António et al. (2021) determined that during this period the bed level changes are greatest. As a result, the error in the bed level measurements made by the LiDAR device becomes smaller relative to the (larger) morphological changes.

In the runs with the morphological evolution also the horizontal position of the maximum run-up, maximum run-down and average run-up were obtained by visual observation. Later, these values were confirmed by video recordings. The maximum run-up on the beach reached 83.21m, the maximum run-down to 76.01m and the average run-up to 79.3m (Figure 3-6). The error for the maximum run-up is ±5cm since the value was obtained by identifying the highest slope part with the wet sand after the wave exposure period. However, the error for the average run-up and maximum run-down is not known since the values were generally approximated based on visual observations.

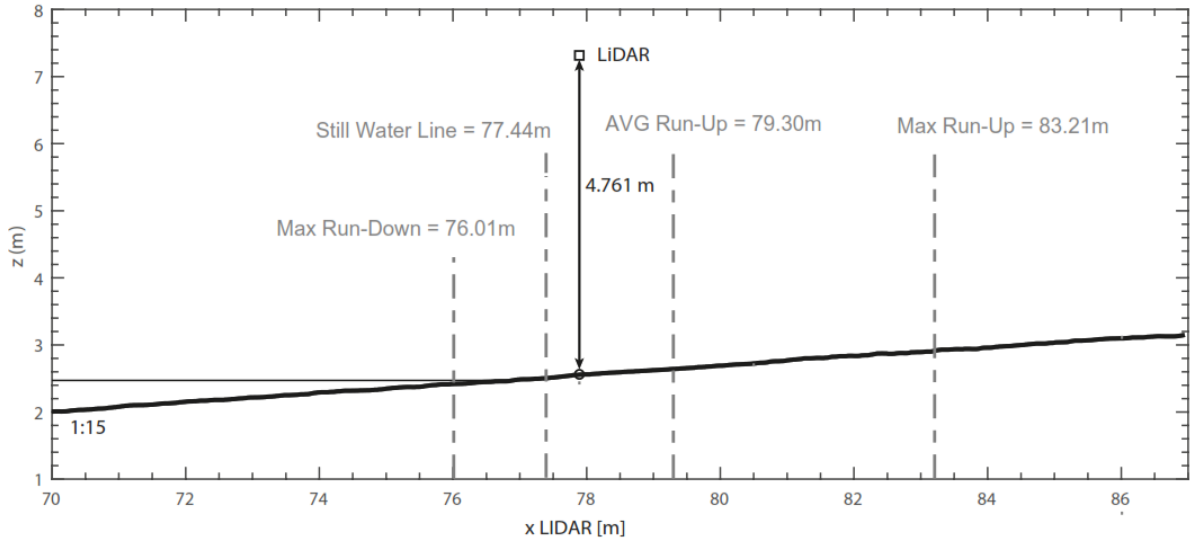

Figure 3-6: Validation Set-Up for Bed Dynamics

3.2 VALIDATION OF LIDAR ACCURACY

Although without data manipulation or in raw format LiDAR measurements only provide laser beam distances between the LiDAR and the object, by making use of cosine and sine functions the distance measurements can be separated into measurements along the x- and y-axis. As mentioned in Section 3.1.1 the accuracy of the LiDAR was measured along the x- and y-axis. The validation setup for each of the axes was different: to validate accuracy along the x-axis the reference boxes were used

while to validate LiDAR accuracy along the y-axis the slope profiler was used.

To validate the LiDAR accuracy along the x-axis, the following steps were implemented:

1. All the measurement points were time-averaged over the whole measurement period (~4000 measurements or ~2.6min) to get the mean profile for the respective validation run. The mean profile was calculated using equation 3-1, where *A* is a vector or a particular point measurement in time, and *N* is the number of scalar observations (~4000).

$$\mu = \frac{1}{N}\sum_{i=1}^{N} A_i \qquad 3\text{-}1$$

2. The standard deviation was calculated for every measurement point in space using equation 3-2.

$$S = \sqrt{\frac{1}{N-1}\sum_{i=1}^{N}|A_i - \mu|^2} \qquad 3\text{-}2$$

3. In the mean LiDAR profile, the point closest to the bottom edge of the box facing the LiDAR was assumed to be a representative point. The closest point was derived by qualitatively looking at the mean LiDAR profile.
4. The mean and standard deviation of the x-position of these measurement points were read.
5. It was checked whether the LiDAR's measured location of the bottom edge of the reference box is within allowed error boundaries compared to the location of the bottom edge of the reference box measured with the sinker, string and ruler.

To validate the LiDAR accuracy along the y-axis, the following steps were implemented:

1. For each validation run with reference boxes, the measurement points representing the box and in the near vicinity of the box were deleted to get rid of the measurement points which are not representative of the bed slope.
2. The three validation runs were compiled and then time-averaged to obtain a final mean profile.
3. The bed levels measured by the profiler were compared to the bed levels measured by the LiDAR. Here, the differences along the y-axis were examined. In particular, if the difference between the measured slopes does not exceed the total error of both devices.

3.3 DATA SMOOTHING

Data smoothing was applied to distance measurements (x-axis), elevation measurements (y-axis) and derived variance. For the distance and elevation measurements, the data smoothing was applied by making use of temporal smoothing with a moving window. As for the variance, it was smoothed spatially up until the point to only retain the general variance function by removing the noise from the data.

The LiDAR measurement runs for a period of about 30-minutes (~500 cross-shore points representing the slope spatially and ~50'000 temporal measurements) are saved in a matrix form. The distance and elevation measurements are saved in separate matrixes. For each of the matrices, rows represent a particular measuring point along the cross-shore beach profile, while columns represent measurements of the elevation of a point in time. To apply the temporal smoothing, a set of particular measurement points were averaged row-wise over a pre-determined window width. To smooth the distance and elevation measurements the choice in favour of the mean was made. The choice could be explained by the fact that the LiDAR measurements are disturbed symmetrically and rarely for the same measurement point there are clear outliers. The general equation of the moving-mean function is presented in the equation, where *p* is a data point, and *k* is the entries of the data-set containing *n* entries. The application equation 3-3 resulted in the matrix with the same dimensions as the raw

matrix. Besides, the visual presentation of column-wise moving mean smoothing is shown in Figure 3-7, where *A* is an original matrix, *B* is smoothed matrix, but arrows show the direction of smoothing. In general, the smoothing window for the distance and elevation measurements is limited to a window of 25 measurements or 1s. The moving window limit is derived from the fact that under present conditions there are several swash events with a duration is ~1s. Since the research goal is to investigate the bed level changes at the inter-swash scale, the larger moving windows are out of consideration since then the results would refer to multiple swash-scale, as a result deviating from the research goal.

$$MM = \frac{1}{k}\sum_{i=n-k+2}^{n+1} p_i \qquad 3\text{-}3$$

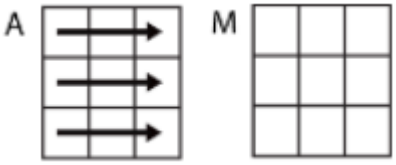

Figure 3-7: Visualization of row-wise smoothing

To calculate and smooth the variance of the static bed, the following steps were implemented:

1. In the first (REFP1) and second (REFP2) run with reference boxes, the measurement points representing the box and in the near vicinity of the box were deleted to get rid of the measurement points which are not representative of the bed slope. The third (REFP3) run was neglected in variance calculation because it had a quantitatively different bed profile compared to the first two runs. Besides, the vertical variance from the runs with water in the flume could not be derived since there was no reference between when the bed was exposed and when it was submerged.
2. The data from the first two runs were compiled in one matrix. This was done to obtain a larger data sample for the variance calculation thus decreasing the variability of the sampling distribution. In the end, the total sample size had ~8000 measurements.
3. The variance was then calculated for each of the cross-shore points using the equation 3-4

$$\sigma^2 = \frac{1}{N-1}\sum_{i=1}^{N}|A_i - \mu|^2 \qquad 3\text{-}4$$

4. The variance was smoothed spatially to obtain the general variance trend while neglecting the noise in the variance. The details regarding the smoothing can be found in Section 5.

3.4 SEPARATING WATER LEVELS FROM BED LEVEL

To separate measurements of the beach and the water surface, first, three different methods were applied to isolate water level from bed level: applying an observed variance filter, applying a decreased variance filter and applying a received signal strength index filter. Second, all the methods were compared with researchers' observation during the experiment and elevation change in time compared to the first beach profile measured.

To isolate the water level from the bed level, i.e., to indicate the water line, with both observed variance and decreased variance values, equation 3-5 was used, where *z* is the elevation measurement for each observation point, while σ^2 is variance (Almeida et al., 2014). The variance in the elevation matrix was calculated by applying equation 3-4 to the LiDAR elevation matrix in the time domain while making use of different moving variance windows about which more details will be provided in the latter sections. In general, equation 3-5 is based on the LiDAR observation principle, that for the bed level measurements the time-variance is smaller than for the measurements with a moving water

surface. Equation 3-5 states that, if the time-variance of the observed elevation at a particular measurement point is larger than the defined threshold (in this case either the observed variance or decreased variance), then the measurement point should be interpreted as water, however, if it is equal or smaller than it is supposed to be bed level. For the

$$z_{bed\ level} = \overline{z_{LiDAR\ (\Delta t)}}\ if\ \sigma^2\ (z_{LiDAR(\Delta t)}) \leq \sigma^2_{threshold} \qquad 3\text{-}5$$

To isolate the water level from the bed level based on the RSSI values the following steps were implemented:

1. First, the RSSI values of the beach profile with the static water level, intersecting with the beach at the 77.4m longitudinal flume distance mark, were extracted into a separate section. The sample size in this case was ~3000 measurements or ~2 minutes.
2. The time-average RSSI value of the sand bed based on the distance to LiDAR was calculated. This was achieved by averaging the extracted data set of raw data with a dry sand bed containing the distance to the slope's point and their respective RSSI value. The relation between RSSI and distance was made since RSSI values are dependent on distance to object as shown in Figure 3-4.
3. The quadratic function was fit to the average sand bed RSSI and distance to LiDAR measurements to obtain the theoretical function representing the distance and RSSI interdependency.
4. The theoretical dry bed measurement of RSSI values was made for the complete profile by utilizing the extrapolation principle from known values and the previously derived quadratic function of RSSI and distance. In particular, the unknown RSSI values for the submerged part of the beach profile were calculated by preserving the shape of the obtained function. This was necessary since during the measurement run the water level retreats further back than the 77.4m longitudinal mark in the flume. Consequently, the extrapolation of the theoretical value to the lower beach face is vital for the successful application of this method.
5. The theoretical RSSI threshold values were validated by comparison of the observed and computed water levels for multiple cases, e.g., at the start of the run and the end of the run, and with the relatively high run-up and relatively low run-down situations. In particular, it was checked how the derived theoretical RSSI beach profiles compare against the measured RSSI values.
6. Equation 3-6 was used to identify the point where the bed level end and the water level starts. Equation 3-6 states as soon as the measured RSSI value deviated from the theoretically derived value for sand by a predetermined threshold, the boundary between water level and bed level was set. The $RSSI_{thresholds}$ were arbitrarily chosen. The values of the thresholds will be presented in the latter sections. The principle of this equation is derived from equation 3-5.

$$z_{bed\ level} = \overline{z_{LiDAR\ (\Delta t)}}\ if\ |RSSI_{Observed} - RSSI_{theoretical}| \leq RSSI_{threshold} \qquad 3\text{-}6$$

Once all the above methods were implemented, the methods were compared with each other to find the best possible solution for tracking the water line in the flume over time. To select the method that tracks the water line the best, all the water lines were plotted over an image showing the relative elevation changes compared to the first bed. This was done by creating a time stack plot, where the first bed profile was subtracted from every measured beach profile in time. As a result, an image was obtained showing how the bed evolves in time compared to the first profile (e.g., Figure 5-1). Here the extracted water lines must follow the erosion and accretion patterns observed, e.g., if in the lower part of the beach profile significant erosion occurs, then it can be assumed that most of the waves are travelling over this area. Likewise, if the upper part of the beach profile experiences

accretion, there must be at least some swash events reaching the upper area of the beach to generate the observed accretion pattern. Also, the water line was compared to the researchers' visual observation values of the average run-up, maximum run-up and run-down mentioned in Section 3.1.2. The selected water line will then be used to demarcate the beach level in the LiDAR data for further analysis of bed level changes at the inter-swash scale.

3.5 BED LEVEL CHANGES

To calculate bed level changes at inter swash scale, multiple steps were taken. At first, a run-down threshold for the swash zone was established. Then, run-down events below the run-down limit were identified. Once the location and time of these run-downs were known, the representative bed profiles for these moments in time were selected. After that, the points and quantities of maximum accretion and maximum erosion for every consecutive profile were determined. Next, the total change in the area (i.e., beach volume) for the consecutive profiles was calculated. Finally, the results of bed level changes were compiled to make distribution plots, analysing the relative contributions of individual erosion/accretion events to the net morphological change of the beach in time.

To calculate the bed level changes in the swash zone at different time scales, a run-down threshold was introduced. It was done to avoid comparing the complete swash zone since then only one profile with a completely uncovered swash zone of the beach slope would be available. This would not allow comparing the beach profile in the lower area due to the presence of the water. As a result, an arbitrary threshold for the run-down threshold was introduced which was equal to the still water line in the flume at the beginning of the run.

To identify run-down events in the extracted water line, a few conditions were applied to the water line data set. First, the water line had to run-down lower than the introduced run-down threshold. Second, the duration between the peaks should be at least 1s to avoid defining the noise in the data as a run-down event.

After the location of maximum run-downs and the time at which they occur were known, the representative bed profiles were selected for further examination. Besides, the exposed bed profiles between swash events have different widths, therefore, the measurement at the run-down maximum was assumed to be representative. The bed profiles for consecutive run-down events were subtracted one from another. This was done to identify the points on the beach slope where maximum accretion and maximum erosion occur. In addition to maximum accretion and erosion values, also the static bed standard deviation at the points of maximum erosion and accretion was selected from the standard deviation profile derived in Section 3.2. This was done to check if observed accretive or erosive events exceed the previously determined standard deviation or, in other words, if the values of maximum erosion and accretion are significant. The maximum accretion and erosion values were also compared to the LiDAR error provided by the manufacturer.

To determine the minimum time scale at which bed level changes could be resolved, the consecutive measurements of the beach profile were examined. The shortest identified swash events were determined. Then, the values of beach accretion and erosion during these events were calculated. After that, it was checked whether there are points in which the maximum accretion or erosion exceeds the static bed standard deviation derived in Section 3.2. If the shortest possible swash event did not fulfil the condition mentioned in step three, the next shortest event was identified and steps 2 to 3 were repeated.

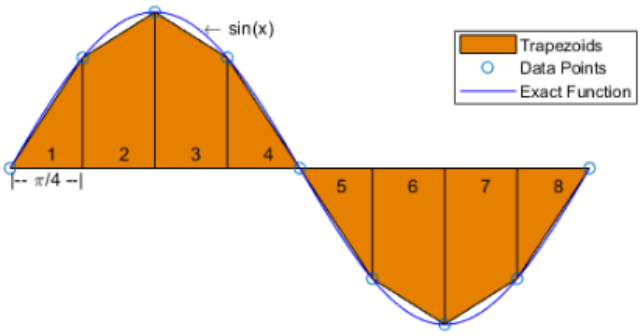

Figure 3-8: Visualization of the method of the trapezoid (The MathWorks, Inc., 2022)

To compare the consecutive profiles at the inter-swash scale, the method of trapezoids was used to derive the cumulative morphological change between beach profiles for consecutive run-down events. This approach was selected due to the limited horizontal resolution of LiDAR. Figure 3-8 shows how the method of the trapezoids discretizes the integration over an interval by dividing the area into trapezoids. The drawback of this method is that it under- or overestimates the total area depending on an integration profile. However, the benefit is that by breaking down the area in trapezoids, the areas could be calculated relatively fast and easy. Equation 4 represents a mathematical expression for the method of trapezoids for the points with unequal spacing between them, where $a=x_1<x_2<...$ $x_n<x_{n+1}=b$ and $x_{n+1}-x_n$ is the spacing between the points. The equation could be used to calculate the area for each of the selected profiles. Once the areas were calculated, the neighbouring values could be subtracted from each other to find the total difference between profiles expressed as the area.

$$\int_a^b f(x)dx \approx \frac{1}{2}\sum_{n=0}^{N}(x_{n+1}-x_n)[f(x_n)+f(x_{n+1})] \qquad 3\text{-}7$$

Once the areas were calculated at the inter-swash scale, the sum of the changes at inter swash scale was compared to the change between the first and the last profile to check whether both are comparable. After that, also the distribution of accretive/erosive events by size was made and morphological changes were also separated into smaller bins to see which of the events had the greatest impact on the beach development.

Last both not least, it was checked whether there is a correlation between the change of the swash zone and event time. This was achieved by calculating the Pearson correlation coefficient presented in equation 3-8 where here μ_A and σ_A are the mean and standard deviation of A, respectively, and μ_B and σ_B are the mean and standard deviation of B.

$$\rho(A,B) = \frac{1}{N-1}\sum_{i=1}^{N}\left(\frac{A_i-\mu_A}{\sigma_A}\right)\left(\frac{B_i-\mu_B}{\sigma_B}\right) \qquad 3\text{-}8$$

4. VALIDATION

In this section, the validation of the LiDAR device is presented. Section 4.1 refers to the validation of the LiDAR measurements along the x-axis. To do so, three separate measurement runs (REFP1, REFP2 & REFP3) with a rectangular box placed at a specific location in the flume were used. To check the LiDAR's accuracy along the y-axis, the LiDAR measurements were compared to the ones measured by the beach slope profiler in Section 4.2.

4.1 HORIZONTAL LIDAR ACCURACY

The LiDAR point measurements, the representative point of the closest bottom edge of the reference box to the LiDAR and the standard deviations of the LiDAR point measurements along both axes for all three reference runs are shown in Figure 4-1, Figure 4-2 and Figure 4-3. The line representing a box face is plotted slightly offset, so the averaged measurement points still could be visible in the plot. The standard deviation was calculated by applying equation 3 to each row (i.e., time series) of the measurements.

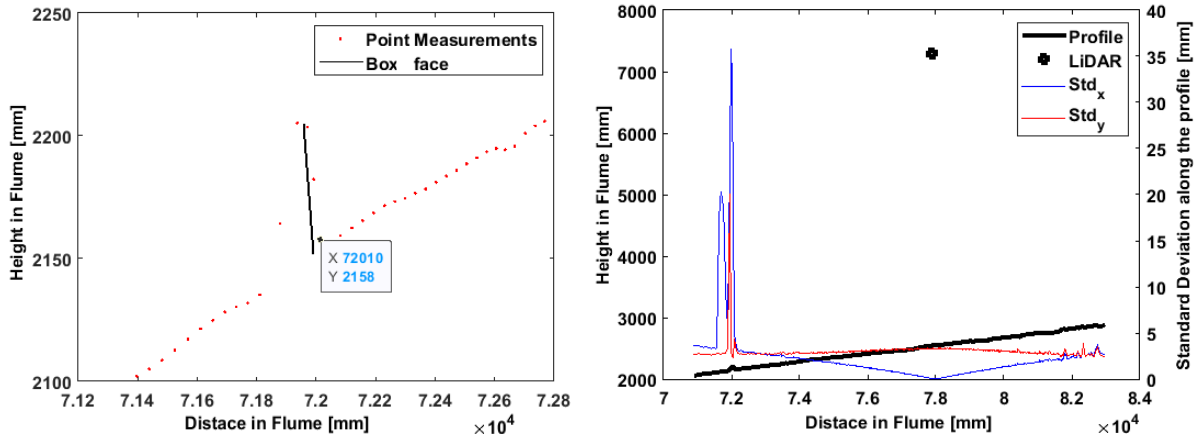

Figure 4-1: Averaged LiDAR Point Location Measurements of Reference Box 1 Closest Bottom Edge to LiDAR (Left) & Standard Deviation Along the Averaged LiDAR Profile in the Measurement Run with Reference Box 1 (Right).

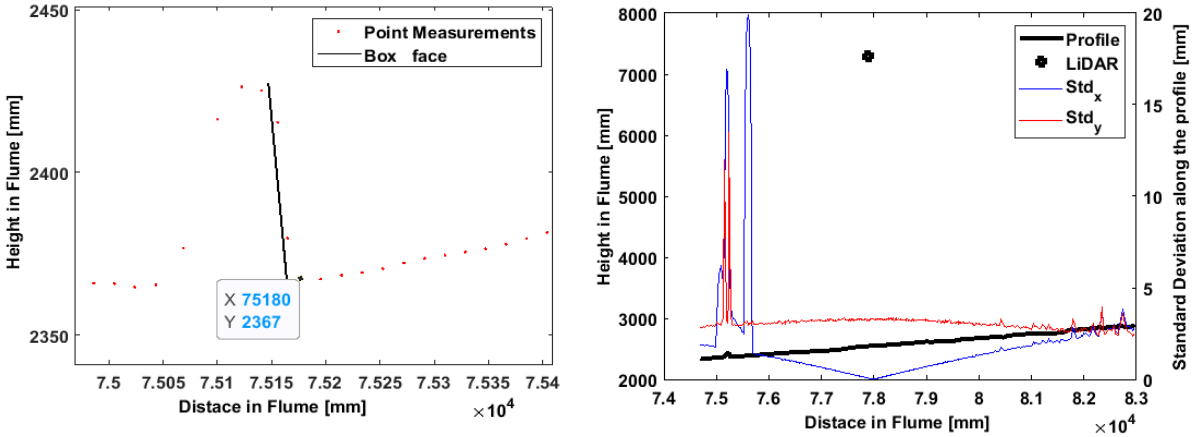

Figure 4-2: Averaged LiDAR Point Location Measurements of Reference Box 2 Closest Bottom Edge to LiDAR (Left) & Standard Deviation Along the Averaged LiDAR Profile in the Measurement Run with Reference Box 2 (Right).

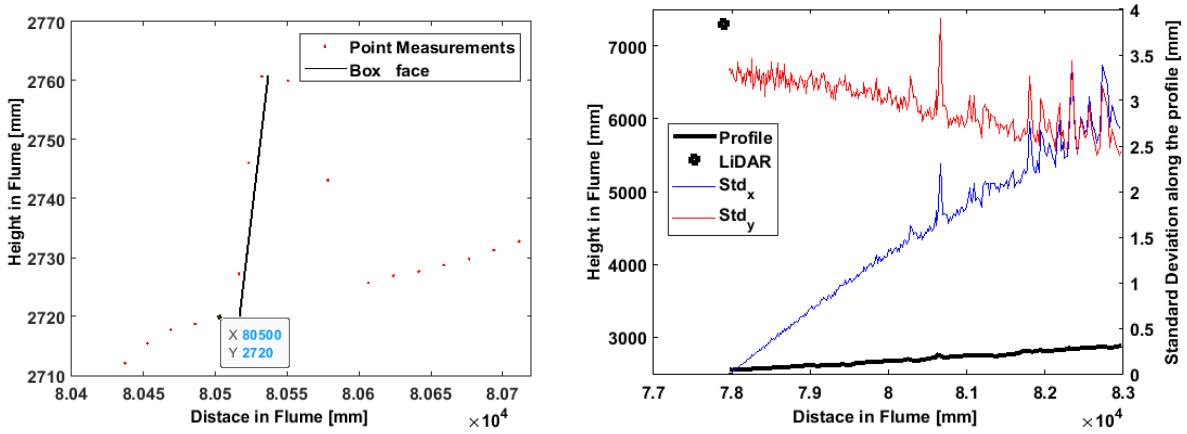

Figure 4-3: Averaged LiDAR Point Location Measurements of Reference Box 3 Closest Bottom Edge to LiDAR (Left) & Standard Deviation Along the Averaged LiDAR Profile in the Measurement Run with Reference Box 3 (Right).

In the figures above it can be observed that the points that are assumed to be representing the closest bottom edge of the boxes to the LiDAR are deviating along the both x- and y-axis. In particular, the representative point of the LiDAR which is interpreted as the edge of the box is offset from its realistic location. This can be derived visually by looking at the red dots and creating extensions that connect the boxes face to the bed slope. As a result, an additional error is made when comparing the value of the observed point and the location of the box's edge measured by the researchers in the flume.

In general, it can be observed that the standard deviation along the x-axis has the lowest deviation observed at the location just below the LiDAR and the standard deviation values increase linearly on both sides as the measurement is being made further away from the LiDAR's nadir (77.891m) as shown in Figure 4-1, Figure 4-2 and Figure 4-3. The standard deviation along the y-axis has a highest just below the LiDAR and is decreasing quadratically as the measurements are made outward from the LiDAR's nadir. In addition, along the x- and the y-axis the standard deviation values increase rapidly for the measurements at the location of the boxes.

The resulting horizontal accuracy for all three reference runs is compiled in table 2. It can be observed that the difference between the LiDAR-measured x-location and the hand-measured positions for all three reference points is smaller than 50mm. However, for the measurement to be within the error interval the total difference between LiDAR and hand measurements could not be larger than 55mm (25mm LiDAR error + 30mm sinker, string and ruler error). As a result, it can be concluded that all of the reference boxes measured with LiDAR are inside the allowed error interval.

Table 4-1: Results of LiDAR Validation Along X-Axis

	REFP1	**REFP2**	**REFP3**
LiDAR measured X-Location [mm]	72010±25	75180±25	80500±25
Hand-measured X-Location [mm]	71960±30	75170±30	80500±30
The Difference Between Measured and Placed X-Location [mm]	50	10	0
Inside/Outside Error Interval	Inside	Inside	Inside

4.2 VERTICAL LIDAR ACCURACY

Before the LiDAR accuracy along the y-axis could be determined, the final LiDAR profile was constructed. This was achieved by making a LiDAR profile out of three previously averaged LiDAR measurement runs without the measurement at the reference boxes and in the vicinity of it. Figure 4-4 shows all three beach profiles separately. In general, the profiles are similar, however, there were a few inconsistencies between profiles noted. At the longitudinal 80.4m distance, in the REFP3 measurement run a distinct pit can be observed that is not present in REFP1 and REFP2. A reason for the shift in a pit location could be related to a human factor, for example, a researcher steps on the profile between the validation runs. Between the 81.8m and 82.6m marks the beach profiles between REFP1, REFP2 and REFP3 have a similar shape but are offset by a few millimetres. The variation in the profile could be related to a human factor or a systematic error of LiDAR.

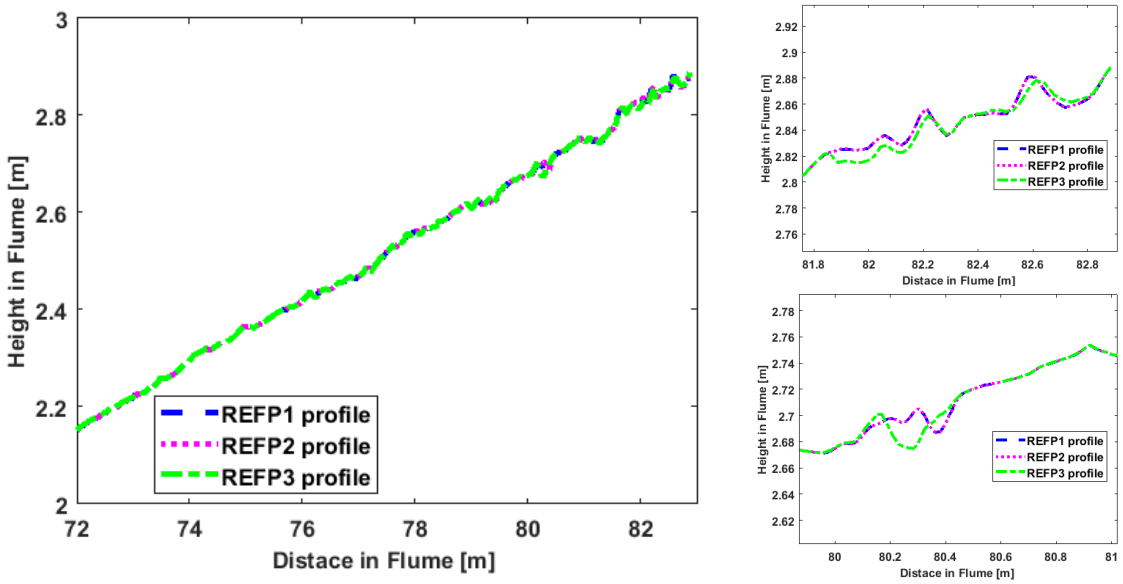

Figure 4-4: Differences in Obtained LiDAR Profiles Between Three Reference Runs

The LiDAR and the bed profiler measurements are compared in Figure 4-5. It can be seen that almost along the full length of the beach profile, there is a difference between the two measured profiles. In the lower section of the beach profile, the LiDAR profile is both higher and has a different shape. In the upper section of the beach profile, there is a pit present in the beach profile measured by LiDAR that is not present in the profiler's beach slope. In addition, it could also be noticed that LiDAR is capable to measure smaller features on the bed slope compared to the beach profiler. The differences could be explained by the contrary spatial resolutions. For LiDAR the spatial resolution is <5mm along the x- and y-axis, while for the bed profiler is 20mm along the x-axis and 10mm along the y-axis. Also, the differences could be explained by the fact that each device made measurements at two separate lateral positions. The LiDAR was measuring bed levels at ±70cm from the side wall of the flume, while the slope profiler was measuring in the middle of the flume (Figure 3-2). Possibly the bed profiles might not match at two separate locations, however, there is no evidence to approve or deny the latter statement.

The quantitative difference between LiDAR's beach slope and the profiler's beach slope is shown in Figure 4-6. It can be seen that in the section from the 72m mark to the 81m mark in the flume, the difference between the profile is below ~30mm. However, further, up the bed profile (81m>) the difference between the profiles even reaches above 50mm due to the presence of the distinct pit on the bed. The spatially averaged difference between LiDAR and the slope profiler is ~10mm.

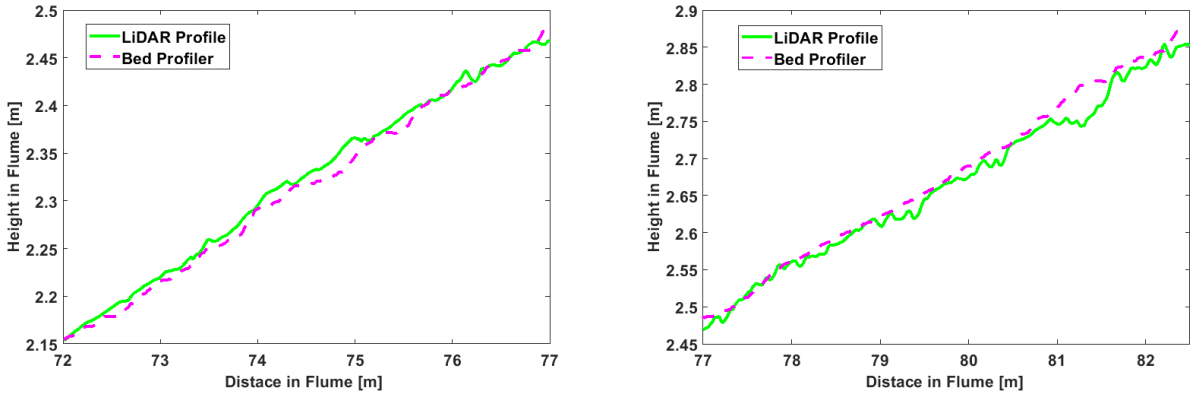

Figure 4-5: Visual Comparison of Beach Slope Measured by LiDAR and Profiler

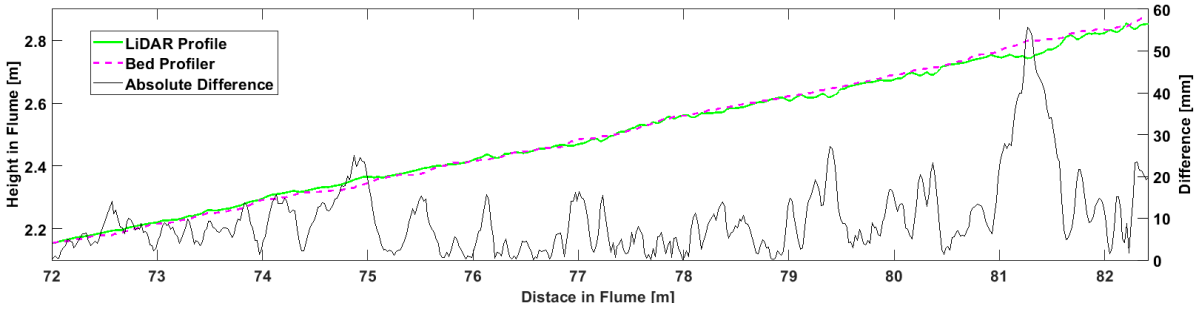

Figure 4-6: Difference Between Averaged LiDAR Profile and Slope Profiler Beach Slope

Figure 4-7 shows the recap of the standard deviation along the y-axis for the LiDAR and the measurement error of the bed profiler. Figure 4-8 compares the absolute difference between the static bed measurements made by LiDAR and the bed profiler along the full length of the bed profile. The *Upper Error Limit* was calculated by adding the theoretical LiDAR error margin (25mm) to the profiler's vertical error margin (10 mm) and *Lower Error Limit* was calculated by adding the measured LiDAR error along the full bed profile (<5mm) to the profiler's vertical error margin (10 mm). In general, the majority of the time, LiDAR can capture the profile within the identified *Upper Error Limit* margin. However, the spatial measurement that lies outside the margin is at points where major inconsistencies between the LiDAR and profiler profiles are present. From the *Lower Error Limit* perspective, still, most of the profile is below the determined threshold and the *Lower Error Limit* is smaller than the spatially averaged difference between LiDAR and the slope profiler. As a result, it can be concluded that LiDAR measurements are capable to measure the static bed level accurately.

From the observed standard error along y -the axis of the LiDAR device along the full length of the profile, it seems that the location along the flume has a minor influence on the inaccuracy of the results since the standard deviation changes relatively minimally. This is shown in Figure 4-7. Therefore, the inaccuracy of dry bed measurements around the y-axis are predictable. As a result, in the next section, where the water level will be separated from the bed level, the expected inaccuracy (standard deviation) of measurements on the beach slope (without water) will be known. This same inaccuracy determines the potential error of bed level changes that are then computed from consecutive LiDAR measurements. In these relative differences between consecutive LiDAR profiles (i.e., temporal bed level changes), the absolute differences between LiDAR and profiler measurements no longer matter.

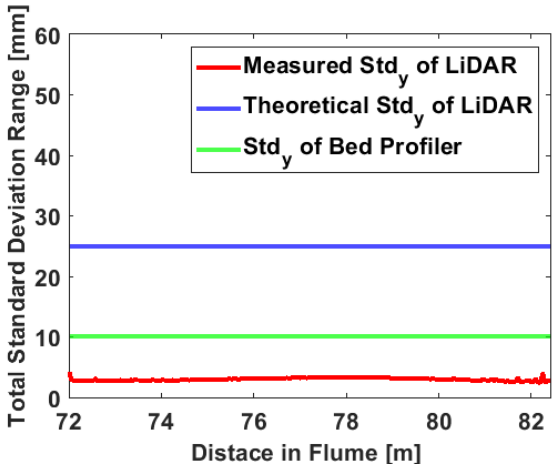

Figure 4-7: Devices' Error Magnitudes

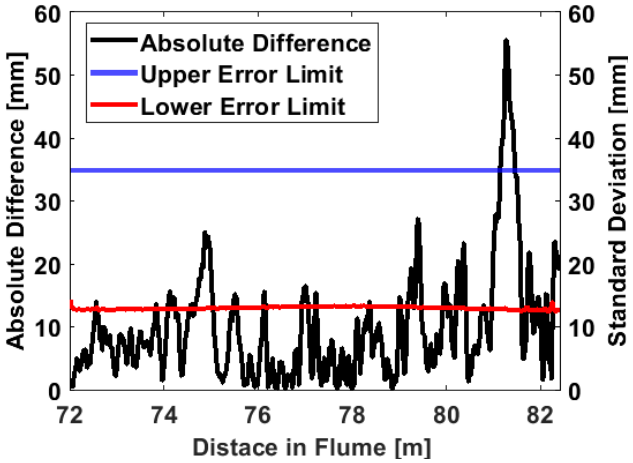

Figure 4-8: Accuracy of LiDAR along the Y-Axis

5. DATA SMOOTHING

Section 5 presents the smoothing of the elevation matrix and the smoothing of variance. First, the section describes the elevation matrix smoothing using different temporal windows. Second, raw vertical variance derivation and its spatial smoothing is described.

To smooth data temporarily, equation 3-3 was used. Besides, also three different arbitrary temporal windows were chosen. To be precise, the size of the moving window was 5 (0.2s), 15 (0.6s), and 25 (1s) measurements large. Again, it must be emphasized, that the upper limit of the smoothing window was chosen to be 1 second. This corresponds to a few shorter swash events observed under present conditions. The results of elevation data smoothing can be observed in Figure 5-1 to Figure 5-4. Besides, the elevation data is presented as the relative vertical change to the first measured profile. This is done to emphasise the profile evolution over time. The time is expressed in consecutive measurement numbers rather than seconds or minutes. This is done for simplicity purposes. The measurement number could be translated into time (seconds) by dividing the measurement number by 25 which is the measurement frequency. It can be observed as the temporal smoothing window increase, the elevation data images become smoother compared to the raw elevation data image. In particular, smaller-scale noise is being eliminated. Besides, at the bottom of the elevation image, the bright yellow coloured part (>20mm vertical elevation change) represents the water line in time. It can be observed that the smoothing had no significant influence on the waterline since the swash event maximum run-ups remain to reach the same distance marks in the flume and swash events occurs at the same moments in time.

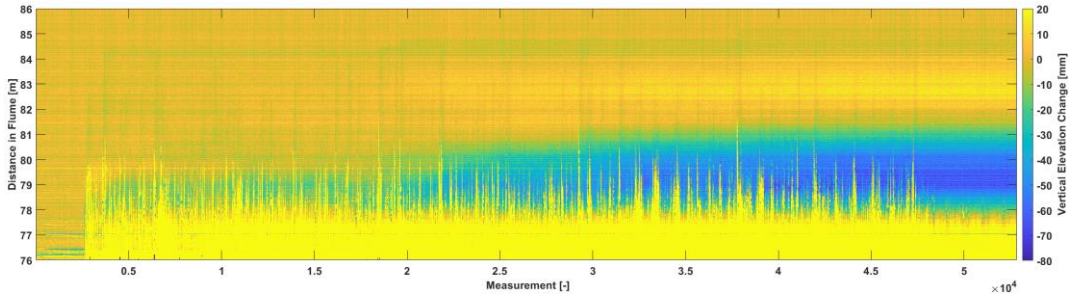

Figure 5-1: Raw Elevation Data

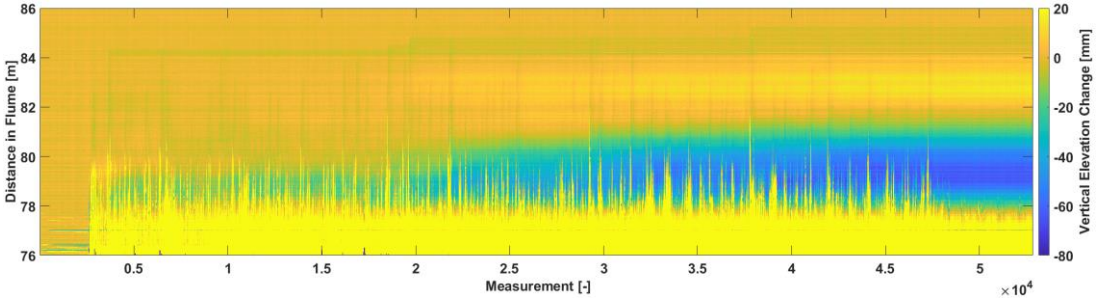

Figure 5-2: Temporarily Smoothed Elevation Data with a Moving Window of 5

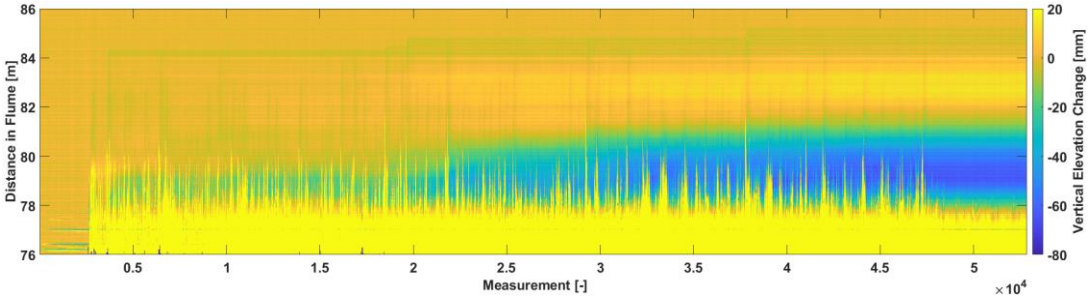

Figure 5-3: Temporarily Smoothed Elevation Data with a Moving Window of 10

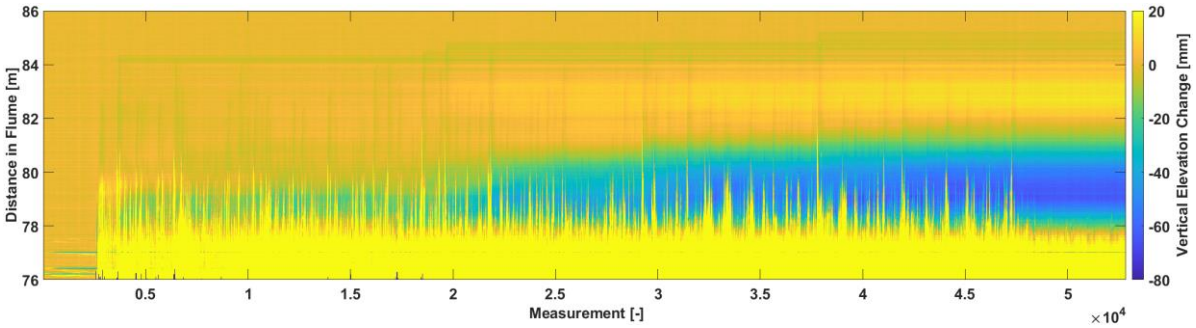

Figure 5-4: Temporarily Smoothed Elevation Data with a Moving Window of 15

To derive the spatial variance of the static beach profile, equation 3-4 was used. The variance profile along the full length of the beach profile is presented in **Error! Reference source not found.**. S ince the variance profile was noisy or rapidly fluctuating vertically, it was decided to filter the randomness from the variance profile, leaving just the general trend of the vertical variance profile. This was achieved by smoothing the raw vertical variance profile with a median function and an arbitrary moving window of 80 measurements in space corresponding to a horizontal distance of ~1m. To smooth data median was used since the method is useful for deducting period trends while outliers are present. The result of vertical variance smoothing is presented in **Error! Reference source not f ound.**.

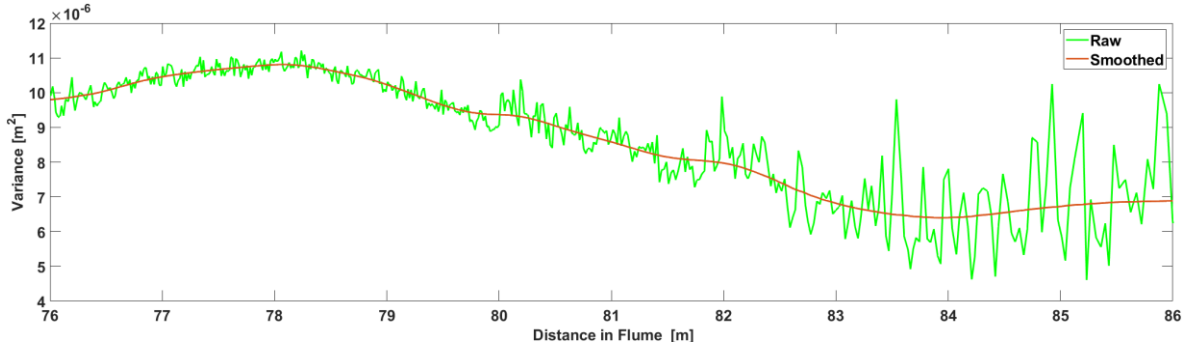

Figure 5-5: The Raw and Spatially Smoothed Representation of Variance Along the Beach Profile

6. SEPARATING WATER LEVEL FROM BED LEVEL

Section 6 consists of four parts. The application of the observed variance method to separate measurements of the water and the beach surface is presented in Section 6.1. Separating water level from bed level using the decreased variance method is detailed in Section 6.2. In Section 6.3 isolating water level from bed level using the received signal strength index is presented. The most successful cases from each of the methods are then compared in Section 6.4.

6.1 OBSERVED VARIANCE

After the elevation matrix was smoothed with three different temporal moving windows, the variance was calculated for each smoothed elevation case. Here, for each of the case variance was calculated again with three different moving windows. The selected windows for variance calculation were 5 measurements or 0.2s, 15 measurements or 0.6s, and 25 measurements or 1s. The variance with the moving window can be calculated by applying 3-3 to the smoothed elevation matrix. Also, here the upper limit of variance windows is limited to 1 second which is the representative time span of a few shorter run-up events.

Once variance was calculated for each smoothed case and the vertical variance of static bed level (interpreted as variance threshold) was known, equation 3-5 was applied to determine the location where the water line ends and bed level starts for each measurement in time. Here, moving from the offshore side to the onshore side, the first point in which the static bed variance was equal to or larger than the variance in the elevation matrix was identified as the point where water levels end and bed level starts. The complete overview of all the cases is provided in Appendix A. The paragraph below summarizes the main findings of equation 3-5 with the observed variance obtained in the validation section variance different identified smoothing and variance windows.

As for the temporal smoothing window of 5 and with variance windows of 5 and 15 the water line is rapidly fluctuating. In particular, along the full length of the obtained water line abrupt momentary vertical lines spanning changes from the submerged beach (where vertical elevation changes are greater than ~+20mm or the border of the yellow area at the bottom of the relative elevation image) to the onshore side of the beach slope (further in the text referred as the spikes). With a variance window of 25, the spikes are almost not present and the detected water line manages to follow the swash pattern (Figure 6-1 and Figure 6-2). Also, the swash events, in most cases, reach the erosion pit's onshore side and some of the events are present in the accretion area located on the upper beach profile. With the temporal smoothing window of 15 and with all respective variance windows moving variance windows, the water level is underestimated than in the case with a temporal window of 5. In particular, the detected run-up events rarely reach the erosion pit's onshore side (81m mark) and almost no swash events are reaching the accretion area (area between 81 and 84m distance mark). As the temporal smoothing window is increased, worse and worse results are obtained. In particular, in the case with a temporal smoothing window of 25 again the water line is even more underestimated (moved more to the offshore side) compared to the previous case, with positions further down the submerged parts of the beach. Besides, as the temporal smoothing window increases, the temporal variability of the water line decreases.

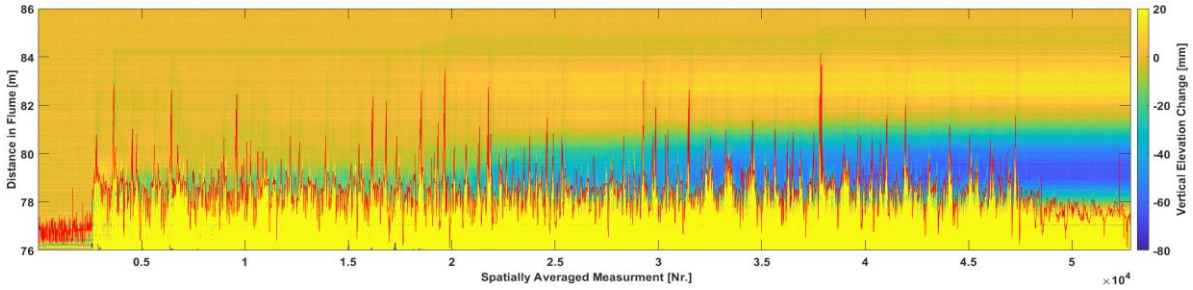

Figure 6-1: Obtained Water Line with Temporal Smoothing Window of 5 and Moving Variance Window of 25

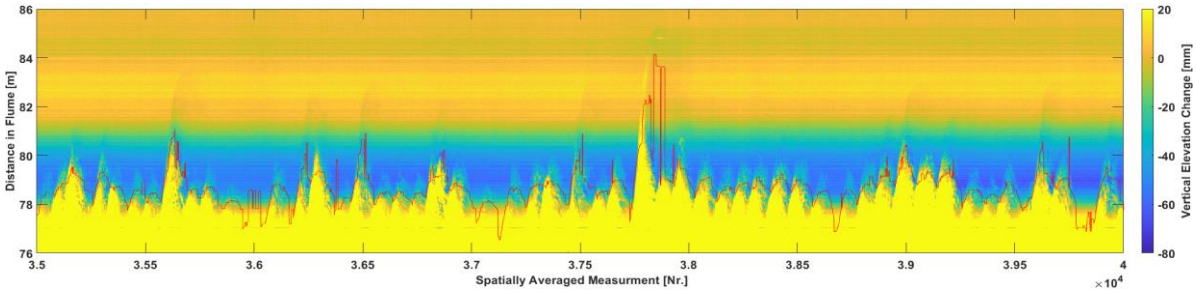

Figure 6-2: Zoomed Section of Obtained Water Line with Temporal Smoothing Window of 5 and Moving Variance Window of 25

The calculated maximum run-up, average run-up and maximum run-down values for each combination smoothing and variance window for observed variance case are compiled in Table 6-1. In general, the maximum run-down for all the cases difference does not exceed more than 9cm in the worst-case scenario. However, the majority of the time, the difference was not larger than 5cm. As for the average run-up, none of the derived cases matches the researchers' observations. In particular, for the majority of the cases, the average run-up was underestimated by roughly 1m compared to the researcher's observations. The largest difference between researchers' observations and calculated values is observed for the maximum run-up. The difference between the two can be as large as 3m in the case with temporal smoothing windows of 15 and 25. This occurred because either elevation smoothing had a larger window than the variance window or the elevation matrix smoothing window was larger than the duration of the swash event peak duration (<0.5s), thus replacing the thinner water column parts of the swash events with the same values the bed level next to the swash event.

Table 6-1: Smoothing Window (Smo Win), Variance Window (Var Win), Maximum Run-Up (Max), Average Run-Up (AVG) and Maximum Run-Down (Min) Values for Each Case with Observed Variance Method

Smo Win [-]	Var Win [-]	Max [m]	AVG [m]	Min [m]
5	5	83.72	78.10	76.02
5	15	84.15	78.37	76.04
5	25	84.15	78.40	76.07
15	5	80.46	77.75	76.01
15	15	83.65	78.07	76.01
15	25	83.65	78.20	76.03
25	5	79.91	77.57	76.01
25	15	80.44	77.98	76.05
25	25	81.67	78.13	76.10
Researchers' Observations During the Flume Experiment				
-	-	83.21	79.30	76.01

In total only one water line from the observed variance method was selected for further comparison (highlighted in yellow in Table 6-1) – one from spatial smoothing and one from temporal smoothing. The selection was based on two conditions. First, the maximum run-up, average run-up and maximum run-down approximately match with researchers' observed values during the flume experiment. Second, in the majority of the swash events, the extracted water lines must follow the

erosion and accretion patterns observed in the relative elevation image.

The case with a temporal smoothing window of 5 and variance window of 25 a was selected for further evaluation. The decision was based on the fact that the water lines extend into the erosion area the majority of the time while at the same time some run-up events reach the upper part of the beach where accretion occurred. In addition, the water line followed the submergence and emergence of the beach (i.e., the swash pattern). However, the maximum run-up was overestimated due to noise present at the location of the maximum run-up. The average run-up was the closest value to the researchers' value in all of the cases, but the maximum run-down was 6cm higher than expected.

6.2 DECREASED VARIANCE

In the previous Section 6.1, it was recognized, that with the derived variance the water line did not follow the submergence of the beach very well. In particular, on the beach slope, the dark yellow and green areas (vertical elevation change between ~-10mm and ~+10mm) above the bright yellow area (~+20mm vertical elevation change) representing the water movement, were separated from the water line. While it was expected that the green area should also be positioned below the isolated water line. At least in the section offshore of the 81m longitudinal mark, where a clear uprush-backwash pattern was visible. As a result, it was decided the decrease the smoothed observed variance and decrease the variance threshold. The value for the decreased variance method was set to $2*10^{-7}$m lower at all spatial points compared to smoothed observed variance. The magnitude by which the smoothed variance was decreased was selected based on the raw variance values observed from roughly 84m distance mark shore-ward. In particular, the magnitude was chosen in a way that the decreased variance would roughly match with the lower raw variance values at the end of the flume, thus not leading to an excessive decrease. The raw observed variance, the smoothed observed variance and decreased observed variance are illustrated in Figure 6-3.

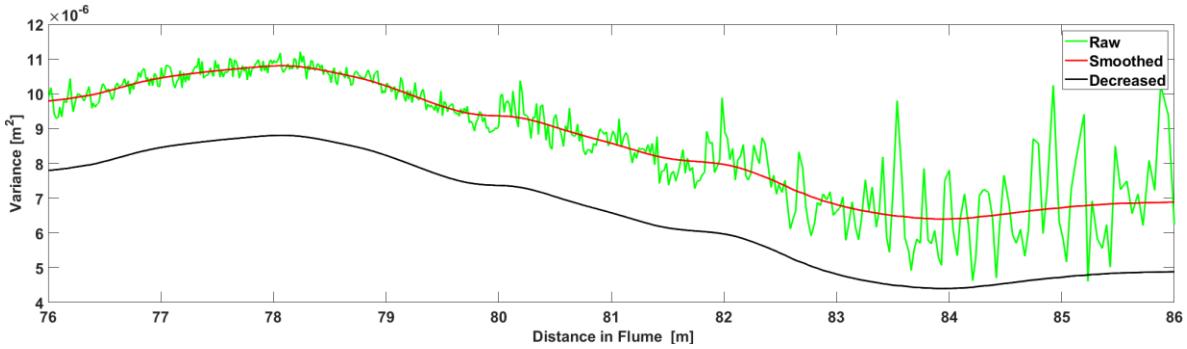

Figure 6-3: The Raw, Smoothed and Decreased Variance

To maintain a consistent approach, temporal smoothing windows and variance windows applied with this method were the same as in Section 6.1 with only one exception. Besides, the same equation was used to derive the water line. The complete overview of all the smoothing and variance window combinations for the decreased variance method is presented in Appendix B.

With the temporal smoothing window of 5, the extracted water lines become smoother as the variance window increases. Although spikes are present, most of the spikes do not exceed the 82m mark. Also, these spikes occur at random moments in time, sometimes it could be at the top of the run-up, sometimes before, during and after the swash event. Especially, with the variance window of 35 (Figure 6-4 & Figure 6-5), it can be seen that a reduction of rapid fluctuating water line pattern in the lower section of the beach profile has been achieved. In addition, the majority of the time, the water line extends up to the onshore side of the erosion pit. Nevertheless, only a few times does it reach the accretion part. However, temporally, the method still only sometimes fails to capture swash events. For example, at $3.77*10^4$ the water line combined two events – one relatively larger and one

relatively smaller into one swash event (Figure 6-5). As for the temporal window width of 15, in all variance window width combinations, the water line is significantly underestimated. Same could the said about all of the cases with a temporal window width of 25.

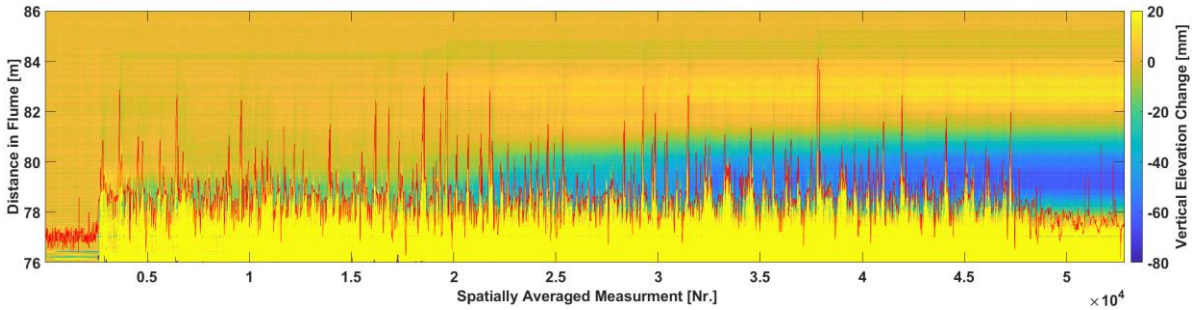

Figure 6-4: Obtained Water Line with Temporal Smoothing Window of 5 and Moving Variance Window of 35

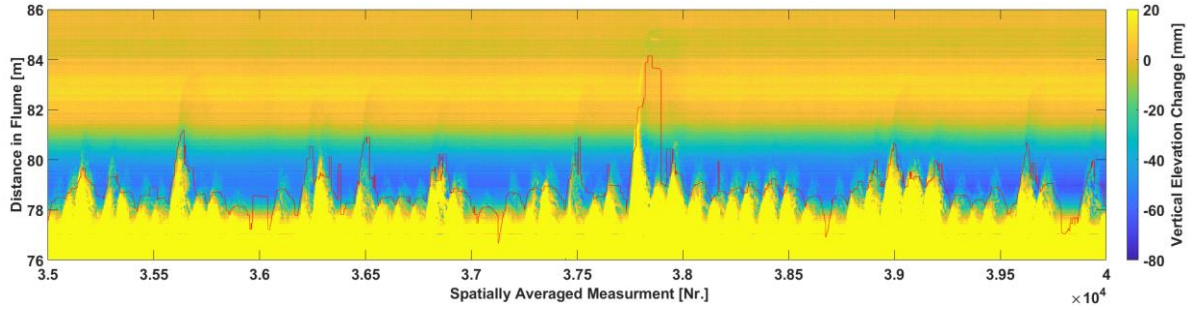

Figure 6-5: Zoomed Section of Obtained Water Line with Temporal Smoothing Window of 5 and Moving Variance Window of 35

In Table 6-2 the maximum run-up, average run-up and maximum run-down values for each combination of spatial and temporal smoothing with the constant variance method have been compiled. In general, the maximum run-down does not deviate from the researchers' observations with more than 6 cm, with three outliers of 10cm, 16cm, and 23cm. The average run-up for the majority of the time is roughly within 1 m distance from the researchers' observation. However, with a maximum run-up, the situation is almost the same as in the previous case.

For further evaluation, a water line constructed with the temporal smoothing method and the combination of a variance window of 35 and a temporal window of 5 was selected. This particular water line was chosen because of the relatively good fit with the relative elevation change image and researchers' observation of maximum run-up, average run-up and maximum run-down. In addition, it was qualitatively noted, that the water line is shifted more onshore than was possible to achieve with the varying observed method (compare Figure 6-1 and Figure 6-2 to Figure 6-4 & Figure 6-5).

Table 6-2: Variance Window (Var Win), Smoothing Window (Smo Win), Maximum Run-Up (Max), Average Run-Up (AVG) and Maximum Run-Down (Min) Values for Each Case with Decreased Variance Method

Smo Win [-]	Var Win [-]	Max [m]	AVG [m]	Min [m]
5	5	84.14	78.24	76.04
5	15	84.18	78.69	76.07
5	25	84.18	78.56	76.24
5	35	84.15	78.56	76.17
15	5	80.46	77.08	76.01
15	15	83.65	78.11	76.01
15	25	83.65	78.24	76.07
25	5	80.04	77.64	76.01
25	15	80.46	78.03	76.05
25	25	83.62	78.17	76.11
Researchers' Observations During the Flume Experiment				
-	-	83.21	79.30	76.01

6.3 RSSI

The section starts with deriving the RSSI across the length of the dry beach profile. Next, the theoretically derived RSSI values are compared with RSSI profile measurements during the flume run to check how well the water run-up can be identified. After that, the method is used to separate the bed level from the water level. Here, both unsmoothed and smoothed data are examined to see which case gives the most accurate results. Once several cases of water level are extracted, the data is compared to both the researchers' visual observation and the relative elevation change in the time image.

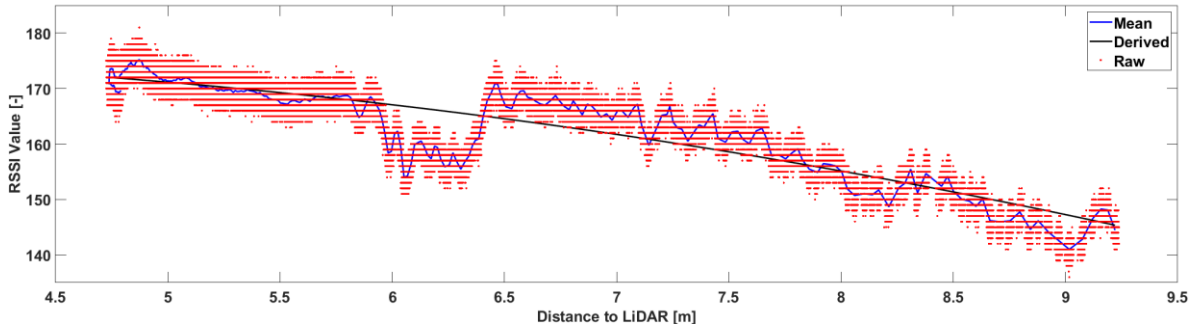

Figure 6-6: The Raw Distance & RSSI Measurement Before Wave Paddle Movement, The Mean Distance & RSSI Measurements, and Derived RSSI Measurement Based on the Distance Measurement

To derive RSSI values of the dry beach slope based on the point distance to LiDAR, the first measurements of the flume run were selected. From the selected temporal data, a temporal mean was calculated. Then, the mean was used to derive the equation to describe the relationship between the RSSI values of the dry beach and the distance between LiDAR and the measurement point. Figure 6-6 shows the raw RSSI data, the mean and the quadratic equation fitted to the data set. The derived quadratic equation is presented in equation 6-1, where $RSSI_{dbt}$ is the theoretical RSSI value representing a dry beach and D is the beach slope's measurement point distance to the LiDAR (in m):

$$RSSI_{dbt} = -0.6312 * D^2 + 2.866 * D + 172.6 \qquad 6\text{-}1$$

Once the theoretical RSSI values of the dry beach profile were known, the theoretical RSSI profile was compared to the raw measurements. For the validation, four cases with different conditions were selected: (1) with the static water level at the beginning of the run, (2) with slightly fluctuating water level and at the end of the run, (3) with water level run-up to 83/84m mark and (4) with water level run-up to 79m mark. For cases (3) and (4) the run-up height was identified by making

use of a previously compiled relative elevation change image. All figures representing these four cases are shown in Figure 6-7 to Figure 6-10. As for case Nr. 1 (Figure 6-7), it can be seen that the theoretical measurements of the dry beach follow the actual RSSI measurements of the dry beach. However, at the ~82m longitudinal mark, a pit-like shape is present. The actual reason for the value drop-off in these particular points is not well-understood. The maximum difference between the theoretically derived RSSI value and the actual measurement in this area is ~10. Besides, it can be observed that RSSI values plummet as the static water line is reached which is located at the x=77.4m mark. For case Nr.2, at the offshore part, where the slightly fluctuating water level is present, the plummeting RSSI value pattern is not evident. Rather, the RSSI value shows a fluctuating pattern. In the area from the ~81m to ~84m distance mark, a gradual onshore declining RSSI profile is present. According to the relative elevation change image, in this area accretion occurred and as a result, the distance to LiDAR decreased. Therefore, it was expected that the raw RSSI values should have been higher in this area compared to case Nr.1 according to Figure 50. The reason for declining RSSI values could be related to the wetting of the sand which could have an impact on the RSSI measurements. In the case Nr.3, from the 80m to 83-84m distance mark the RSSI values do not experience the significant drop-off in values as in the case Nr.1. This could be explained by the fact that the LiDAR laser beam actually can penetrate the shallow water in the swash zone. Nevertheless, the difference between the theoretical and raw measurements is assumed to be satisfactory to successfully separate water run-up from bed level. Case Nr.4 is similar to case Nr.2. Here, both RSSI values of dry bed and water follow the same pattern.

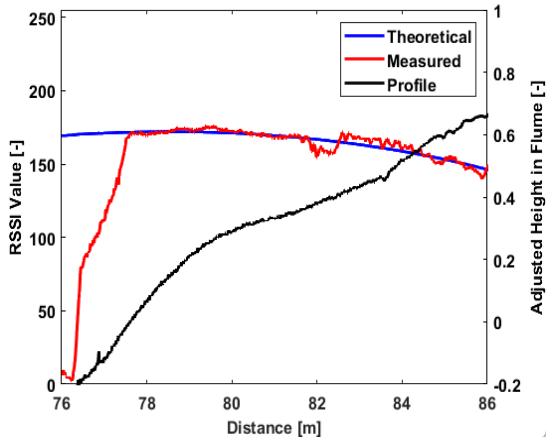

Figure 6-7: Validation of Theoretically Derived RSSI Values for Dry Bed Slope at the Start of the Run with Static Water Line at ~ 77.4m Distance (Case Nr.1)

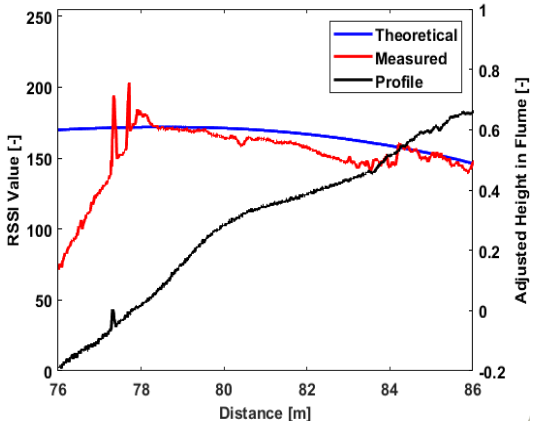

Figure 6-8: Validation of Theoretically Derived RSSI Values for Dry Bed Slope at the End of the Run with Static Water Line at ~ 78m Distance (Case Nr.2)

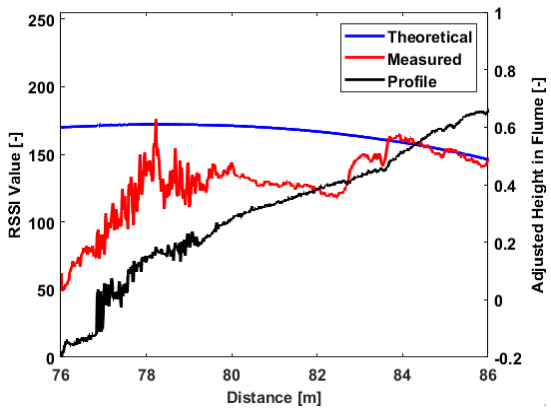

Figure 6-9: Validation of Theoretically Derived RSSI Values for Dry Bed Slope at the Middle of the Run with Moving Water Line at ~ 83/84m Distance (Case Nr.3)

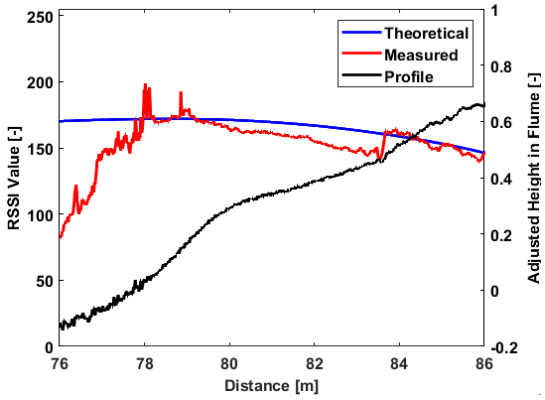

Figure 6-10: Validation of Theoretically Derived RSSI Values for Dry Bed Slope at the Middle of the Run with Moving Water Line at ~ 79m Distance (Case Nr.4)

Similar to the observed and decreased variance method, also in this case temporal smoothing with the same moving average windows was applied to maintain a consistent approach. To derive the water line with the RSSI method, equation 3-6 was used. However, here, instead of variance an RSSI threshold value was introduced. Here three arbitrary values were selected: 5, 10 and 15. The complete overview of all the smoothing combinations and thresholds is presented in Appendix C.

With a temporal smoothing window of 5 and an RSSI threshold of 5, spikes are present in the water line. In particular, most of the spikes occur at the swash lens maximum run-up location. Besides, these spikes have odd behaviour. In particular, the spikes seem to have the same upper limit for some time and then the upper limit changes to a different value, which is not a realistic scenario. Another odd observation is that the spikes seem to correlate with relatively larger swash events. As the RSSI threshold is increased, the number of spikes is decreased. With the threshold of 15, the presence of spikes completely disappears. As for the water line, it follows the higher parts of the swash events at the bottom of the relative elevation image (the bright yellow shade or >~20mm) while maintaining a rapidly fluctuating pattern. The increase in the threshold results in a water line shift towards the offshore side and had a minor effect on the temporal variability of the swash events. With a temporal smoothing window of 15 and 25, the results are comparable to the ones with a temporal smoothing window of 5.

However, there are few distinct results. Firstly, the increase of the spatial smoothing window only led to a less rapid fluctuating pattern of the detected water line. In other words, the larger the smoothing window became, the smoother the extracted water line was. Secondly, as the smoothing window increased, the peaks of the swash events were reduced. As a result, the water line did not manage to follow the observed accretion and erosion pattern in the relative vertical elevation change image. Thirdly, especially with a threshold of 10 and temporal smoothing windows of 15 and 25 the swash events extending above the 81m distance mark have a distinct rectangular swash lens pattern (Figure 6-11 and Figure 6-12).

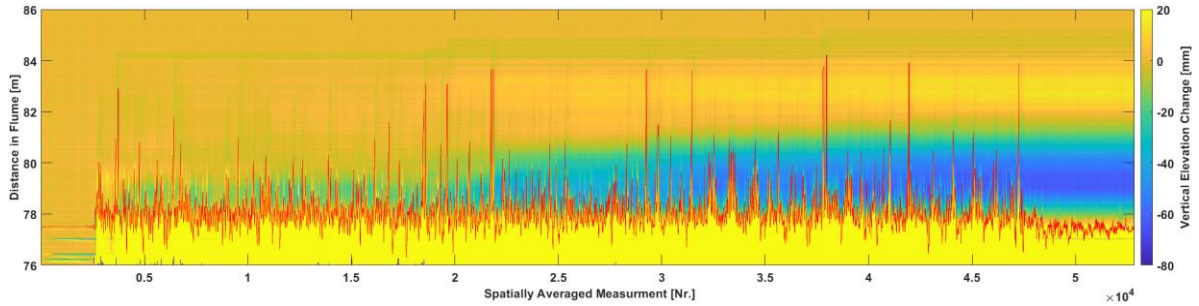

Figure 6-11: Obtained Water Line with Temporal Smoothing Window of 15 and RSSI Threshold of 10

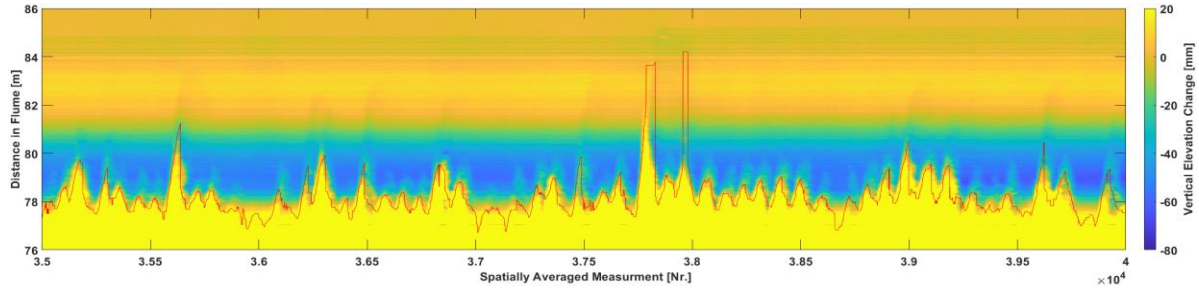

Figure 6-12: Zoomed Section of Obtained Water Line with Temporal Smoothing Window of 15 and RSSI Threshold of 10

In Table 6-3 maximum run-up, average run-up and maximum run-down values for each combination of temporal smoothing with the RSSI method have been compiled. The run-up maximum values with the RSSI threshold of 5 and 10 are ~84.21m with every spatial window. This could be

explained by the presence of spikes in the extracted water lines. However, the maximum run-up values decrease as the RSSI threshold is increased to 15. As for the average run-up, the run-up decreases as the RSSI threshold increases. This happens because with larger RSSI threshold values the water line is moved more offshore as a result of decreasing the average run-up values. Besides, the increase in the average run-up values is observed with increasing spatial windows. Also, it was observed that as the smoothing window increases, the maximum run-down moves more onshore. The last two observations could be explained by the fact that once the larger smoothing window is applied, the water line becomes less staggered while restricting the water line's presence in the area between the 78m and 80m distance mark.

Table 6-3: Threshold Values (Thres.), Smoothing Window (Smo Win), Maximum Run-Up (Max), Average Run-Up (AVG) and Maximum Run-Down (Min) Values for Each Case with RSSI Method

Smo Win [-]	Thres. [-]	Max [m]	AVG [m]	Min [m]
5	5	84.21	78.06	76.17
5	10	84.21	77.89	76.14
5	15	83.48	77.78	76.09
15	5	84.22	78.24	76.51
15	10	84.21	78.01	76.30
15	15	83.67	77.89	76.27
25	5	84.22	78.34	76.74
25	10	84.21	78.06	76.40
25	15	83.69	77.92	76.30
Researchers' Observations During the Flume Experiment				
-	-	83.21	79.30	76.01

The combination with the temporal window of 15 RSSI threshold of 10 has been chosen for further elevation. Also, in this case, the average run-up has been underestimated and the maximum run-up and maximum run-down overestimated. However, this combination allows relatively smooth water line tracking at the higher run-up parts at the bottom of the relative elevation matrix. In addition, the duration of the higher run-ups has a much more accurate representation although the shape is rectangular rather than wave-like.

6.4 COMPARISON BETWEEN METHODS AND SELECTED COMBINATIONS

The three selected water lines are compared to each other in this section. After the comparison of the methods, one of the methods will be selected for further utilization in Section 7 to calculate the bed level changes.

In Figure 6-13 and Figure 6-14 the comparison between the previously selected detected water lines is shown. In Figure 6-13 it can be seen that decreased variance (DV) method has multiple swash events, where the peak of the water line is shifted more onshore compared to the observed variance (OV) and RSSI method (RSSI). However, the latter could be explained by the noise present in the extracted water lines. In particular, the reason for the DV peaks to be higher is due to random spikes in the extracted water lines as is presented at measurement Nr. 38170 in Figure 6-14. Furthermore, by comparing the DV to OV, it can be seen that no actual benefit could be gained. In particular, for the most part, the DV and OV water lines are following the same trend besides a few minor exceptions e.g., at measurement Nr. ~37840 where DV follows the relatively larger swash event more smoothly than OV and at measurement Nr. ~36000 where DV has a constant water line while OV has a more rapidly fluctuating pattern. Besides, sometimes it is vice versa, where the OV tracks the swash lens more smoothly than DV, e.g., at measurement Nr. 36850. By comparing RSSI to DV or OV, two observations have been made. First, the RSSI seems to be better at representing the temporal variability of the water line and thus helps in isolating individual swash events. This can be noticed in Figure 6-14 between measurement Nr. 38150 and 38580. Here, the range between uprush and

backwash is larger for RSSI than for variance methods, thus moving the water line more offshore, especially during the uprush and backwash parts. Second, for most of the swash events where the water line extends above the 80m mark, the maximum uprush of RSSI is comparable to OV or DV. Furthermore, in some cases, it does match (e.g., at measurement Nr. 35640), but in some cases, the maximum uprush of RSSI is underestimated (e.g., at measurement Nr. 37480).

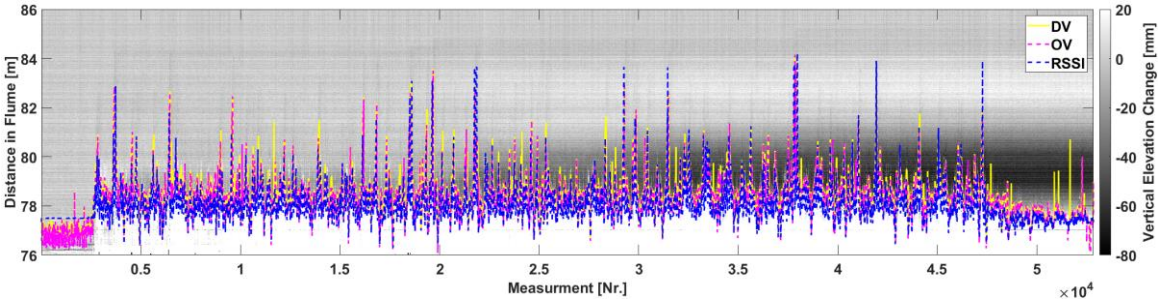

Figure 6-13: Comparison of Derived Water Lines with Different Methods and Window Combinations. DV – Decreased Variance Method, OV – Observed Variance Method, and RSSI –Relative Signal Strength Index Method

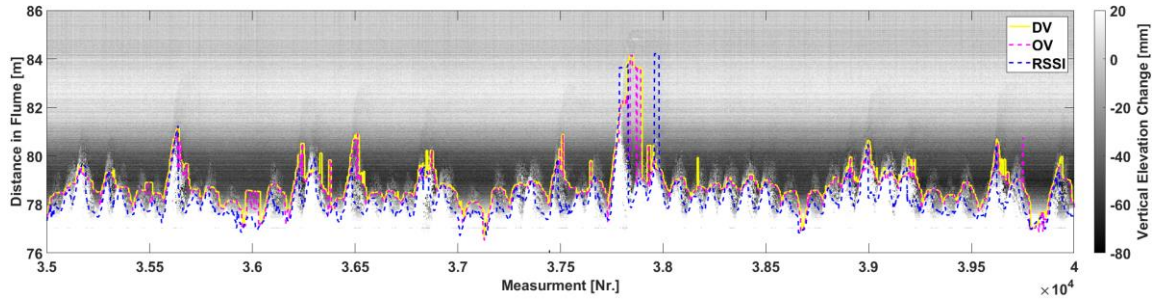

Figure 6-14: Zoomed Section of Comparison of Derived Water Lines with Different Methods and Window Combinations

For further analysis, the OV detection of the water line was selected due to its relatively low noise pattern, which follows relativity well with the wave swash lens in a relative elevation image. The match with the researchers' observations could be better, but for none of the cases, a perfect match was obtained. RSSI methods are neglected, although these methods appear to isolate the swash pattern the best. The reason to neglect the RSSI water line in the further analysis is that this method is underestimating the water line. In particular, if the identified run-down event value is found near the run-down threshold value (78m in this case, more information about what is it is why is necessary can found in Section 3.5 and Section 7), upon close inspection of the water line it still appears to be above the predetermined run-down threshold value. The latter is represented in Figure 68, where although, the RSSI method states that water retreats up until the 77.99m mark, in the LiDAR profile onshore of 77.99m mark still fluctuation bed pattern can be observed. The fluctuation bed pattern is a representation of water, not a dry bed. As a result, if these profiles with selected run-down limits with the RSSI method would be used to calculate the bed level changes, parts of water in the swash would be included in the dry bed beach profiles, leading to errors in the computed bed level changes.

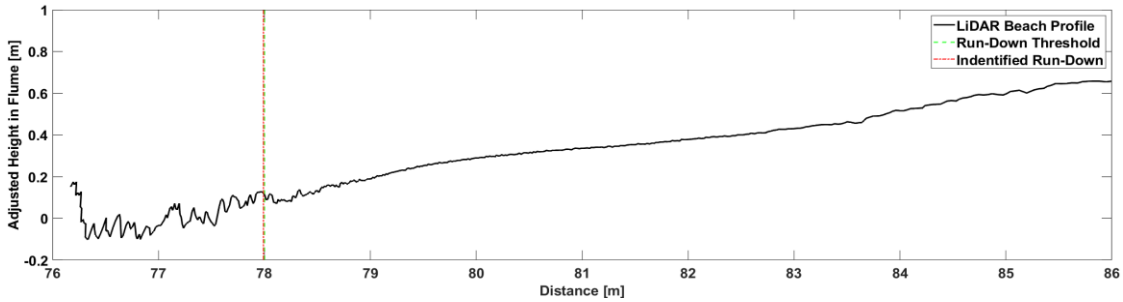

Figure 6-15: The Extracted Beach Profile with a Measurement Point of 21780 with Arbitrary Taken Threshold at 78m Mark

7. BED LEVEL CHANGES

Following the selected detection method for the water line, the run-down events below a defined threshold value are identified. Once the occurrence time of the run-down events is identified, then at these points in time beach profiles are selected. After that, the maximum erosion and maximum accretion points for every consecutive beach profile are calculated. Next follows the change in the total area between the consecutive profiles and the net morphological development of the beach profile. Then, distribution plots are presented of the morphological changes in the swash zone to examine their contribution to the net change of the beach profile. Finally, the correlation between swash event change and event time has been determined.

Figure 7-1 presents the water line and the identified run-downs below the threshold value of the 78m distance mark. The arbitrary threshold value of 78m was selected based on two criteria. First, the threshold had to be below the average run-up value of the selected water line (78.40m) to maximize the number of identified run-downs. Second, the threshold value had to be to the offshore side as much as possible to allow for a comparison of wider beach profiles. In total, 166 run-downs have been detected. The average time between detected run-down events is 10.96s or ~3 peak periods of the incoming waves. Besides, the periods with a non-working wave paddle (warm-up (<~2 min) and cool-down time (>~32.3 min)) have been neglected.

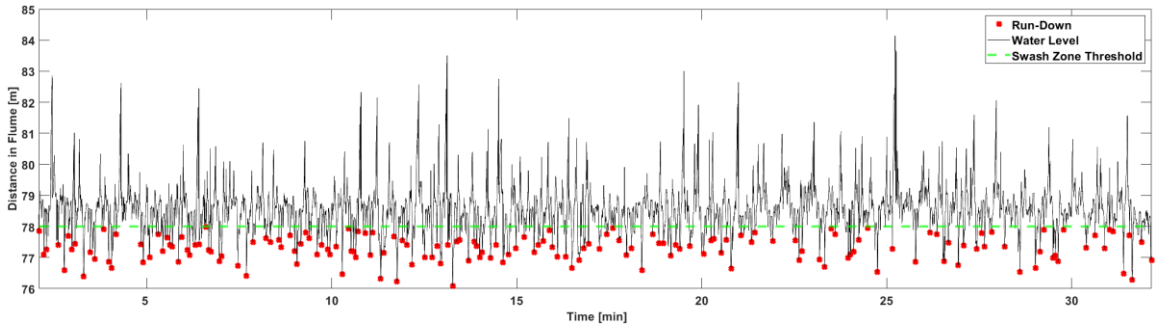

Figure 7-1: Derived Water Line with Identified Troughs and Threshold Line at 78m Mark

Figure 7-2 presents the percentage distribution plots of the time interval between the detected run-down events. It can be observed that the distribution is skewed to the left side or the side with the shortest inter-swash periods. The majority of the events (147 out of 165 or 89%) are shorter than the 5 peak periods of the incoming waves or 17.5s. Also, three events are longer than the 10 peak period of the incoming waves or 35s. The long swash events could be explained by the fact that during the flume run, the swash events do not retreat below the defined run-down threshold. However, during these events, the water line approaches the threshold at least once before again moving onshore and then moving offshore and crossing the threshold. The latter can be observed in Figure 7-1 between 25.9min and 25.47min.

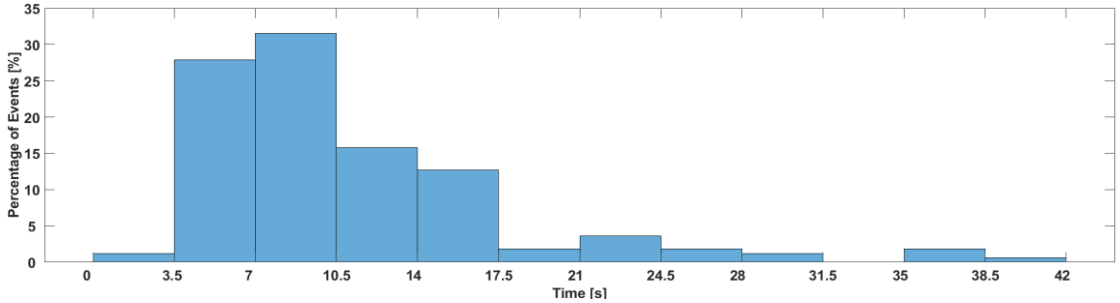

Figure 7-2: Percentage Distribution of Time Interval Between Detected Run-Down Events Expressed as Time(s)

Figure 7-3 shows the maximum erosion and accretion observed between consecutively identified run-downs. For both accretion and erosion, the majority of the events stay within 10mm or 1cm boundaries, and the magnitude of the events does not exceed ~16mm. The error margin for accretion and erosion was based on the LiDAR error provided by the manufacturer (Table 3-1). None of the maximum accretion or erosion values after each swash event exceed the LiDAR error margin. As a result, it can be concluded that swash events are causing a non-significant elevation change in the beach profile.

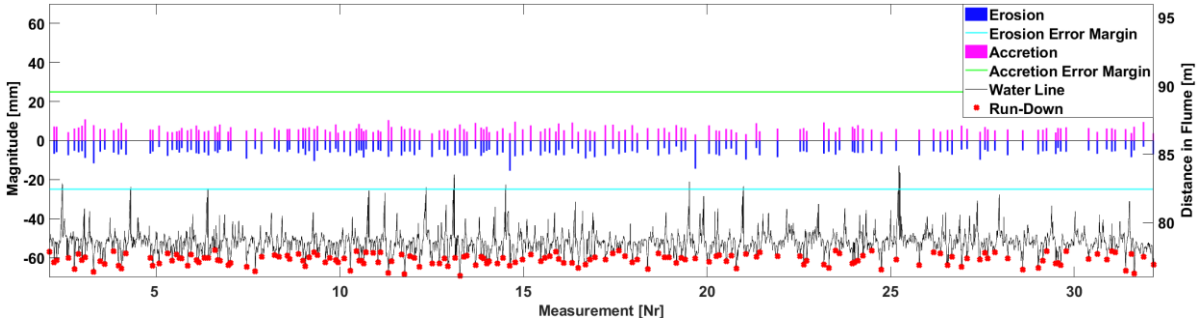

Figure 7-3: Maximum Accretion and Maximum Erosion Observed Between Consecutive Beach Profile with Provided Error

The error described by the LiDAR manufacturer does not provide a detailed description of the error along each axis (x and y) separately rather it is a total error along both axes at the same time. Therefore, assuming the total error of 25mm to be representative for both axis at the same time could be an overestimation. To see, how the assumed error influences the results Figure 7-4 was made. Here, the maximum accretion and erosion values were compared to the observed error value along the y-axis derived in Section 4.2. None of the detected maximum accretive magnitudes was smaller than the observed error at the point where the maximum accretion had been detected. Only two observed maximum erosion values were smaller than the observed error at the representative points. These two events were located at 18.58min and 31.38min measurements. Based on the results obtained from Figure 7-4, opposite results to the previous paragraph are found. To be precise, almost every identified swash event is causing a significant elevation change.

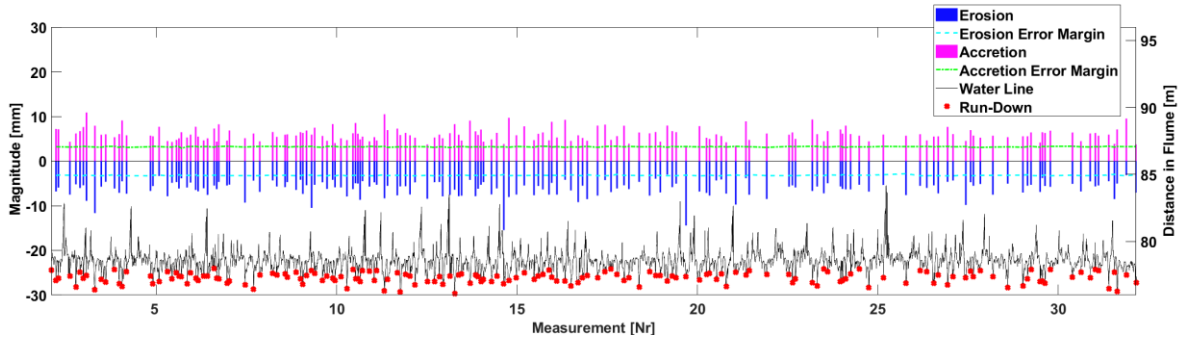

Figure 7-4: Maximum Accretion and Maximum Erosion Observed Between Consecutive Beach Profile with Observed Error

The contrary results could be explained by the fact that the difference between provided and observed error margin is roughly ~20mm. The difference between the error margins is larger than the magnitude of all observed maximum accretive and erosive events. Furthermore, the value provided by the manufacturer may be conservative and to be assumed as general and therefore not representative of the beach slope. This could be explained by observations made from Figure 4-1 to Figure 4-3. Here, the LiDAR error only sharply increases in the places, where the same measurement moving ~0.16 degrees to one or other side could have a relatively sharp increase or decrease in the value e.g., measurement of the reference box. However, since the beach slope's bed level is relatively flat, the error decreases respectively as shown in the mentioned figures. Therefore, it is assumed that the

provided error by the manufacturer is too conservative to be applied for this case.

Also of interest was the minimum possible time scale at which significant elevation changes could be detected. By making use of the data in Figure 7-3, the shortest possible time scale at which significant accretion and erosion occurred was found. For the accretion and erosion, the same event was detected – between the run-down at ~6.40min and the run-down at ~6.44min, which was 3.4 s or about the peak period of the incoming waves. The maximum accretion occurred at the 79.29m mark with a magnitude of 8mm, while the maximum erosion occurred at the 79.61 m mark with a magnitude of 4mm. At the point of maximum accretion, the pit in the beach profile was filled with sand, while, at the point of erosion, the sand ripple was washed away. This is illustrated in Figure 7-5. Besides, the run-up separating bed profiles reached the 80.51m mark. However, the confidence in the measurement accuracy could be defined as low due to the following reasons. First, the maximum accretion and erosion are in the same order of magnitude as the observed measurement error. Second, maximum accretion and erosion are based on the single-point measurement. In both cases, the point measurements are located at peaks of the different lines between profile measurements. Furthermore, in the vicinity of the peaks, the difference between the two profiles is a few mm smaller. As result, these peaks could just be caused by noise patterns in the measurement profile rather than actual bed level change induced by the swash event.

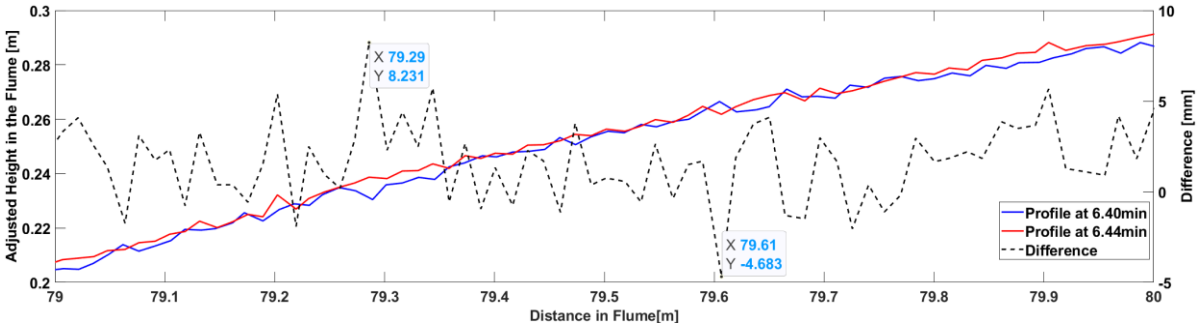

Figure 7-5: Changes Between Profiles at Minimum Time Scale

Figure 7-6 shows the difference between the first measured beach profile and the last measured beach profile at the end of the run. In the area between 78m and 80.5m, erosion has occurred. In the area between 80.5m and 83m, sand accretion has formed. After the 83m mark, no significant changes in the beach profile evolution have occurred. In general, the beach profile erosion had occurred. The total change in the area between the first and last profile was 0.05m^2.

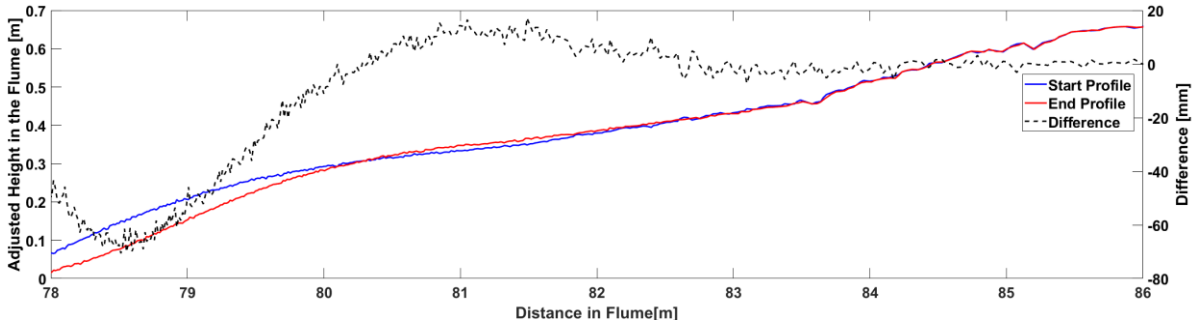

Figure 7-6: The Beach Profile at the Start of the Run and the End of the Run

Figure 7-7 and Figure 7-8 show the percentage distribution of bed level changes at the point of maximum accretion (81.49m) and erosion (78.51m) respectively. As for the maximum accretion, the bed level changes skewed, with a greater occurrence of accretion (positive) events. Most of the observed bed level changes occurring at the point of the maximum accretion are in between -2 and 2mm bed level change values. As for the point of maximum erosion, the distribution of the events has

not had a clear pattern, in other words, it is random. Similar to point of maximum accretion, also most of the bed level changes for the maximum erosion are in the boundaries between -2 and 2mm. In both cases, most of the event bed level changes measured by the LiDAR can be considered insignificant since the values are below the observed error.

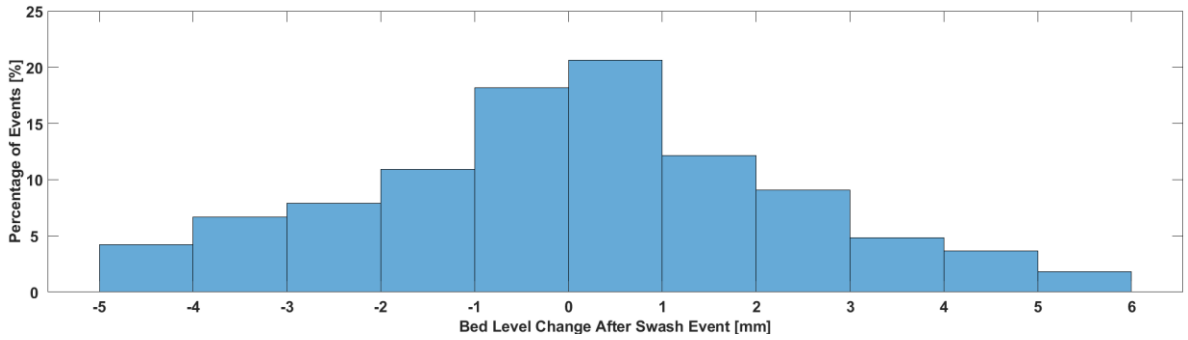

Figure 7-7: Percentage Distribution of Bed Level Change at Point of Maximum Accretion

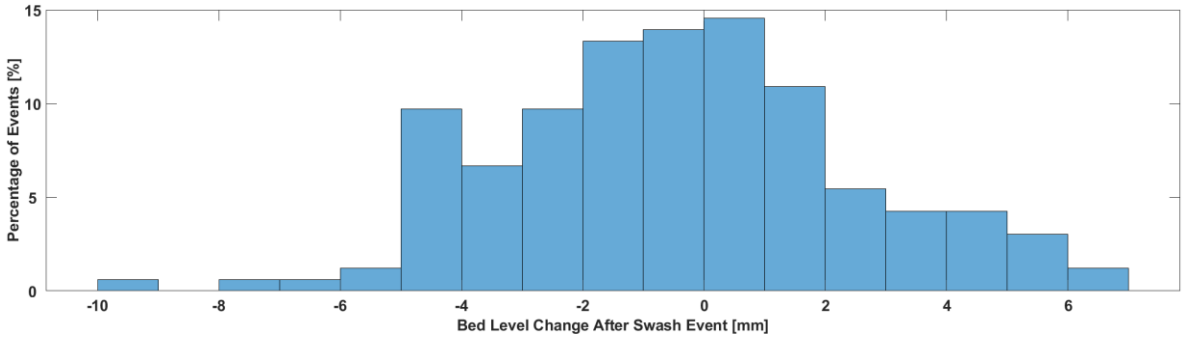

Figure 7-8:Percentage Distribution of Bed Level Change at Point of Maximum Erosion

Figure 7-9 shows the total beach slope's morphological change over time. The total morphological change between consecutive profiles does not exceed 0.025m2, while the majority of the events do not induce more change than 0.01m2. Events which are on the scale same as the net morphological of the whole measurement period were not detected, however, some of the measured inter-swash events induce the change in the area that was in the same order of magnitude as the net morphological change over the whole period. Over time the accretion is alternating with erosion. To validate that calculated changes in the area at the inter-swash scale are realistic, the sum of changes at the inter-swash scale was compared to the total change in the area between the first and last profile. The same value was calculated by subtracting the area of the last measured beach profile from the first measured beach profile and the sum of changes in the area at the inter-swash scale (0.05m^2). To conclude, with LiDAR it is not only possible to observe inter-swash changes at one particular point on the slope, but also along the full beach profile.

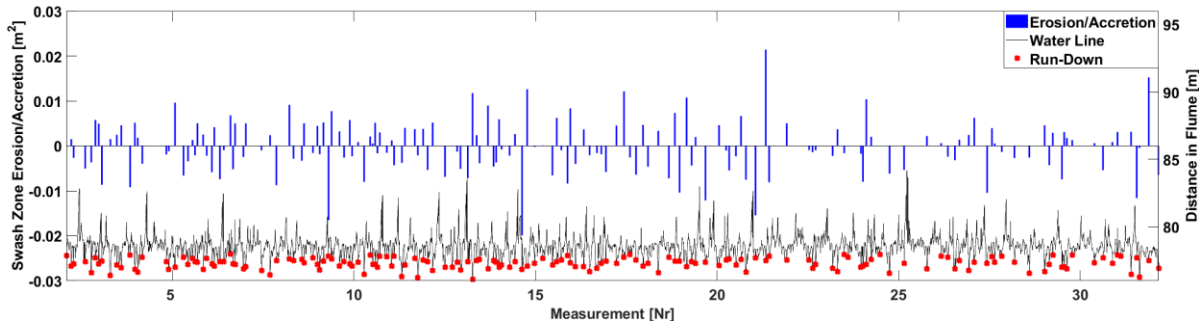

Figure 7-9: Total Beach Slope's Erosion/Accretion (positive-accretion, negative-erosion)

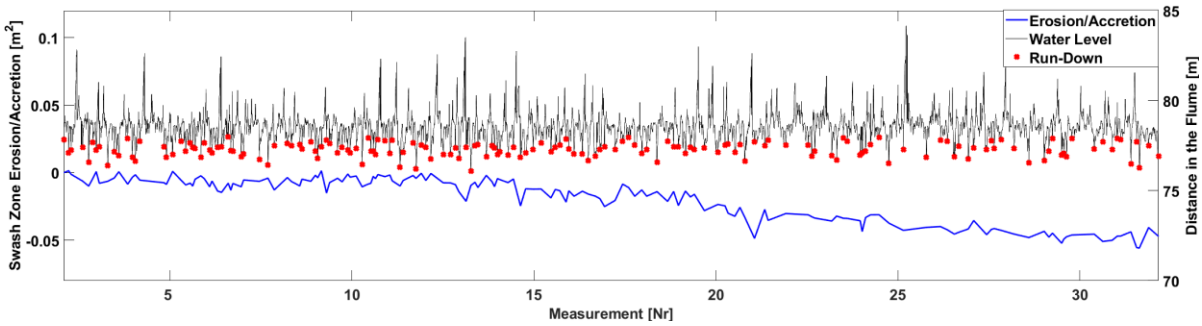

Figure 7-10: Cumulative Morphological Change of the Beach Slope

The net morphological evolution of the swash zone is shown in Figure 7-10. The net morphological change up until ~13min measurement remains almost 0 while the change in area is experiencing fluctuations. The fluctuating pattern remains also after the ~13min measurement. However, in addition to fluctuation also a gradual erosion of the swash zone occurs. In addition, it can be noticed that after relatively large erosion events (at ~9.2min, at ~14.4min and ~21.2min) the beach experiences accretion that almost returns to the previous state.

Figure 7-11 presents the difference between bed level profiles which is representative of maximum area change (~0.02m^2) after the swash event. The event occurred at ~21m in the flume run. The swash event between the bed level reached the 82.64m mark. The accretion of the bed slope was observed. Although the difference between the profiles is rapidly fluctuating, the general trend of accretion can be observed between the 79.5m and 82.5m marks. Figure 7-12 presents bed level profiles that are representative of minimum area change (2*10^{-5}m^2) after the swash event. The swash event between profiles reached the ~80m mark. The difference between bed levels is fluctuating around the 0 mm mark while kept in the boundaries between -4 and 4mm.

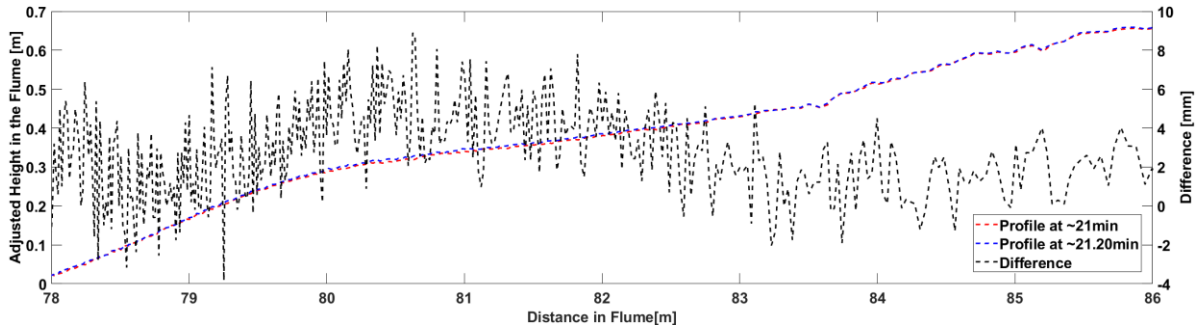

Figure 7-11: Difference Between Bed Profiles with Maximum Area Change

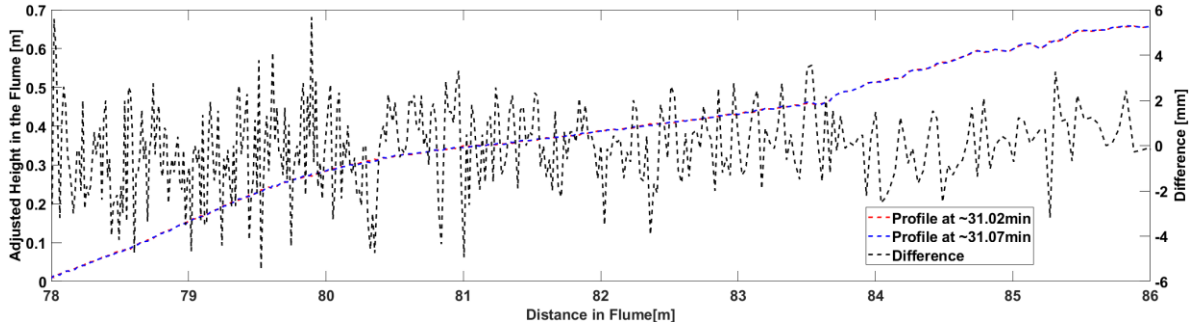

Figure 7-12: Difference Between Bed Profiles with Minimum Area Change

Figure 7-13 presents the distribution plots of the detected morphological changes in the swash zone expressed as a percentage of the occurrence. Here, the distribution of 165 events is presented in bins of 0.05m^2 large. In particular, the larger the magnitude of the erosive or accretive events, the fewer events occur. The distribution indicates that the accretive and erosive events are normally distrusted while skewed to the erosive side. The skewness is explained by the erosive nature of the measurement run.

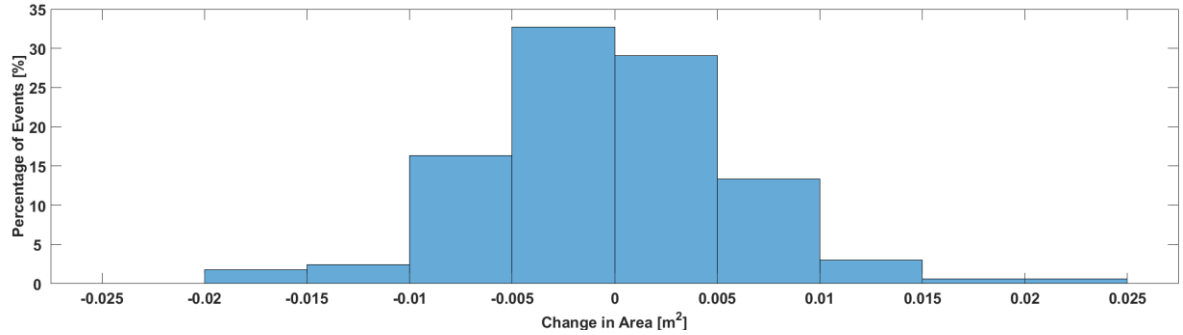

Figure 7-13: Percentage Distribution of Change in Area

Table 7-1 presents an overview of the bin size and their representative number of events and the total change induced. Most of the total change was induced by the events in the bins up to 0.010m^2, while the events in the bins from 0.015m^2 up to 0.025m^2 caused from 4x to 7x less change in the beach volume. Looking at the net contribution or the same bin sizes from accretion and erosion, it could be noticed that although the total induced change bins from 0.000m^2 to 0.005m^2 were larger compared to some of the other bins, the net contribution to the area change is neglectable. While the largest net change was caused by 0.005m^2 to 0.010m^2 bin followed by 0.015m^2 to 0.020m^2.

Table 7-1: Bins, Number of Events and Their Contribution to Total Change in Area (positive- accretion, negative- erosion)

Bin size [m²]	Number of Events in Bin [Nr.]	Total Change Induced by Events in the Bin [m²]	Net Change Induced by Same Size Bins [m²]
from 0.025 to 0.020	1	0.0214	0.0214
from 0.020 to 0.015	1	0.0152	-0.0366
from 0.015 to 0.010	5	0.0576	0.0130
from 0.010 to 0.005	22	0.1402	-0.0434
from 0.005 to 0.000	48	0.1201	-0.0016
from 0.000 to -0.005	54	-0.1217	-
from -0.005 to -0.010	27	-0.1836	-
from -0.010 to -0.015	4	-0.0446	-
from -0.015 to -0.020	3	-0.0518	-
Sum of Values	165	-0.0472	-0.0472

Figure 7-14 presents a correlation between the swash zone change and the time of the swash events. The correlation between swash event and event time has a Pearson coefficient of 0.01 meaning that no correlation was found between the two variables. The reason why no correlation was found could be explained by the fact that relatively longer swash events (> few seconds) is representing a group of relatively larger and smaller swash events for which the water does not retreat below a 78m mark. As a result, the mix of events induces both accretion and erosion during the same swash event leading to a relatively smaller net change in the swash event.

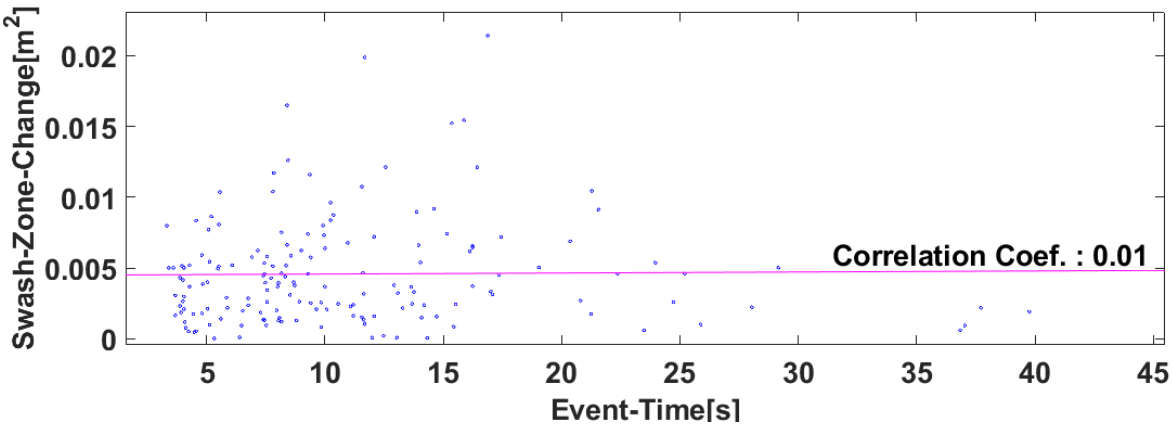

Figure 7-14: Correlation Between Change in Swash Zone and Event Time

8. DISCUSSION

In this section, the results of the research are discussed. For each of the three components (comparison/context, practical implication and uncertainties) of the research, a separate subsection is presented.

Comparison/Context

Vousdoukas et al. (2014) studied the swash zone morphodynamics with the use of LiDAR. Vousdoukas et al. (2014) stated that measurements by ultrasonic sensors are more accurate than LiDAR measurements. In particular, the difference between ultrasonic sensors and LiDAR (SICK LMS291) bed level measurements along the vertical axis was in general ~ 4.00mm, however, in some cases it could reach up to 20mm. Blenkinsopp, Mole, & Peirson (2010) studied time-varying free-surface profiles across the swash zone using an industrial LIDAR (SICK LMS511). Blenkinsopp, Mole, & Peirson (2010) found that the static bed level horizontal error is ~5.00mm and vertical error is up to ~2.50 mm. In this research, the LiDAR (SICK LMS511) error of static bed measurement was below ~5.00mm along the both horizontal and vertical axis. In general, the results between similar, however, the differences between the results could be explained by a variety of factors e.g., the use of different LiDAR devices that what difference errors, the position of the LiDAR relative to slope, materials (sand) surface reflectivity, and the LiDAR beam footprints at the point measurement.

Almeida et al. (2014) studied gravel beach dynamics during high wave energy conditions with LiDAR SICK LD-OEM3100 (statistical error of ±38mm). Almeida et al. (2014) applied the same variance method (equation 3-5) to separate water and bed levels by defining arbitrary thresholds for separating the water level from the bed level. The researchers concluded that parts of the swash lens at which the water level is <15mm were not captured. Similar to Almeida et al. (2014), in this research parts of the swash lens where the water column was shallower than ~20.00mm were not captured accurately. Comparable values across research indicate that method has the threshold for the water level. In other words, if the water column is thinner than the previously mentioned values, the LiDAR is not capable anymore to distinguish water level from bed level. The reason for it could be found explained by the fact, that if the water column is already thinner than ~40.00mm, the LiDAR beams can penetrate the water column. As result, the measurement of water level is interpreted as water level.

For the maximum bed elevation changes along a vertical dimension that can occur at the inter-swash scale, Vousdoukas et al. (2014) observed events that induced changes in general up to ~10.00mm. However, also events with a magnitude of ~100.00mm were observed. The relatively larger changes in the bed profile were associated with the swash berm's avalanching. However, the maximum morphological change at the inter-swash scale value found in this research was only 16.00mm, which is almost 1 order of magnitude smaller than in the research done by Vousdoukas et al. (2014). This difference in the observations of both studies could be related to the shape of the beach, its morphological state and the wave conditions it was exposed. Although the beach slopes were the same (1:15) in both experiments, the wave conditions to which these slopes were exposed were different. For example, in Vousdoukas et al. (2014) waves were 0.51m in height and the wave period was 7s while in this research wave height was 0.55m and the wave period was 3.5s. Although in general steeper waves in this study should have caused more bed level changes than in Vousdoukas et al. (2014), the opposite was found.

The findings of this research were similar to the findings by Blenkinsopp et al. (2012) who analysed the sediment fluxes in the swash zone over various tidal cycles:

1. The net morphological change of the swash zone was characterized by frequent reversal between accretion and erosion (Figure 7-10).

2. Relatively larger accretive or erosive events were balanced by relatively smaller events that do not allow the beach face volume to rapidly accrete or erode (Figure 7-10).
3. Accretive and erosive events were normally distributed (Figure 7-13). In addition, isolated swash events which were in the same order of magnitude as the net morphological development of the beach were also observed.

Although Blenkinsopp et al. (2012) made use of a natural environmental setting where wave heights and wave periods were varied in the range of 0.9m to 4.1m and 5s to 13s, the sediment grains were 0.4mm large and tidal amplitude up to 4.3m was present, similar morphological evolution of the beach slope was also captured in this study. These findings suggest, that the beach slope has a general pattern of evolution thus indicating a predictable behaviour of the swash zone. Besides, since the relatively smaller events do mix with relatively larger events, to successfully capture the behaviour of the beach slope, both relatively smaller and larger morphodynamical events have to be captured accurately.

Practical Implications

The LiDAR measurements with relatively high spatial and temporal density in the raw format required data processing for further analysis of the natural processes. Even after data processing, not all natural processes can be completely captured. In particular, one of the most challenging aspects is separating the water level from the bed level in the swash zone. Both previous and this research shows that if the LiDAR is used to capture the swash run-up lens, parts of the run-up events where the water depth is less than ~20mm cannot be captured accurately. However, based on the interest of the research, it is possible to apply different methods to extract the water line according to the need of the research. For example, if the temporal variability of the water line is of interest, then it is advised to apply the RSSI method since it can capture the temporal variability much more accurately than the variance method. In addition, by applying this method, it was noticed, that the method tends to underestimate the water line on the beach slope, in other words, the derived water line with this method tends to be located more offshore than realistically occurring. However, if bed levels are of interest and the water level needs to be separated from the bed level, then it is recommended to apply the variance method due to its ability to better capture the upper limits of the swash lens, which is achieved by the methods ability to follow the thinner water column parts on the beach slope.

The findings of the study show that when LiDAR is applied to study bed level changes induced by swash events, the majority of the time, the bed level changes are either below the LiDAR error margin or in the same magnitude as the LiDAR error. This indicates, that the bed level changes could not be interpreted as significant or, in other words, not accurate enough to deterministically state that the measurements are accurate at the inter-swash scale.

Also, no correlation between the swash event duration and the swash zone change was not found. Other researchers in the field (Li, 2016), state that change in the swash zone is related to the water velocities, wave steepness, wave irregularity and spectral width factor. Although it can be roughly estimated that longer events are related to higher water velocities, the longer events in this research represented a set of swash events rather than one particular uprush and downrush. As a result, in the longer swash events both accretion and erosion occurred rather than only one of the latter.

Uncertainties

The LiDAR manual (SICK AG, 2017) does not specifically address the LiDAR error along each of the axes (horizontal and vertical) separately, but the total error along both axes is presented. Therefore, separating measurements for each axis and making an assumption that the total error of 25mm occurring in both directions is the maximum error for each of the axes might not be the entirely correct approach.

When validating the extracted water lines, the researcher observation of maximum run-up, average run-up and maximum run-down during the flume experiment was made using. Especially, for average run-up and maximum run-down, the error boundaries in which the measurement values could vary were not indicated by researchers. As a result, when validating the water lines, it was impossible to deterministically say, if extracted average run-up and maximum run-down were within allowed error boundaries or not.

Also, the LiDAR error under dynamic conditions remains unknown, thus limiting the definitive conclusion of the accuracy of the extracted water line and bed level changes. Although the LiDAR error of the water line under dynamic conditions could be determined by making use of the water line data gathered with AWG, the data was not used in this research due to miscommunication between the parties. Besides, Vousdoukas et al. (2014) mentioned that under wave conditions the LiDAR error can increase by an order of magnitude. So, in this case, the error increased from ~5.00mm to roughly ~50.00 mm which could partly explain the relatively large difference (~1m) between the extracted maximum run-up value and researched observed maximum run-up value.

One of the uncertainties related to bed level changes is the accuracy of the LiDAR measured static bed profiles before and after slopes exposure to wave conditions. Although based on the validation section, the static bed profiles should be accurate, to further introduce unambiguous evidence of LiDAR accuracy, the LiDAR and bed slope profiler data could be compared. However, in this case, it was not done due to miscommunication between parties involved in the research.

9. CONCLUSIONS

The current research aimed to determine whether the LiDAR can be used to quantify inter-swash morphodynamic changes to explore the contribution of individual swash events to the longer-term, event-averaged morphological evolution on a sandy beach. Below the findings related to each of the research questions are summarized.

How accurate is the LiDAR data?

For all of the boxes, the box's representative edge was detected with the LiDAR within the theoretical error margin. The theoretical error margin along the x-axis consisted of the sum of the LiDAR error provided by the manufacturer (±25.00mm) and the manual measurement error (±30.00mm). Besides, the LiDAR error along the x-axis for the majority of the spatial point representing the bed profile did not exceed 5.00mm. However, at the points of the reference boxes, the error could reach up to ~35.00mm.

The LiDAR accuracy along the y-axis was evaluated by comparing the beach slope measured with LiDAR to the beach slope measured with an automated slope profiler. Along the y-axis, the upper error limit consisted of the LiDAR error provided by the manufacturer (±25.00mm) and the slope profiler error along the y-axis (±10.00mm) sum and the lower error limit LiDAR error along the full bed profile (<±~4.00mm) to the profiler's vertical error margin (±10.00 mm). Although for most of the profiles, the LiDAR measurements were the below both error margins, there were parts in which the difference between the bed profiles measured exceeded the defined margin. The points at which the latter occurred were related to inconsistencies between the measured bed profiles e.g., at the 81.5m distance mark the error between profiles exceeded the defined error margins due to the presence of a pit only in the bed level measured by slope profiler.

Under present laboratory conditions, it was found that the LiDAR error along both the axis of static bed level is roughly ±5.00mm, which was derived based on the calculations of the standard deviation. Therefore, when studying the inter-swash morphological changes on the beach, the LiDAR error must be included as part of the measurement value.

How to identify swash events in the LiDAR data?

To separate the bed level from the water surface in LiDAR measurements, two general methods can be applied: filtering based on the measurement variance (Almeida et al., 2014) and based on relative signal strength index (RSSI). Additionally, the variance method was applied using the observed static bed variance or a decreased observed variance threshold. The variance method was found to be capable to follow the thinner parts run-up lens much more closely than the RSSI method based on the relative elevation image. However, the RSSI method is predicting the temporal variability of the water line better than the variance method and thus helps in isolating individual swash events. Nevertheless, the RSSI method cannot capture water columns thinner than ~20mm.

To identify the separate swash events, a run-down threshold must be applied to the water line. The selected threshold is required to only capture the events in which the run-down exceeds the threshold value, hence serving as a point where one swash event ends and the following starts.

In total 165 swash events were identified. The average period of the determined swash events was 11.0s or ~3 peak periods of the incoming waves. The swash events had a skewed distribution, with a greater occurrence of events with shorter periods. The majority (147 out of 165) of the swash events were shorter than 17.5s. Only a few events were observed with a length of≥ 35s.

To calculate the bed level changes for individual swash events and a group of swash events scale, the water level derived with overserved static bed variance was found most appropriate, since it does not underestimate the water line which then could interfere with bed level calculations.

What is the contribution of individual swash events or groups of swash events to the total net morphological change of the beach?

When examining if the swash events could cause significant bed level changes at point measurements contrary measurements were found. In particular, if the LIDAR's manufacturer error is applied not measurements, then none of the observed bed level changes at the inter-swash scale could be considered significant. However, if the observed error is applied to determining bed level values, almost every point bed level change could be defined as significant. However, in this case, the LiDAR error and the determined bed level changes are in the same order of magnitude indicating low confidence in the measured values.

When applied the observed LiDAR error to determine the smallest time scale at which accretion and erosion greater than the computed error margin observed were 3.4s. This event occurred at the 6^{th} min of the flume run. However, also here the confidence in the detected value remains low. Over a ~30minute period the beach experiences a maximum erosion of ~71mm at the 78.51m mark and maximum accretion of ~22mm at the 81.49m distance mark in the flume. Most of the observed bed level changes occurring at the point of the maximum accretion and erosion are between -2 and 2mm which is below the observed LiDAR error or in other words insignificant. Inconsistency has been noted in the representation of the erosion and accretion pattern in the relative elevation image. In Figure 7-6, where the beach profile at the start and end is shown, it can be seen that the erosion pit ends at approximately 80m, while the accretion area spans from ~80m to ~83m. However, in the relative elevation image the erosion pit extends up to the 81m mark and the accretion area is located between 81m to 84m (Figure 5-1).

In total out of 165 swash events, 77 were accretive and 88 erosive. In general, the distribution of the events was skewed to the erosive side. For all events, the total induced morphological change of the swash zone was smaller than $0.025m^2$. Most of the bed level changes were induced by events that caused less than $0.005m^2$ accretion or erosion. However, from the net perspective, accretive and erosive events with magnitudes between 0.005 to 0.010 m^2 had the largest impact on the beach development which is between one-fourth and one-half of the total morphological change of the bed profile. Besides, no correlation between event time and swash zone change was found.

Although the LiDAR can detect the changes in bed level at an inter-swash scale, most of the bed level changes measured are considered insignificant or, in other words, smaller than the device error made for each measurement. Therefore, it is recommended not to use SICK LiDAR LSM511 to detect bed level changes at the inter-swash scale unless proven otherwise.

10. RECOMMENDATIONS

Following the findings of this study, several recommendations for further research are summarized below:

1) To further improve the LiDAR accuracy of the measurements a hybrid measurement system could be utilized as mentioned by Vousdoukas, et al., (2014). In particular, a variety of measurement devices could be used to measure the same phenomenon, for example, water levels at the same time could be measured with a precise video monitoring system, LiDAR and ultrasonic sensors. Once the data is gathered, it then could be compared to each other to achieve higher accuracy of the data. Additionally, Blenkinsopp, Mole, & Peirson (2010) mentions the post-processing of the LiDAR data is required. In particular, in this research, the focus was only time-dimension, but Blenkinsopp, Mole, & Peirson (2010) emphasizes that post-processing of spatial dimension is also required.
2) To increase the sample size and further evaluate the LiDAR accuracy of the bed level under static conditions, the profiler bed level data of bed level before and after wave exposure could have been used.
3) To determine the LiDAR error under dynamic conditions (e.g., the accuracy of the temporally varying water line), the neglected AWG data sets of the research could be used.
4) The method of RSSI separating the bed level from the water level provided promising results. Especially, it was able to capture the temporal variability of the water line better than the method of variance. Therefore, it is advised to investigate this method further. In particular, a more robust prediction model for the RSSI values of sand is necessary because, at the current state, the theoretical derived dry bed RSSI values at the end of the flume run did not match the measured values as close as the ones at the beginning of the run (Figure 6-7 and Figure 6-10).
5) If the flume experiment is redone, the location of the LiDAR monitoring device could be changed to the swash zone to achieve better accuracy. For example, since the LiDAR error is based on the object's distance to the device, the device could also be located closer to the beach profile itself, thus also limiting the beam diameter and horizontal spacing between the beams.

11. BIBLIOGRAPHY

Aagaard, T., & Hughes, M. (2006). Sediment suspension and turbulence in the swash zone of dissipative beaches. *Marine Geology*, 117-135. doi:dx.doi.org/10.1016/j.margeo.2006.01.003

Almeida, L., Almar, R., Blenkinsopp, C., Senechal, N., Bergsma, E., Floc'h, F., . . . Viet, N. (2020). Lidar Observations of the Swash Zone of a Low-Tide Terraced Tropical Beach under Variable Wave Conditions: The Nha Trang (Vietnam) COASTVAR Experiment. *Marine Science and Engineering*, 1-18. doi:doi:10.3390/jmse8050302

Almeida, L., G.Masselink, Russel, P., & Davidson, M. (2014). Observations of gravel beach dynamics during high energy wave. *Geomorphology*, 15-27. doi:10.1016/j.geomorph.2014.08.019

Austin, M., Masselink, G., O'Hare, T., & Russel, P. (2009). Onshore sediment transport on a sandy beach under varied wave conditions: Flow velocity skewness, wave asymmetry or bed ventilation? *Marine Geology*, 86-101. doi:10.1016/j.margeo.2009.01.001

Bagnold, R. (219-232). The shearing and dilatation of dry sand and the “singing” mechanism. *Proc. R. Soc. Math. Phys.*

Baldock, T. &. (2006). Field observations of instantaneous water slopes and horizontal pressure gradients in the swash-zone. *Cont. Shelf Res.*, 574-588. doi:10.1016/j.csr.2006.02.003

Bergsma, E., Blenkinsopp, C., Martins, K., Almar, R., & De Almeida, L. (2019). Bore collapse and wave run-up on a sandy beach. *Continental Shelf Research*, 132-139. doi:10.1016/j.csr.2019.01.009

Blenkinsopp, C. E., Mole, M. A., & Peirson, W. L. (2010). Measurements of the time-varying free-surface profile across the swash zone were obtained using an industrial LIDAR. *Coastal Engineering*, 57(11-12), 1059–1065. doi:10.1016/j.coastaleng.20

Blenkinsopp, C., T. ,., M. ,., & R. P. (2010). Validation of volume continuity method for estimation of cross-shore. *Coastal Engineering*, 953-958. doi:10.1016/j.coastaleng.2010.05.005

Blenkinsopp, C., Turner, I., Allis, M., Peirson, W., & Garden, L. (2012). Application of lidar technology for the measurement of time-varying free-surface profiles in a laboratory wave flume. *Coastal Engineering*, 1-5. doi:10.1016/ j.coastaleng.2012.04.006

Brocchini, M., & Baldock, T. (2008). Recent advances in modelling swash zone dynamics: Influence of surf-swash interaction on nearshore hydrodynamics and morphodynamics. *Reviews of Geophysics*, 1-21. doi:10.1029/2006RG000215

Caceres, I., & Alsina, J. M. (2012). A detailed, event-by-event analysis of suspended sediment concentration in the swash zone. *Continental Shelf Research*, 61-76. doi:10.1016/j.csr.2012.04.004

Chardón-Maldonado, P., Pintado-Patiño, J., & Puleo, J. (2015). Advances in swash-zone research: Small-scale hydrodynamic and sediment transport processes. *Coastal Engineering*, 1-18. doi:10.1016/j.coastaleng.2015.10.008

Conley, D., & Inman, D. (1994). Ventilated oscillatory boundary layers. *Journal of Fluid Mechanics*, 261-284.

Deltares. (2017, November 20). *Study of sand-grain movement in the swash zone*. Retrieved from deltares.nl: https://www.deltares.nl/en/news/study-of-sand-grain-movement-in-the-swash-zone/

Dionísio Antónioa, S., Werf, v. J., Horstman, E., Cáceres, I., Alsina, J., Zanden, v. J., & Hulscher, S. (2021). Influence of beach slope on morphological changes and sediment transport under irregular waves. *Not Yet Published*, -.

Grasso, F., Michallet, H., & Barthelemy, E. (2011). Sediment transport is associated with morphological beach changes forced by irregular asymmetric, skewed waves. *Journal of Geophysical Research*, 116-126. doi:10.1029/2010JC006550

Hardisty, J. (1986). A morphodynamic model for beach gradients. *Earth Surface Processes and Landforms*, 327-333.

Harry, M., Zhang, H., Lemckert, C., Colleter, G., & Blenkinsopp, C. (2018). Observation of surf zone wave transformation using LiDAR. *Applied Ocean Research*, 88-98. doi:doi:10.1016/j.apor.2018.05.015

Hughes, M., & Baldock, T. (2020). *The Swash Zone.* Brisbane: NSW Department of Planning Industry and Environment. doi:10.1016/b978-0-08-102927-5.00008-4

Hughes, M., & Moseley, A. (2007). Hydrokinetic regions within the swash zone. *Continental Shelf Research*, 2000-2013. doi:10.1016/j.csr.2007.04.005

Komar, P. (1998). Beach Processes and Sedimentation. *Englewood Cliffs, NJ.: Prentice-Hall*.

Kranenburg, W. R. (2012). Net currents in the wave bottom boundary layer: on waveshape streaming and progressive wave streaming. *J. Geophys. Res. Earth Surf.*, F03005. doi:10.1029/2011JF002070

Larson, M., Kubota, S., & Erikson, L. (2004). Swash-zone sediment transport and foreshore evolution: Field experiments and mathematical modelling. *Marine Geology*, 61-79. doi:10.1016/j.margeo.2004.08.004

Li, Z. (2016). Relationship between high-frequency sediment-level oscillations in the swash zone and inner surf zone wave characteristics under calm wave conditions. Open Geosciences. doi.org/10.1515/geo-2016-0058

Martins, K., Blenkinsopp, C., & Zang, J. (2016). Monitoring Individual Wave Characteristics in the Inner Surf with a 2-Dimensional Laser Scanner (LiDAR. *Journal of Sensors*, 20-31. doi:dx.doi.org/10.1155/2016/7965431

Masselink, G. &. (1998). Field investigation of sediment transport in the swash zone. *Continental Shelf Research*, 1179-1199. doi:10.1029/2005JC002893

Masselink, G., & Puleo, J. (2006). Swash-zone morphodynamics. *Continental Shelf Research*, 661-680. doi:10.1016/j.csr.2006.01.015

Masselink, G., Russell, P., Turner, I., & Blenkinsopp, C. (2009). Net sediment transport and morphological change in the swash zone of a high-energy sandy beach from swash event to tidal cycle time scales. *Marine Geology*, 18-35. doi:10.1016/j.margeo.2009.09.003

Nielsen, P., Robert, S., Moller-Christiansen, B., & Olivia, P. (2001). Infiltration affects sediment mobility under waves. *Coastal Engineering*, 105-114.

Pedrozo-Acuña, A. d.-A.-F. (2011). Laboratory investigation of pressure gradients induced by plunging breakers. *Coastal Engineering*, 722-738. doi:10.1016/j.coastaleng.2011.03.013

Pritchard, D. &. (1-23). On the transport of suspended sediment by a swash event on a plane beach. *Coastal Engineering*.

Puleo, J., Beach, R., Holman, R., & Allen, J. (2000). Swash zone sediment suspension and transport and the importance of bore-generated turbulence. *J. Geophys. Res. Oceans*, 17021-17044. doi:dx.doi.org/10.1029/2000JC900024

Shields. (1936). Application of similarity principles and turbulence research to a bed-load movement. *Technical Report*.

SICK. (2022). *Product Portfolio for detection and ranging solutions*. Retrieved from 2D LiDAR sensors: https://www.sick.com/ag/en/detection-and-ranging-solutions/2d-lidar-sensors/lms5xx/lms500-20000s01/p/p476045?ff_data=JmZmX2lkPXA0NzYwNDUmZmZfbWFzdGVySWQ9cDQ3NjA0NSZmZl90aXRsZT1MTVM1MDAtMjAwMDBTMDEmZmZfcXVlcnk9JmZmX3Bvcz0xNCZmZl9vcmlnUG9zPTE0JmZmX3BhZ2U9MS

SICK AG. (2017). *LMS5xx Laser Measurement Sensor Operating Instruction.* Waldkirch: SICK AG.

Sobel, I., & Feldman, G. (2014). An Isotropic 3x3 Image Gradient Operator. *Computer Science*. doi:10.13140/RG.2.1.1912.4965

Sou, I., Cowen, E., & Liu, P. (2010). Evolution of the turbulence structure in the surf and swash zones. *J. Fluid Mech.*, 193-216. doi:dx.doi.org/10.1017/S0022112009992321

Stringari, C., & Power, H. (2021). LiDAR Observations of Multi-Modal Swash Probability Distributions on a Dissipative Beach. *Remote Sensing*, 1-16. doi:doi.org/10.3390/rs13030462

The MathWorks, Inc. (2022, August 9). *MathWorks*. Retrieved from MathWorks Help Center: https://se.mathworks.com/help/matlab/ref/trapz.html

Van Thield De Vries, J. (2009). Dune erosion during storm surges. *Deltares Select Series*.

Vousdoukas, M. I., Kirupakaramoorthy, T., Oumeraci, H., de la Torre, M., Wübbold, F., Wagner, B., & Schimmels, S. (2014). The role of combined laser scanning and video techniques in monitoring wave-by-wave swash zone processes. *Coastal Engineering*, 150-165. doi:10.1016/j.coastaleng.2013.10.013

Zanden, v. d., Cáceres, I., Eichentopf, S., Ribberink, J., Werfd, v. d., & Alsina, J. (2019). Sand transport processes and bed level changes are induced by two alternating laboratory swash events. *Coastal Engineering*, 1-20. doi:doi.org/10.1016/j.coastaleng.2019.103519

Zhang, Q., & Liu, P.-F. (2008). A numerical study of swash flows generated by bores. *Coast.Eng.*, 1113-1134. doi:dx.doi.org/10.1016/j.coastaleng.2008.04.010

APPENDIX A - VARYING VARIANCE

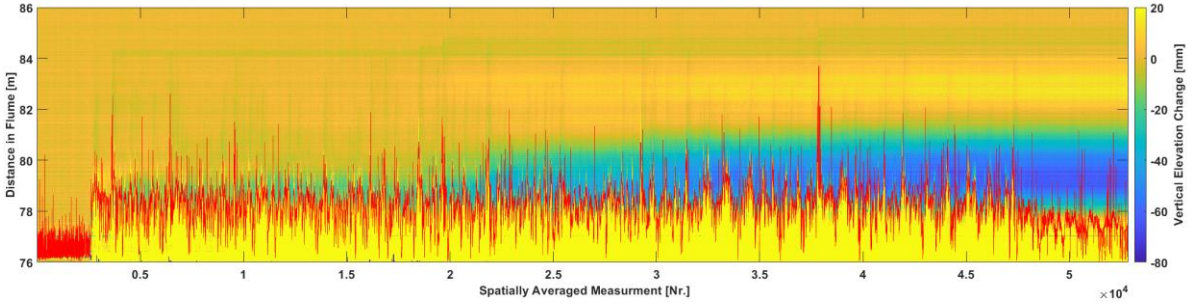

Figure 11-1: Temporal Smoothing with Variance Window of 5 and Temporal Window of 5

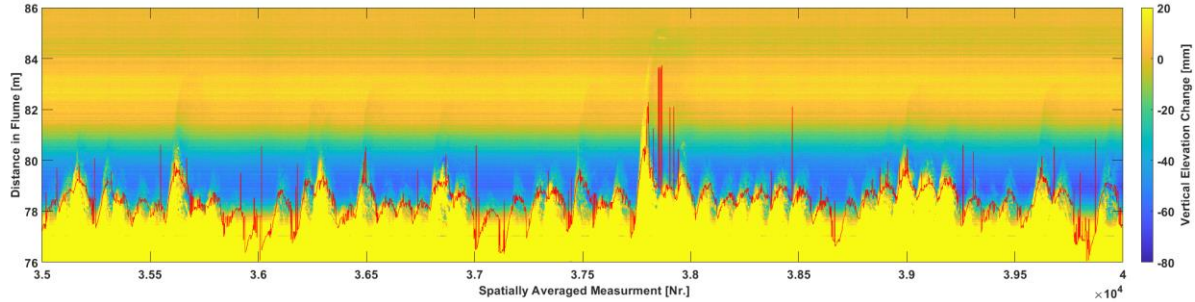

Figure 11-2: Zoomed Section of the Temporal Smoothing with Variance Window of 5 and Temporal Window of 5

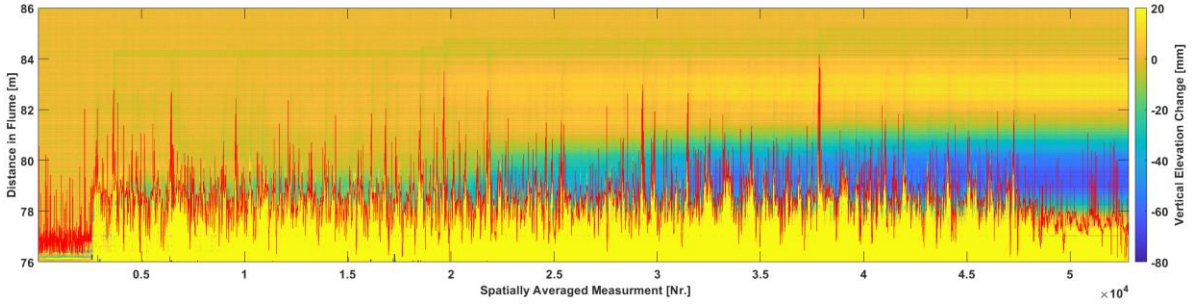

Figure 11-3: Temporal Smoothing with Variance Window of 15 and Temporal Window of 5

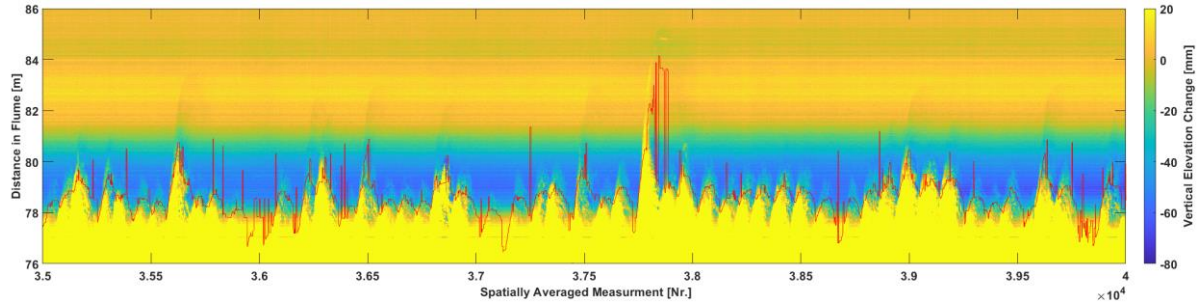

Figure 11-4: Zoomed Section of the Temporal Smoothing with Variance Window of 15 and Temporal Window of 5

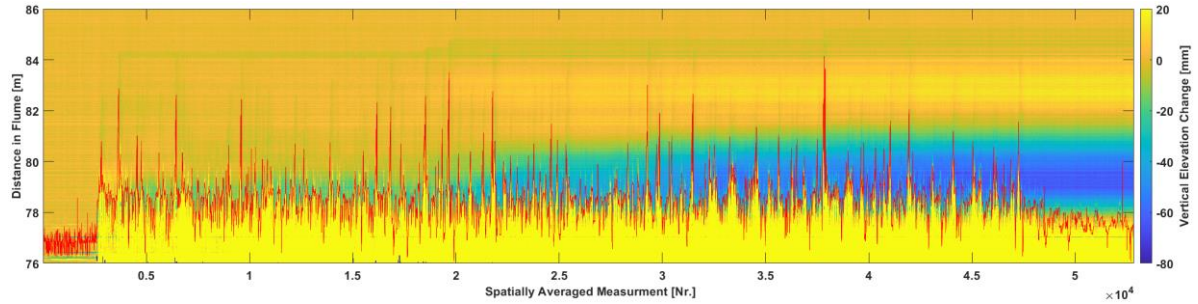

Figure 11-5: Temporal Smoothing with Variance Window of 25 and Temporal Window of 5

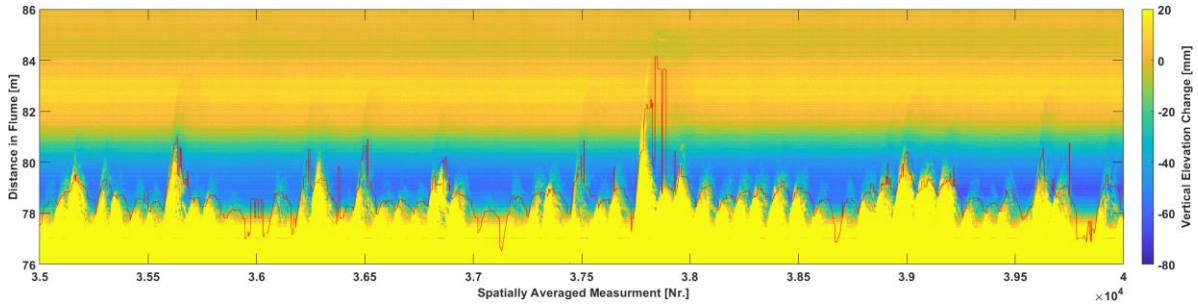

Figure 11-6: Zoomed Section of the Temporal Smoothing with Variance Window of 25 and Temporal Window of 5

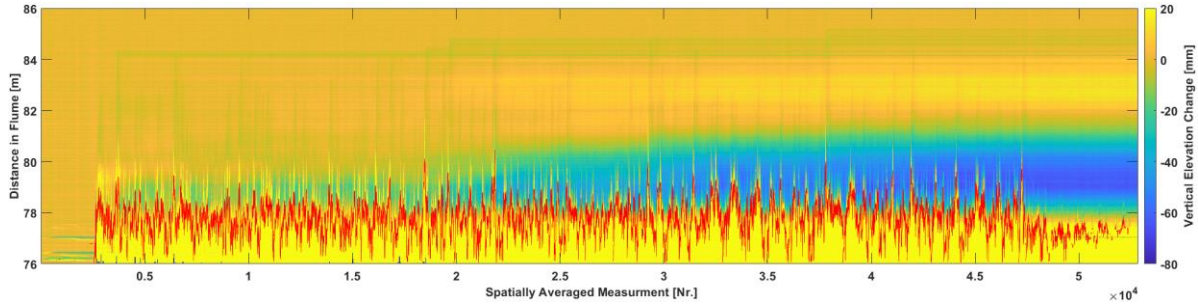

Figure 11-7: Temporal Smoothing with Variance Window of 5 and Temporal Window of 15

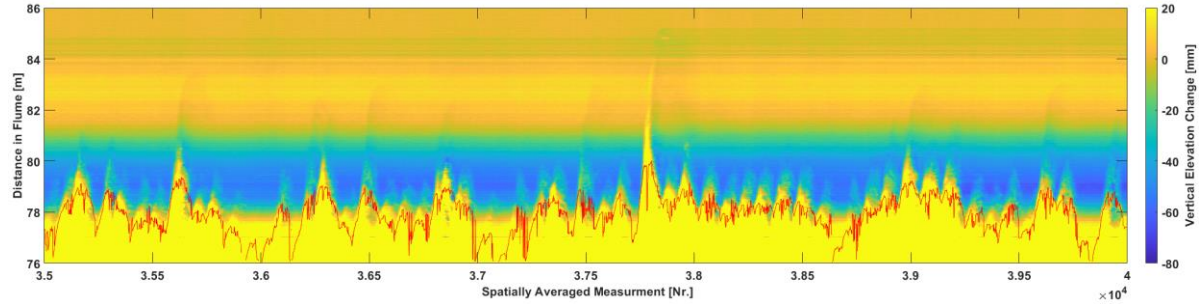

Figure 11-8: Zoomed Section of the Temporal Smoothing with Variance Window of 5 and Temporal Window of 15

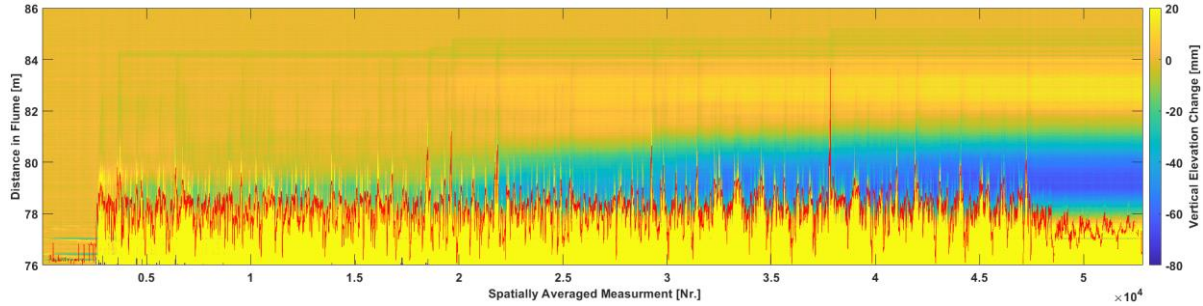

Figure 11-9: Temporal Smoothing with Variance Window of 15 and Temporal Window of 15

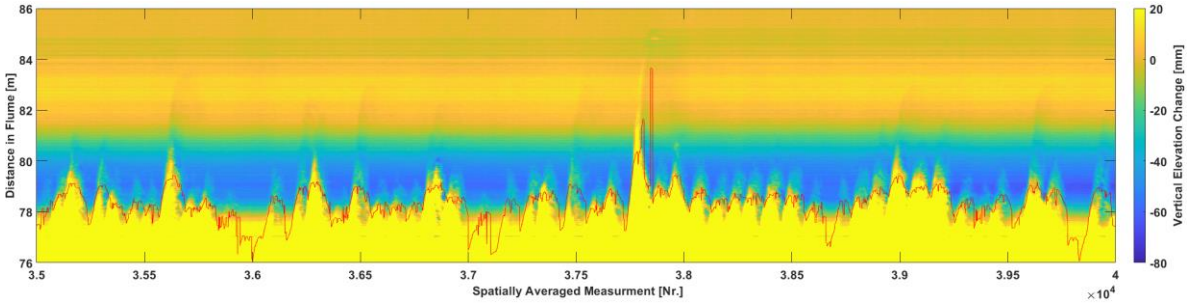

Figure 11-10: Zoomed Section of the Temporal Smoothing with Variance Window of 15 and Temporal Window of 15

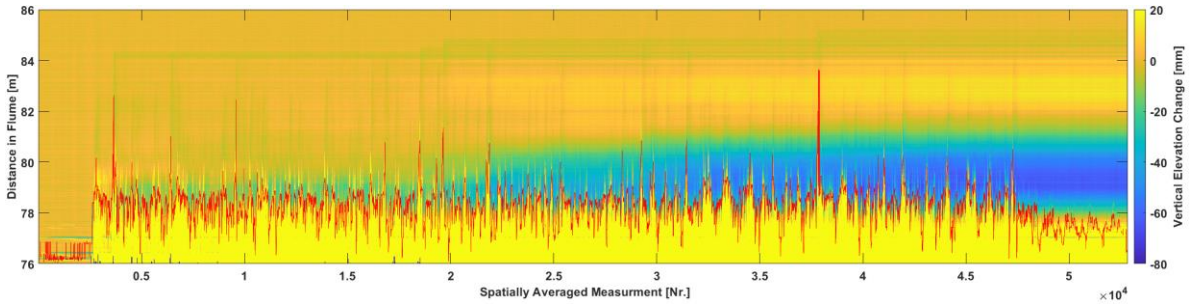

Figure 11-11: Temporal Smoothing with Variance Window of 25 and Temporal Window of 15

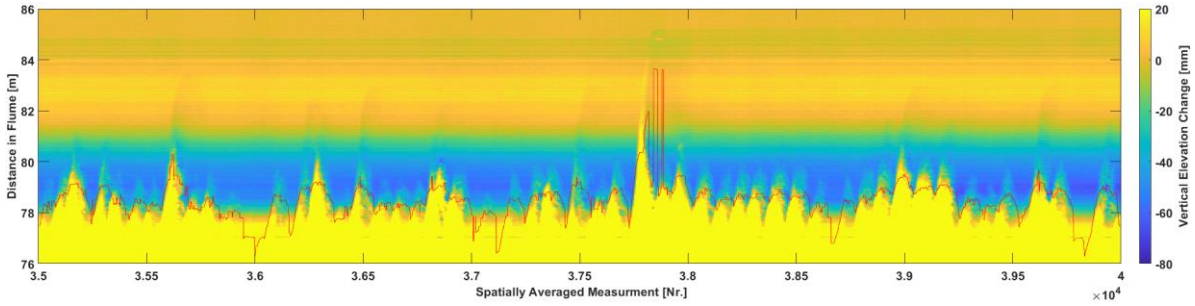

Figure 11-12: Zoomed Section of the Temporal Smoothing with Variance Window of 25 and Temporal Window of 15

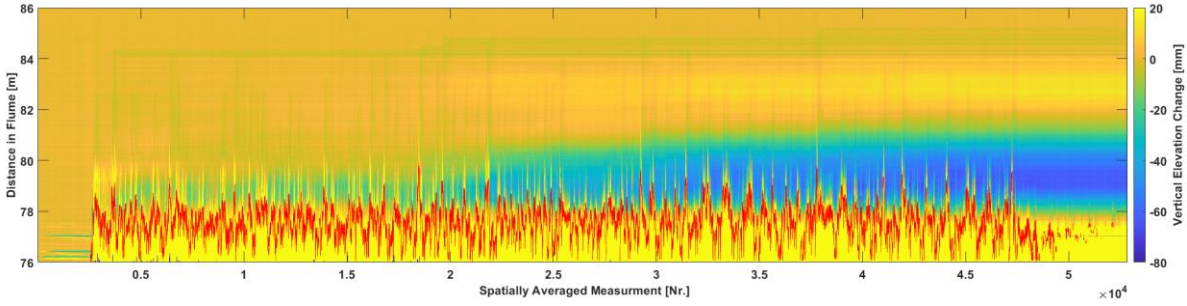

Figure 11-13: Temporal Smoothing with Variance Window of 5 and Temporal Window of 25

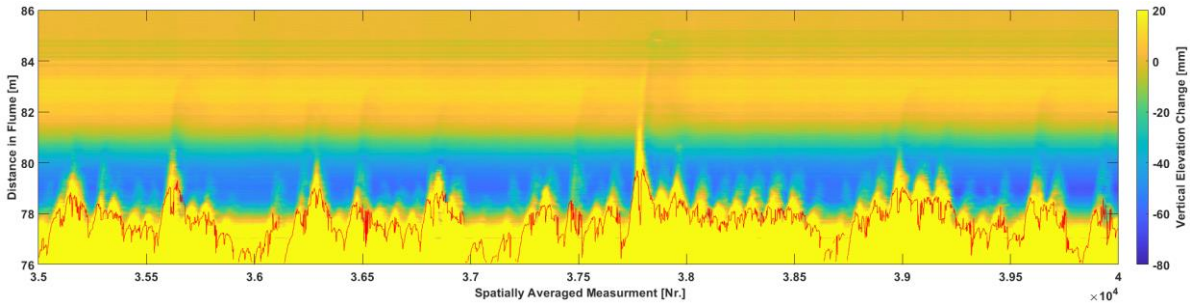

Figure 11-14: Zoomed Section of the Temporal Smoothing with Variance Window of 5 and Temporal Window of 25

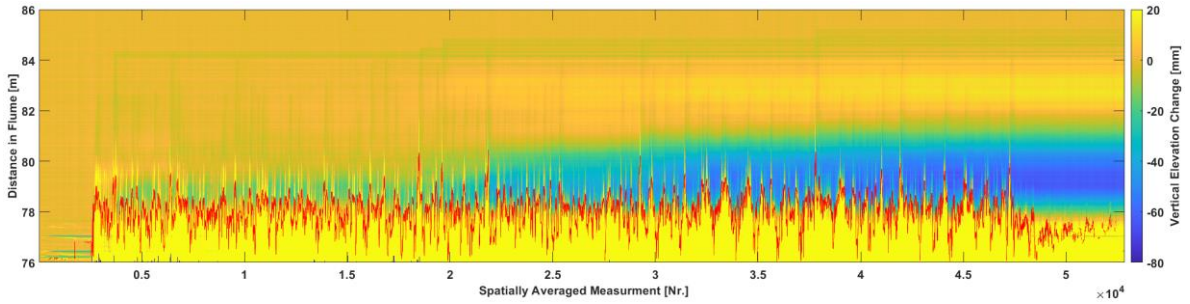

Figure 11-15: Temporal Smoothing with Variance Window of 15 and Temporal Window of 25

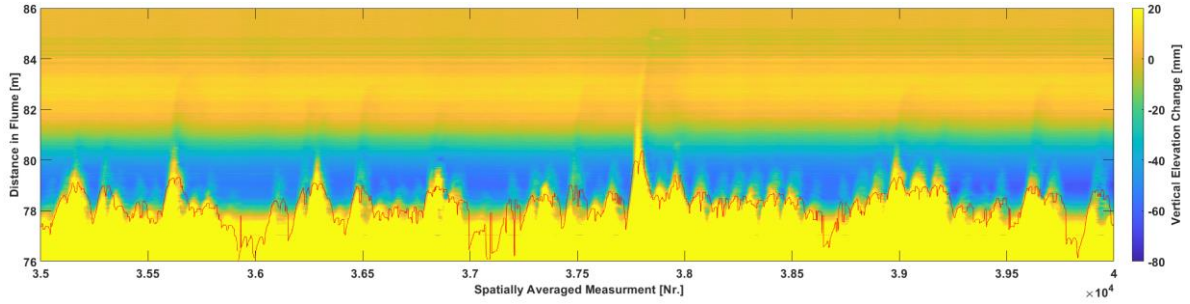

Figure 11-16: Zoomed Section of the Temporal Smoothing with Variance Window of 15 and Temporal Window of 25

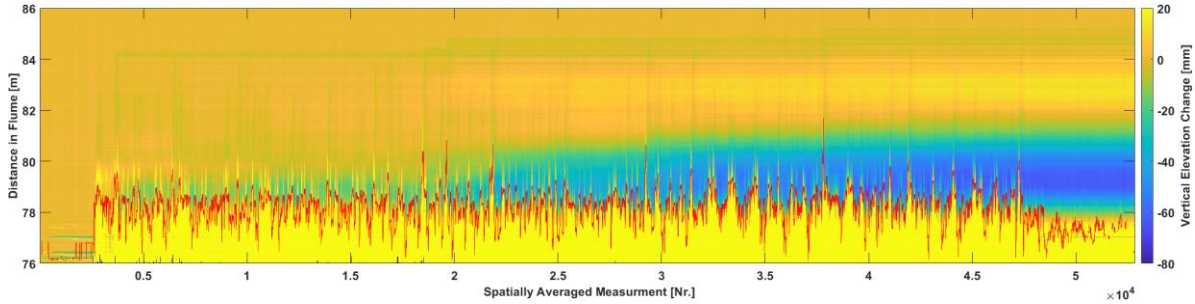

Figure 11-17: Temporal Smoothing with Variance Window of 25 and Temporal Window of 25

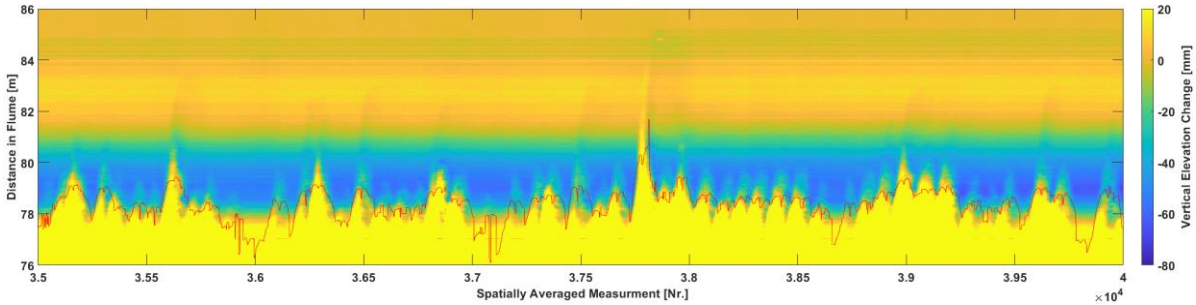

Figure 11-18: Zoomed Section of the Temporal Smoothing with Variance Window of 25 and Temporal Window of 25

APPENDIX B - DECREASED VARIANCE

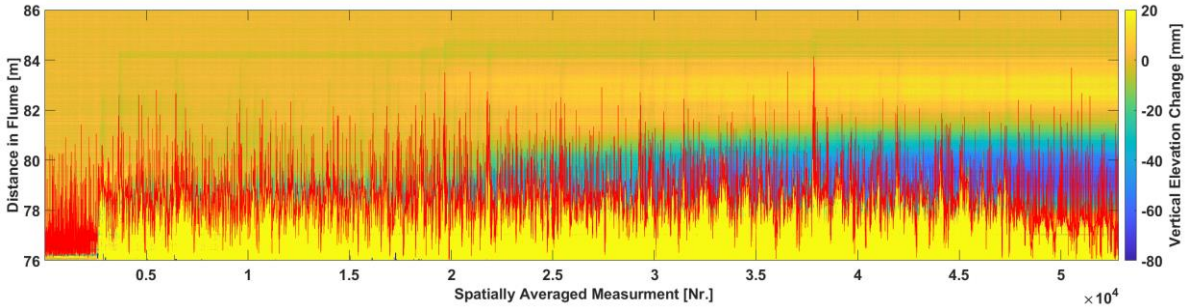

Figure 11-19: Temporal Smoothing with Variance Window of 5 and Temporal Window of 5

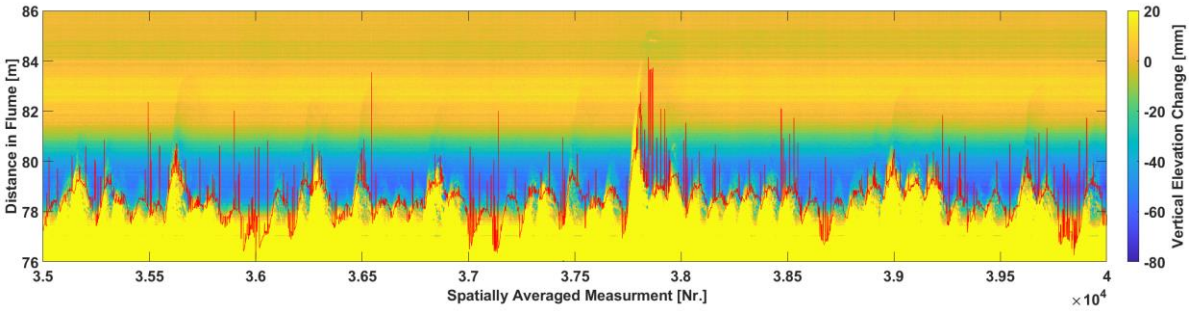

Figure 11-20: Zoomed Section of the Temporal Smoothing with Variance Window of 5 and Temporal Window of 5

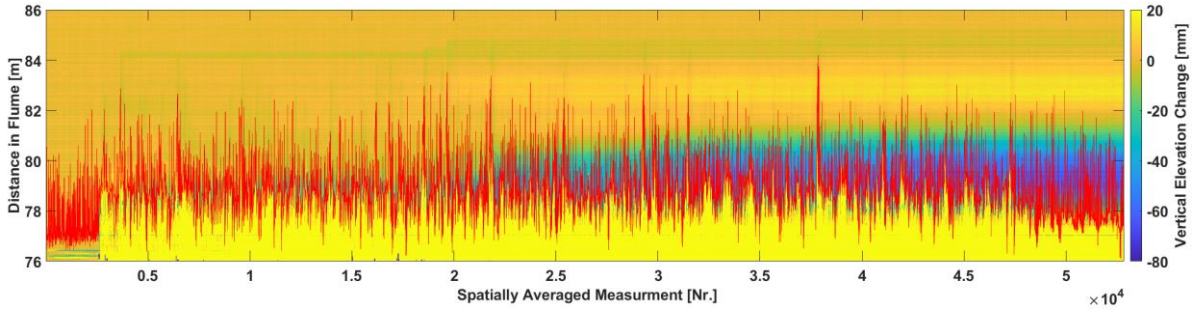

Figure 11-21: Temporal Smoothing with Variance Window of 15 and Temporal Window of 5

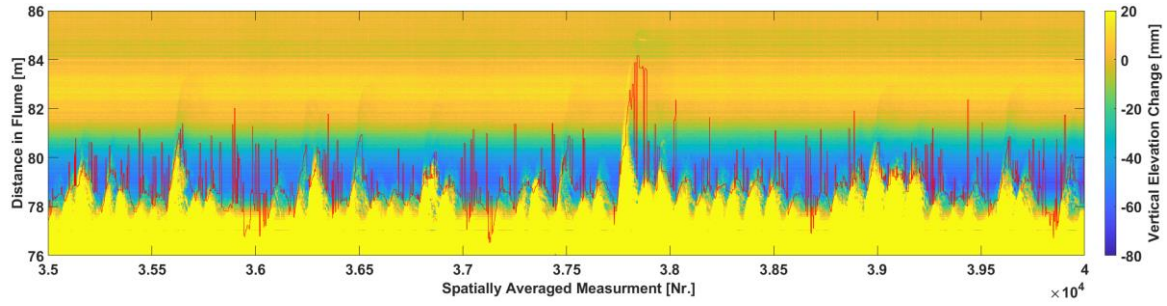

Figure 11-22: Zoomed Section of the Temporal Smoothing with Variance Window of 15 and Temporal Window of 5

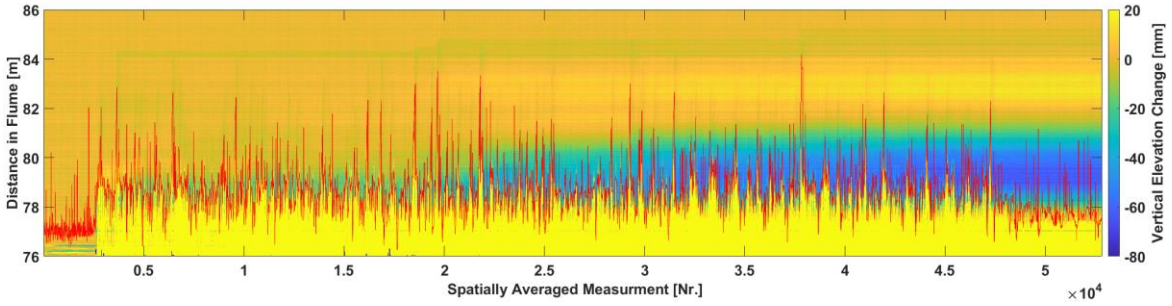

Figure 11-23: Temporal Smoothing with Variance Window of 25 and Temporal Window of 5

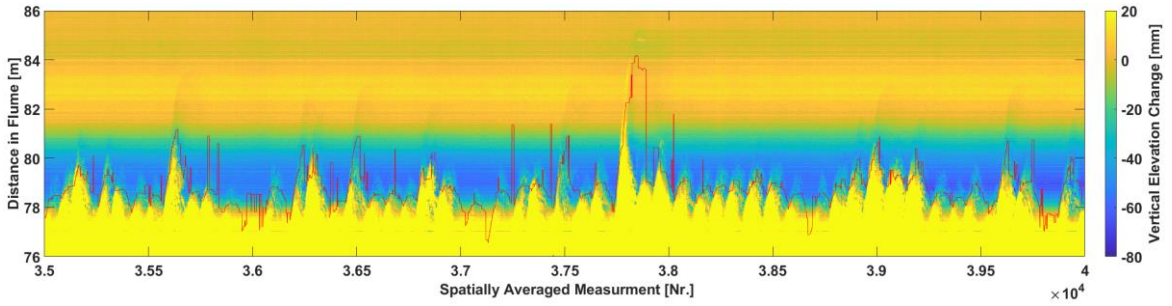

Figure 11-24: Zoomed Section of the Temporal Smoothing with Variance Window of 25 and Temporal Window of 5

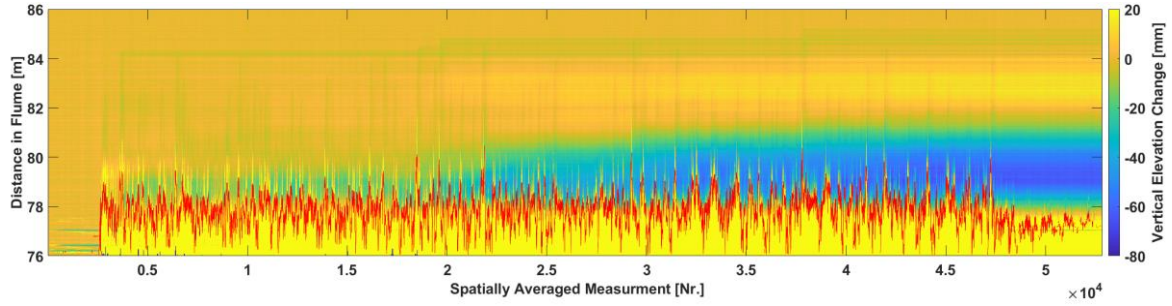

Figure 11-25: Temporal Smoothing with Variance Window of 5 and Temporal Window of 15

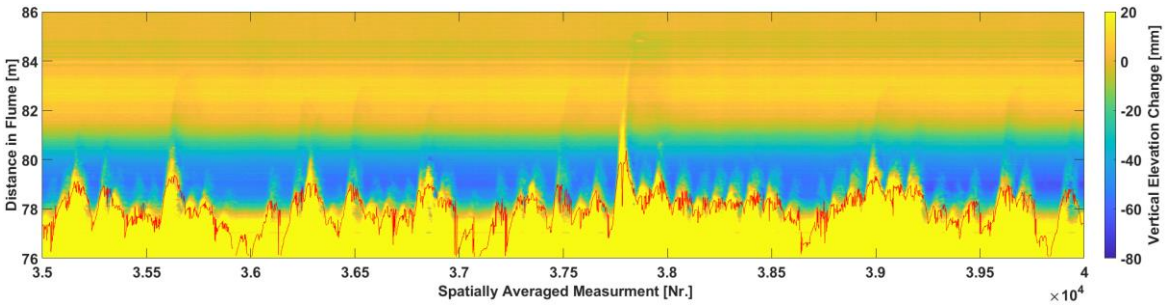

Figure 11-26: Zoomed Section of the Temporal Smoothing with Variance Window of 5 and Temporal Window of 15

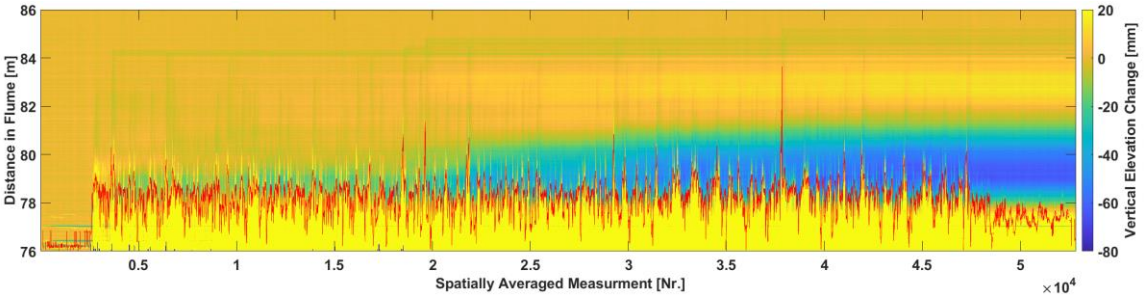

Figure 11-27: Temporal Smoothing with Variance Window of 15 and Temporal Window of 15

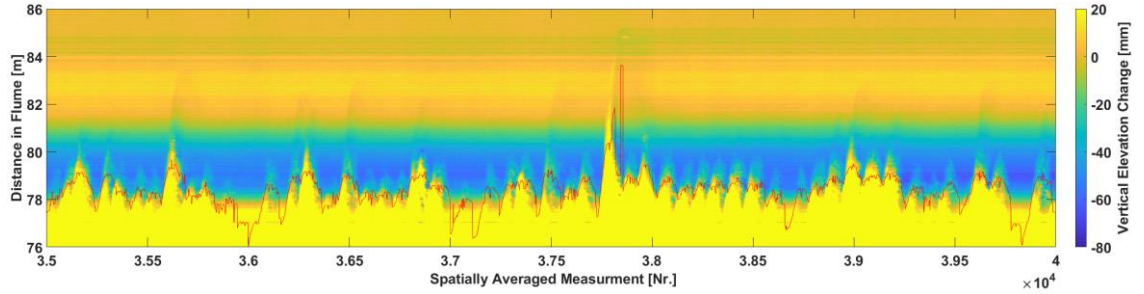

Figure 11-28: Zoomed Section of the Temporal Smoothing with Variance Window of 15 and Temporal Window of 15

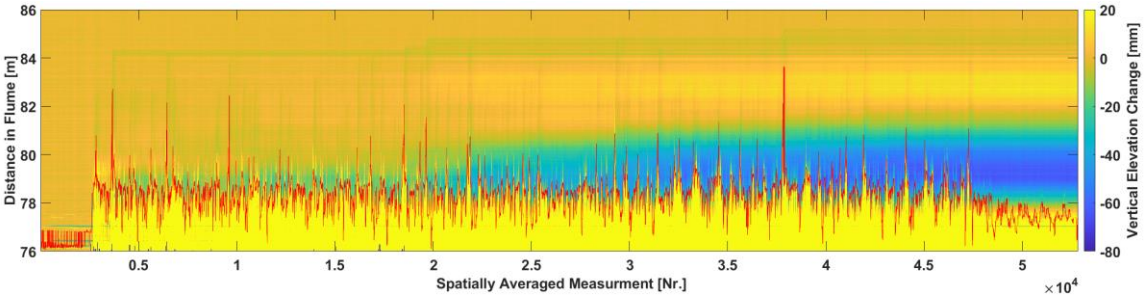

Figure 11-29: Temporal Smoothing with Variance Window of 25 and Temporal Window of 15

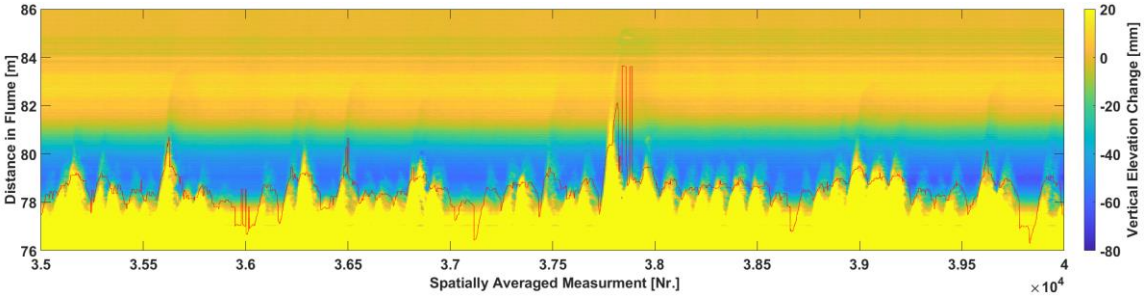

Figure 11-30: Zoomed Section of the Temporal Smoothing with Variance Window of 25 and Temporal Window of 15

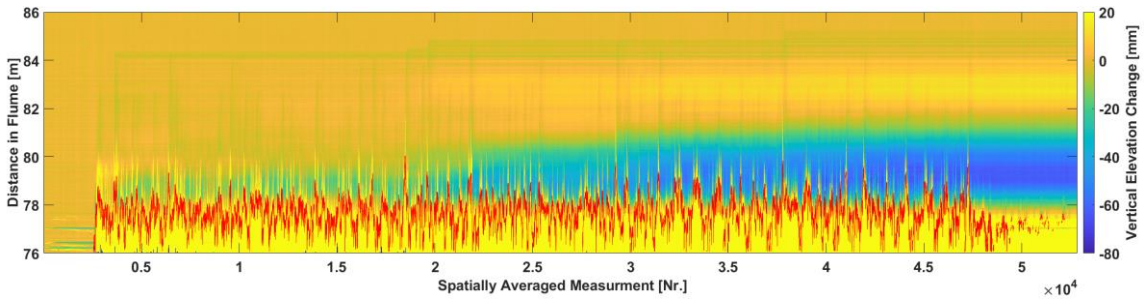

Figure 11-31: Temporal Smoothing with Variance Window of 5 and Temporal Window of 25

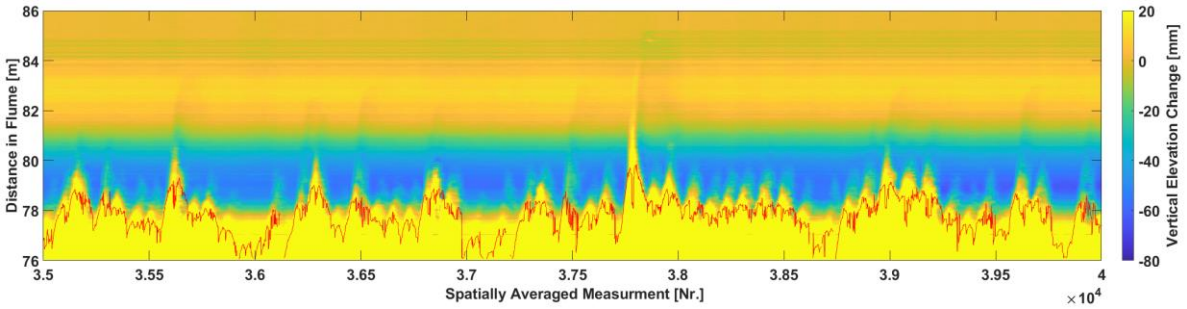

Figure 11-32: Zoomed Section of the Temporal Smoothing with Variance Window of 5 and Temporal Window of 25

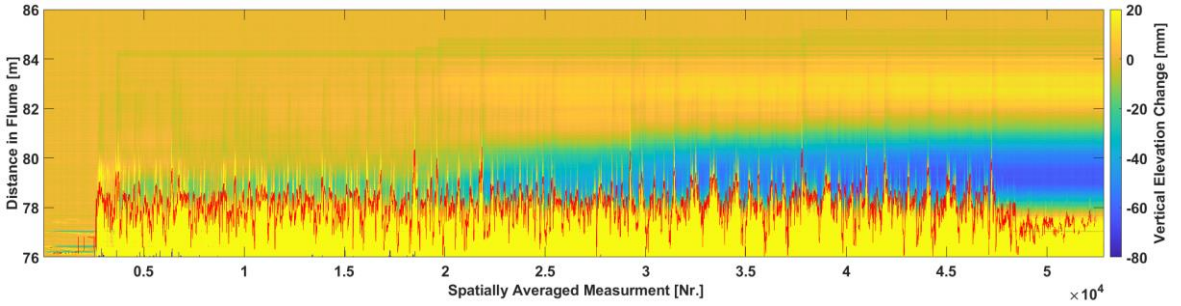

Figure 11-33: Temporal Smoothing with Variance Window of 15 and Temporal Window of 25

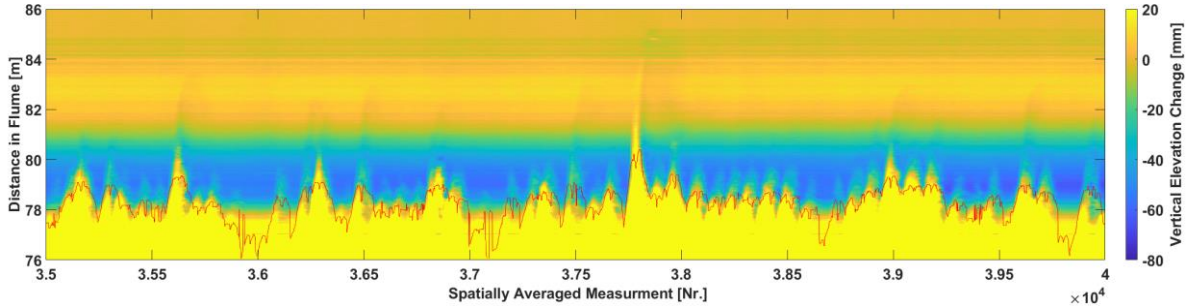

Figure 11-34: Zoomed Section of the Temporal Smoothing with Variance Window of 15 and Temporal Window of 25

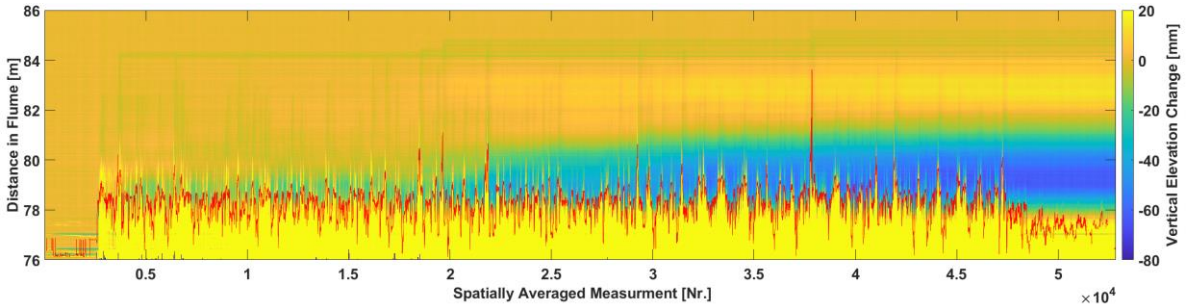

Figure 11-35: Temporal Smoothing with Variance Window of 25 and Temporal Window of 25

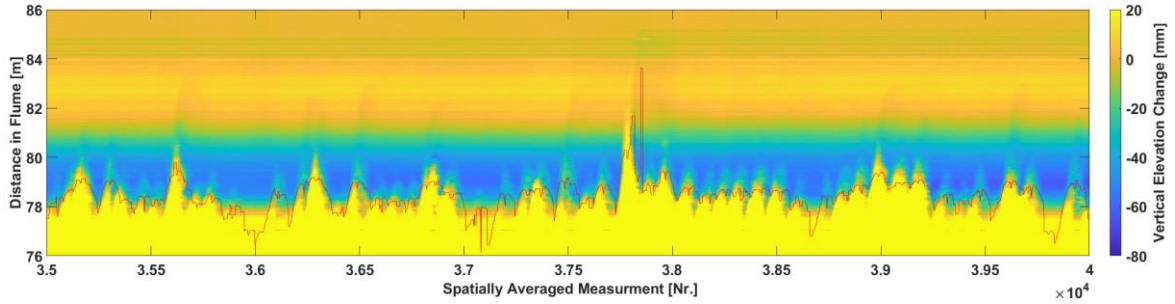

Figure 11-36: Zoomed Section of the Temporal Smoothing with Variance Window of 25 and Temporal Window of 25

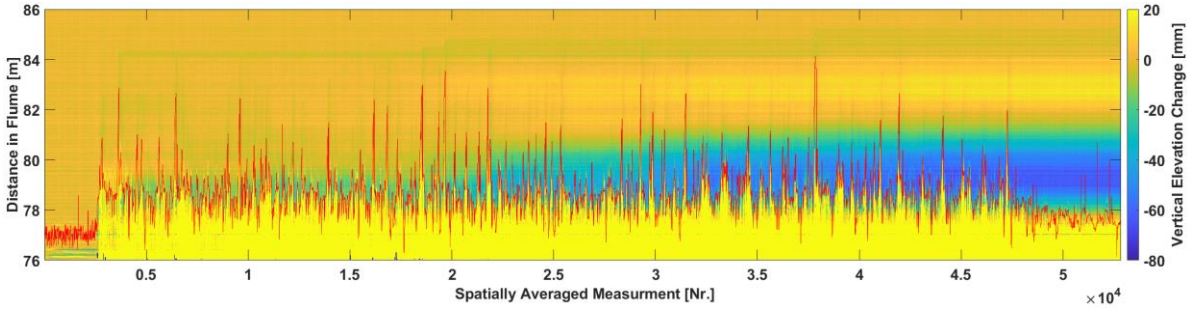

Figure 11-37: Temporal Smoothing with Variance Window of 35 and Temporal Window of 5

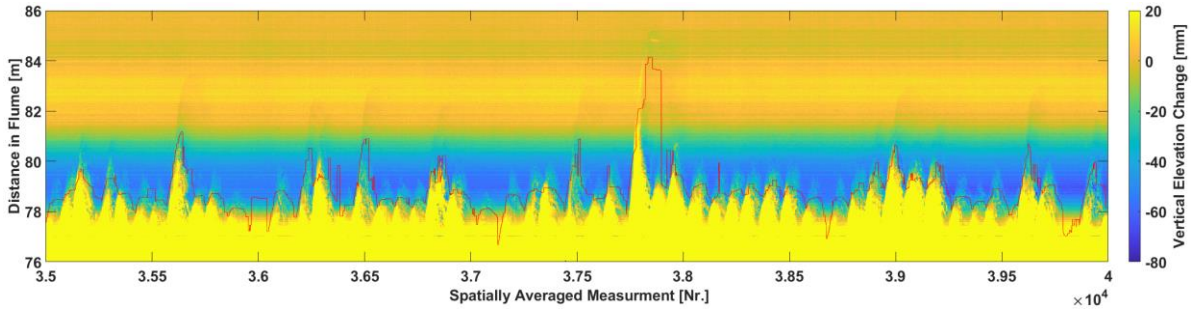

Figure 11-38: Zoomed Section of the Temporal Smoothing with Variance Window of 35 and Temporal Window of 5

APPENDIX C – RSSI METHOD

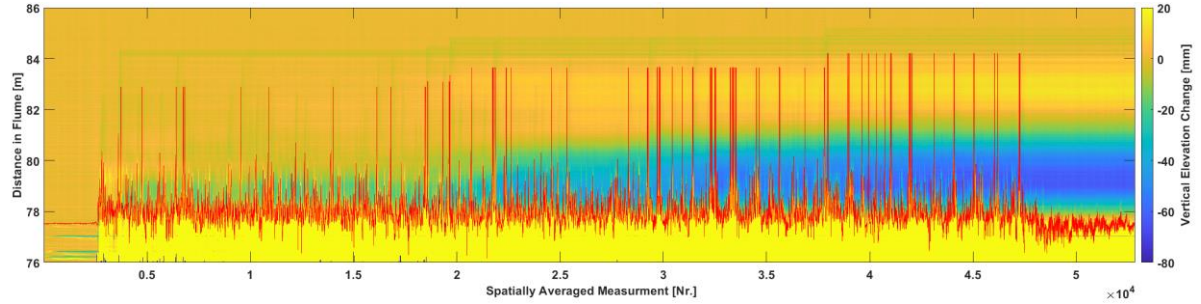

Figure 11-39: Obtained Water Line with Temporal Smoothing Window of 5 and RSSI Threshold of 5

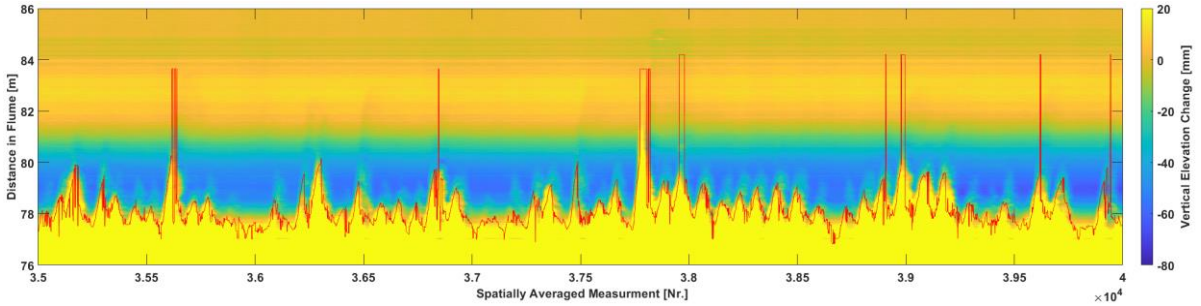

Figure 11-40: Zoomed Section of Obtained Water Line with Temporal Smoothing Window of 5 and RSSI Threshold of 5

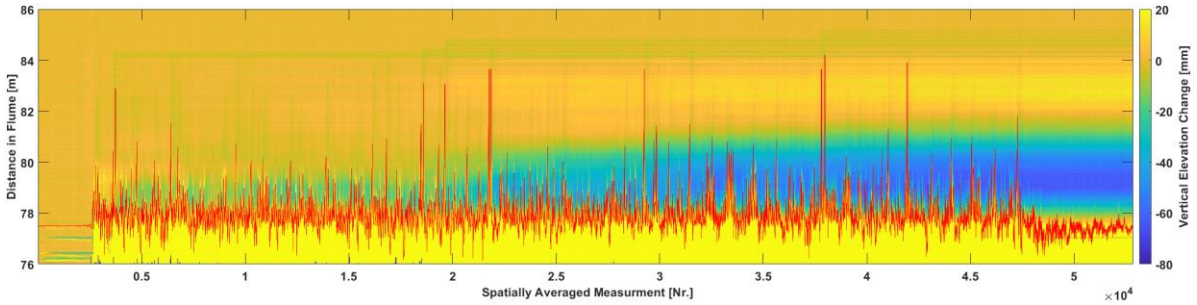

Figure 11-41: Obtained Water Line with Temporal Smoothing Window of 5 and RSSI Threshold of 10

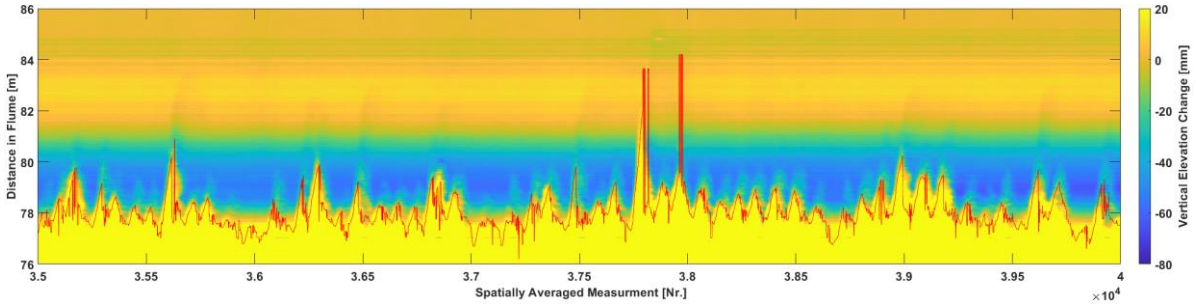

Figure 11-42: Zoomed Section of Obtained Water Line with Temporal Smoothing Window of 5 and RSSI Threshold of 10

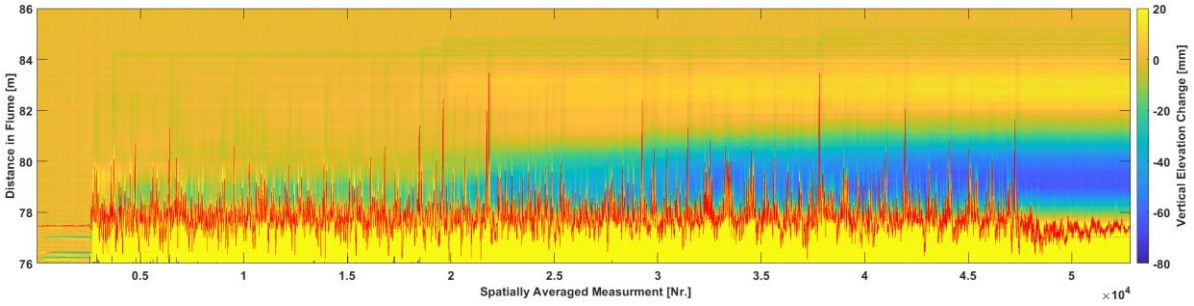

Figure 11-43: Obtained Water Line with Temporal Smoothing Window of 5 and RSSI Threshold of 15

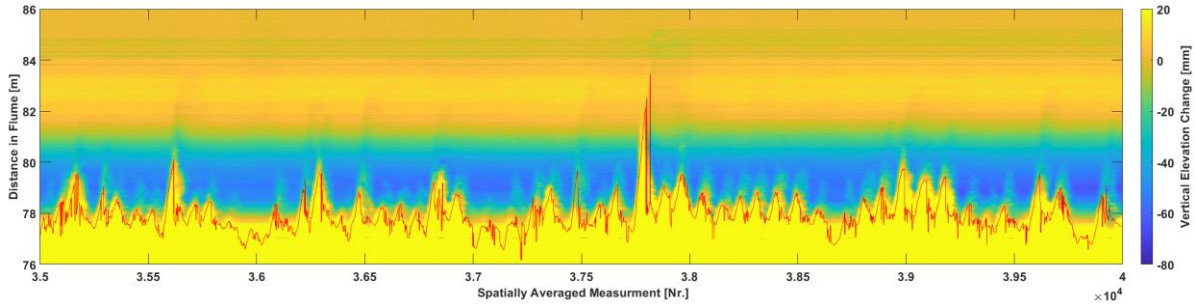

Figure 11-44: Zoomed Section of Obtained Water Line with Temporal Smoothing Window of 5 and RSSI Threshold of 15

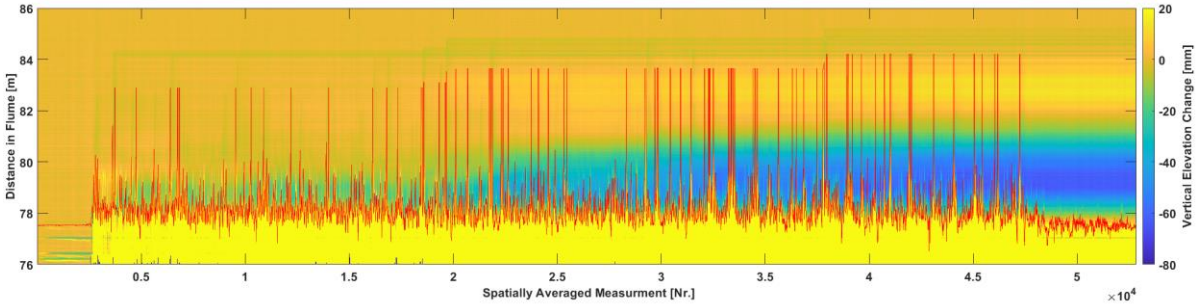

Figure 11-45: Obtained Water Line with Temporal Smoothing Window of 15 and RSSI Threshold of 5

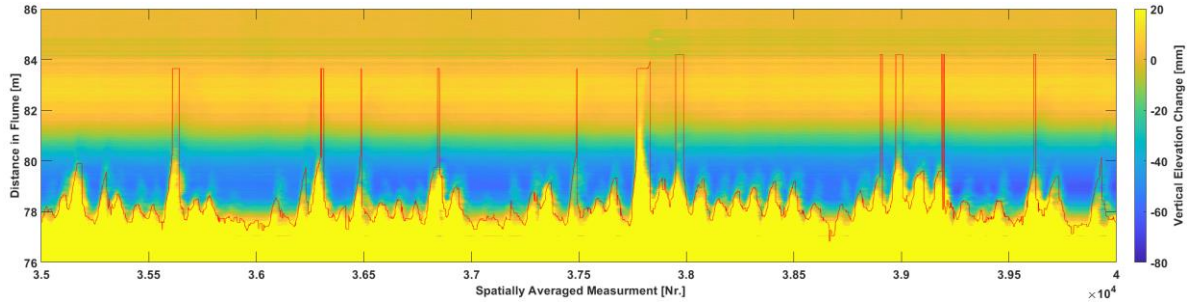

Figure 11-46: Zoomed Section of Obtained Water Line with Temporal Smoothing Window of 15 and RSSI Threshold of 5

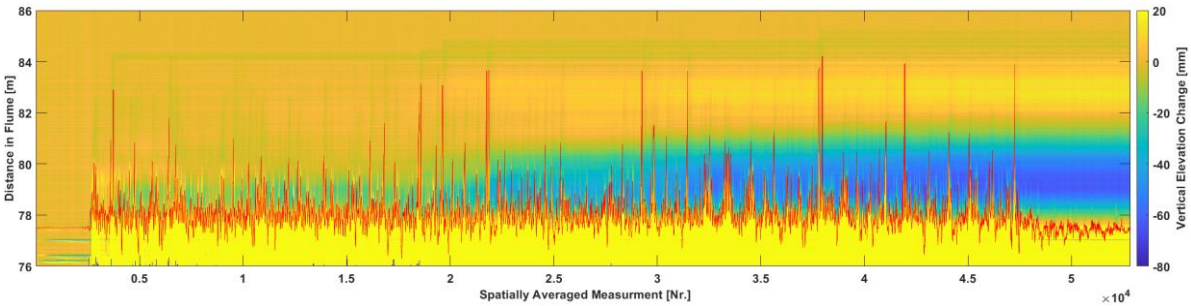

Figure 11-47: Obtained Water Line with Temporal Smoothing Window of 15 and RSSI Threshold of 10

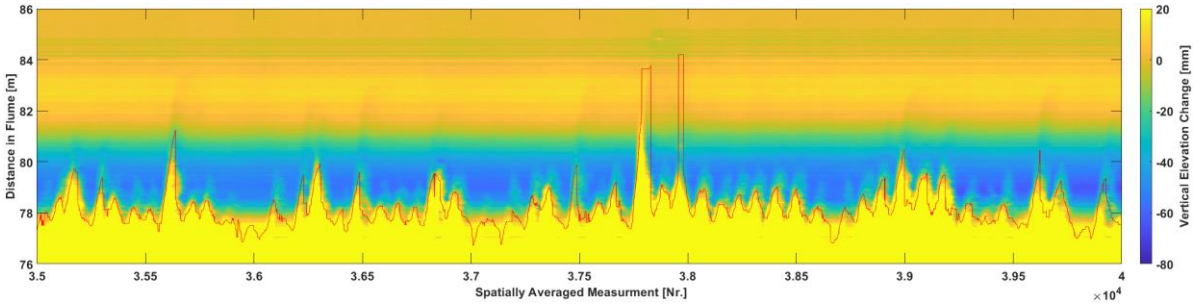

Figure 11-48: Zoomed Section of Obtained Water Line with Temporal Smoothing Window of 15 and RSSI Threshold of 10

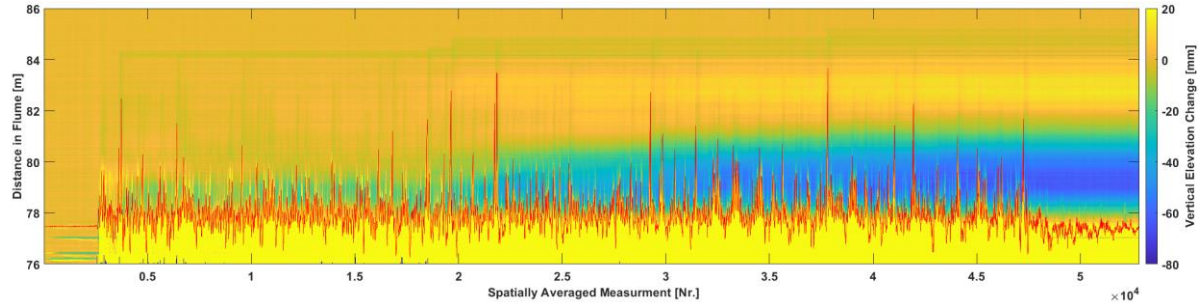

Figure 11-49: of Obtained Water Line with Temporal Smoothing Window of 15 and RSSI Threshold of 15

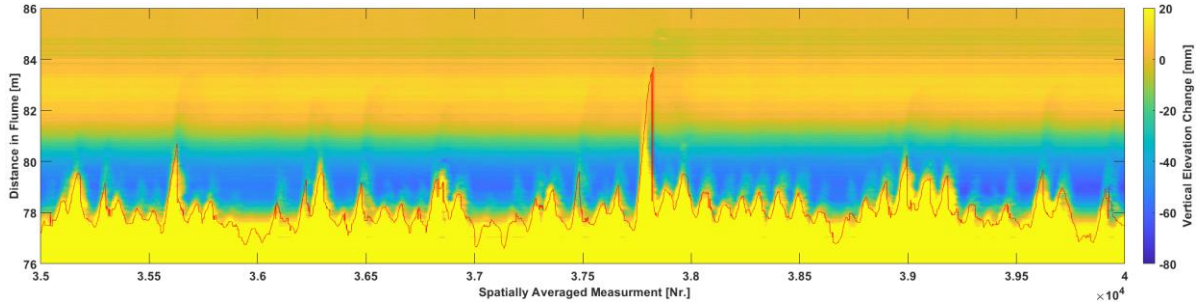

Figure 11-50: Zoomed Section of Obtained Water Line with Temporal Smoothing Window of 15 and RSSI Threshold of 15

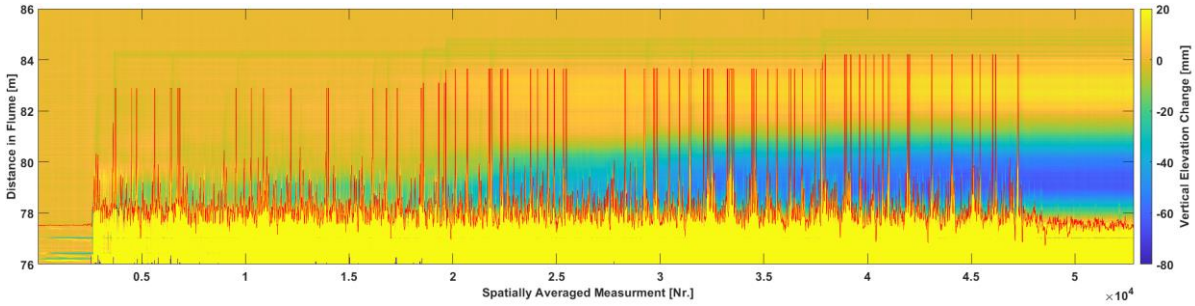

Figure 11-51: Obtained Water Line with Temporal Smoothing Window of 25 and RSSI Threshold of 5

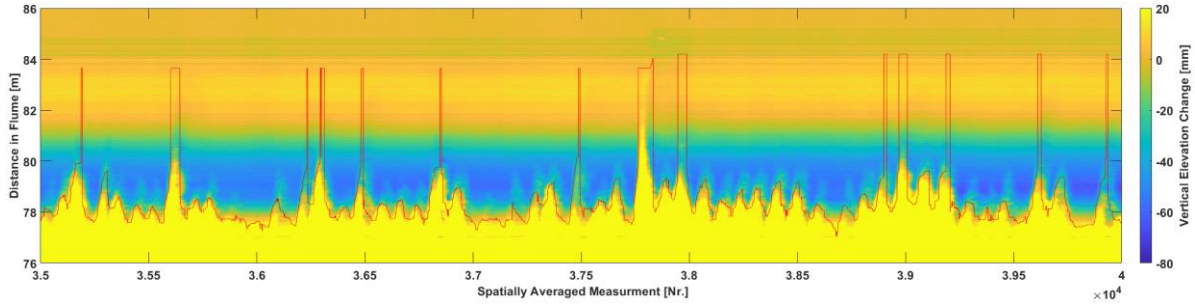

Figure 11-52: Zoomed Section of Obtained Water Line with Temporal Smoothing Window of 25 and RSSI Threshold of 5

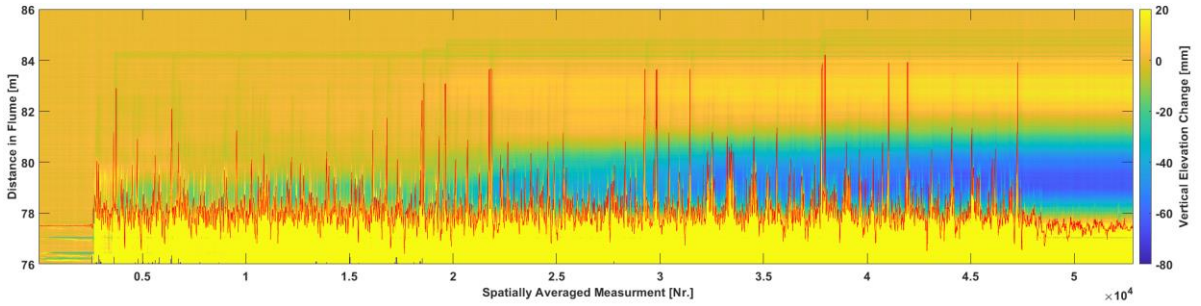

Figure 11-53: Obtained Water Line with Temporal Smoothing Window of 25 and RSSI Threshold of 10

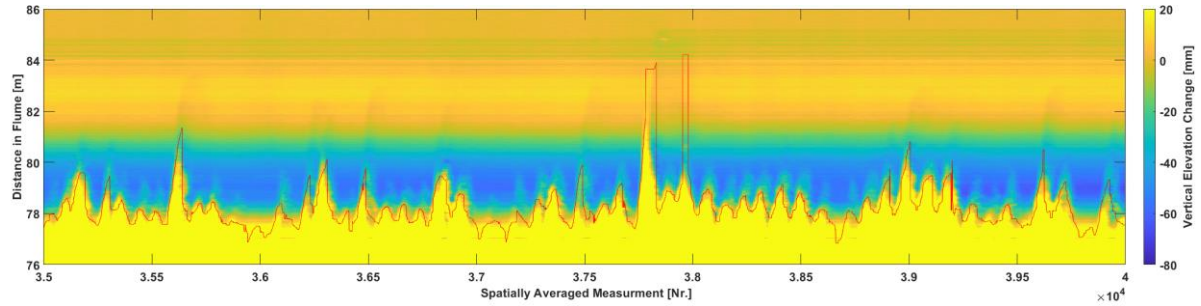

Figure 11-54: Zoomed Section of Obtained Water Line with Temporal Smoothing Window of 25 and RSSI Threshold of 10

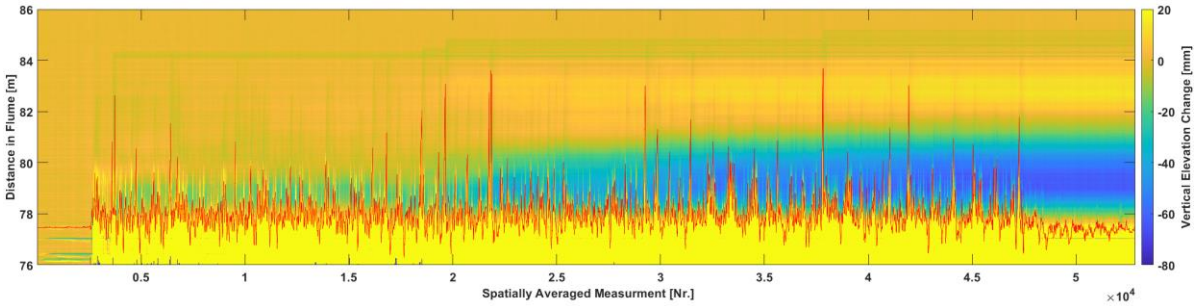

Figure 11-55: Obtained Water Line with Temporal Smoothing Window of 25 and RSSI Threshold of 15

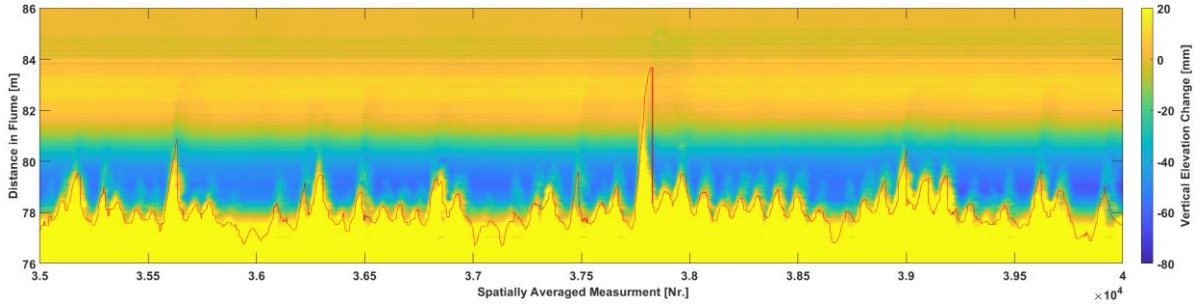

Figure 11-56: Zoomed Section of Obtained Water Line with Temporal Smoothing Window of 25 and RSSI Threshold of 15

UNIVERSITY OF TWENTE
Drienerlolaan 5
7522 NB Enschede

P.O.Box 217
7500 AE Enschede

P +31 (0)53 489 9111

info@utwente.nl
www.utwente.nl

UNIVERSITY OF TWENTE
Drienerlolaan 5
7522 NB Enschede

P.O.Box 217
7500 AE Enschede

P +31 (0)53 489 9111

info@utwente.nl
www.utwente.nl